BLIND DECONVOLUTION OF STILL IMAGES USING HYBRID COMPUTING

by

Tanweer Ahmad Cheema

A dissertation submitted to M.A.J.U. in partial fulfillment of the requirements for the degree of

DOCTOR OF PHILOSOPHY

Department of Electronics Engineering

Faculty of Engineering and Sciences

MOHAMMAD ALI JINNAH UNIVERSITY

2005

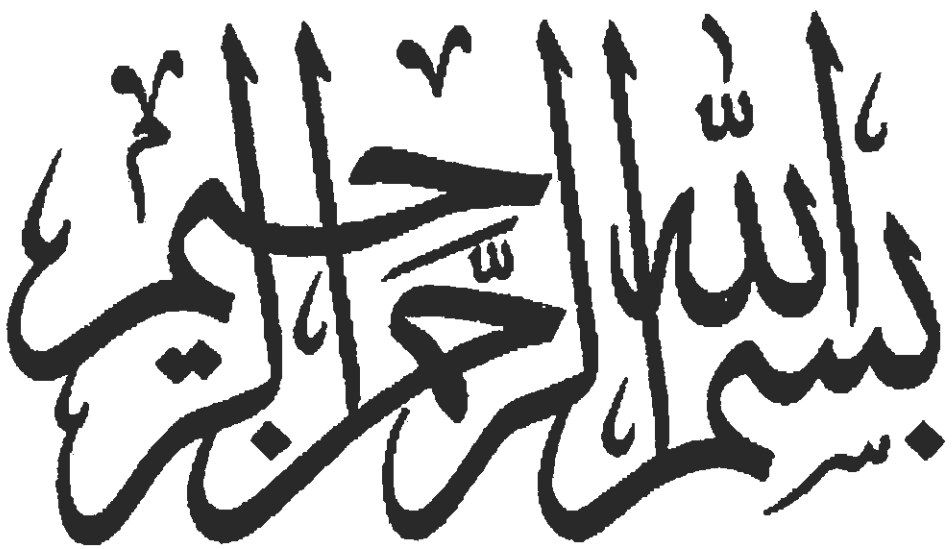
بسم الله الرحمن الرحيم

DEDICATED TO

HOLY PROPHET (P. B. U. H.)
THE GREATEST SOCIAL REFORMER

&

MY WORTHY PARENTS

Abstract

Restoration of images degraded by unknown blur is a difficult problem. It is called blind image restoration. The unknown blur can be of linear or nonlinear nature. It can also be space invariant or space variant making the blind image restoration problem all the more challenging. Sometimes it is necessary to simultaneously identify the blur and restore the image, a problem that we have addressed in this thesis. The assumption is that coefficients of image model are controlled by autoregressive(AR) process while that of blurring model are controlled by moving average (MA) process. Moreover, a natural assumption about most of the images in practical applications is that they are smooth in nature.

We have used three layered artificial neural networks (ANN) to embed naturally the AR process between its first two layers and MA process between its last two layers. The genetic algorithms (GA) have been used to avoid getting stuck in local minima. The first major work has been the extension of the network to handle nonlinear space-invariant degradations in the images by incorporating nonlinear ARMA model using the concept of Volterra filters. This approach can cater for the sharp contrasts which may come in the degraded images as well. The second major work has been the adaptation of the ANN to handle the space variant blur. The image and hence forth, the layers of ANN are divided into blocks and each block is categorized according to the level of activity. Thus the weights between the layers are no more universal and space invariant but they can vary from block to block according to the activity. This kind of freedom results in better results in case of space variant blurs and even space invariant blurs. The third major work has been the extension of the cost function. The two extra terms in cost function take into account the human visual perception system. They match the second order statistics (local variances) of the images at different layers and give improvement in the visual quality of the images.

Gradient based learning algorithms have been developed for the fast convergence to the solution. Several degraded images have been restored. The results have been compared with some of the important current techniques in the literature using improvement in signal to noise ratio (ISNR) of restored images and normalized mean square error (NMSE) of estimated blur as figures of merit.

List of Publications and Submissions

1. **T. A. Cheema**, I. M. Qureshi, A. Jalil, and A. Naveed, "Artificial neural networks for blur identification and restoration of nonlinearly degraded images", *International Journal of Neural Systems*, vol. 11, no. 5, pp. 455–461, 2001.
2. **T. A. Cheema**, I. M. Qureshi, A. Jalil, A. Naveed, "Blurred image restoration of nonlinearly degraded images using ANN and nonlinear ARMA model", *Journal of Intelligent Systems*, vol. 11, no. 5, pp. 299–312, 2001.
3. **T. A. Cheema**, I. M. Qureshi, A. Hussain "Blind Image Deconvolution Through Space-variant Neural Network Approach", *IEE Electronic Letters*, vol. 41, No. 6, pp. 308-309, 2005.
4. **T. A. Cheema**, I. M. Qureshi, A. Hussain and T. S. Durrani, "A New Space-variant Neural Network Approach to Blind Image Deconvolution", submitted to *IEE Proc. of Signal, Vision, and Image Processing.*
5. **T. A. Cheema**, I. M. Qureshi, A. Jalil, and A. Naveed, "Blur and Image Restoration of Nonlinearly Degraded Images using Neural Networks based on modified Nonlinear ARMA Model", Submitted to Arabian Journal of Science and Engineering (AJSE).
6. A. Jalil, I. M. Qureshi, **T. A. Cheema** and A. Naveed, "Feature Extraction of Hand Written Characters by using Non-linear and Unsupervised Neural Networks", *Journal of Information Science and Engineering (JISE)*, vol. 21, no. 2, pp. 453-473, 2005.
7. A. Naveed, I. M. Qureshi, **T. A. Cheema,** and A. Hussain "Blind Equalization of Communication Channels with Equal Energy Sources Using a Combined HOS-SOS Approach", submitted to *IEICE Trans. on Commun.*

8. **T. A. Cheema**, I. M. Qureshi, A. Jalil, and A. Naveed, "Blur and image restoration of nonlinearly degraded images using neural networks based on modified ARMA model", IEEE 8th International Multitopic Conference INMIC 2004, Lahore, Pakistan, pp.102-107, 2004.

9. A. Naveed, I. M. Qureshi, A. Jalil and **T. A. Cheema,** "Blind equalization and estimation of channel using artificial neural networks", IEEE 8th International Multitopic Conference INMIC 2004, Lahore, Pakistan, pp.184-190, 2004.

10. I. M. Qureshi, **T. A. Cheema**, A. Naveed and A. Jalil, "Genetic algorithms based artificial neural networks for blur identification and restoration of degraded images", *Pakistan Journal of Information and Technology*, vol. 2, no. 1, pp. 21-24, 2003.

11. A. Jalil, I. M. Qureshi, A. Naveed and **T. A. Cheema**, "Feature extraction by using non-linear and unsupervised neural networks" *Pakistan Journal of Information and Technology (PJIT)*, vol. 2, no.1, pp. 40-43, 2003.

12. I. M. Qureshi, A. Naveed, **T. A. Cheema** and A. Jalil, "Artificial neural networks for microstructure analysis of rolling process", *Pakistan Journal of Information and Technology (PJIT)*, vol. 2, no.1, pp. 65-68, 2003.

The research publications which are included in this dissertation are 1- 4.

Acknowledgement

I humbly praise and thank ALMIGHTY ALLAH, The compassionate and The merciful, Who gave health, thoughts, affectionate parents, talented teachers, helping friends and opportunity to contribute to the vast body of knowledge. Peace and prayers for His Prophet HAZRAT MUHAMMAD (S.A.W.) Whose incomparable life is the glorious model for humanity.

I offer my sincerest thanks to my supervisor, Dr. Ijaz Mansoor Qureshi, for his illustrious advice, useful suggestions, kind and dynamic supervision throughout the research work. His personal interest, valuable suggestions, most co-operative affectionate behavior, constructive and thoughtful criticism resulted in the completion of this dissertation.

I am desirous of expressing my gratitude for scholastic guidance, utmost co-operation, untiring advises and benevolence of my co-supervisor Dr. Amir Hussain. I would have felt helpless without his guidance which led me To this successful ending. Warm thanks cannot compensate for his deep concern about this work.

I am also thankful to all my class fellows and friends whose good wishes and encouragement enabled me to complete this dissertation successfully. I offer my heartfelt gratefulness to Mr. Abdul Jalil for his help and guidance during the course of study which also cannot be forgotten. I am also extremely indebted to my friend Mr. Aqdas Naveed for his invaluable support. Lastly Mr. Imran Shahzad deserves thanks for his help to me.

I also wish to express my feeling of gratitude to my parents, brothers, sisters, cousins and all the relatives, who prayed for my health and brilliant future. Mr. Ghias Malik deserves my thanks for his support in the typing of this manuscript. Last but not

least, I offer my profound gratitude to my wife for being patient and co-operative throughout my research period.

(TANWEER AHMAD CHEEMA)

Contents

List of Figures

List of Tables

List of Symbols

a_{kl}	Noncausal minimum variance representation NMVR coefficients (AR coefficients).
h_{mn}	Space invariant point spread function (PSF)
$h_{m_1n_1m_2n_2}$	Nonlinear Space invariant point spread function (PSF)
$x(i,j)$	True image
$\hat{x}(i,j)$	Estimate of the true image
$y(i,j)$	Distorted or degraded image
$\hat{y}(i,j)$	Estimate of observed distorted/degraded image
$v_1(i,j)$	Zero mean white Gaussian noise in image model
$v_2(i,j)$	Zero mean white Gaussian noise in degradation model
S_a	Support of image model coefficients a_{kl}
S_h	Support of degradation model coefficients h_{mn}
$\sigma_{v_1}^2$	Variance of zero mean white Gaussian noise in image model
$\sigma_{v_2}^2$	Variance of zero mean white Gaussian noise in degradation model
$E_2(w)$	Auto-associative error between layer 1 and 2.
$E_3(w)$	Hetero- associative error between layer 2 and 3
L_1	First 2-D layer of the neural network
L_2	Second 2-D layer of the neural network
L_3	Third 2-D layer of the neural network

Chapter 1

Introduction

1.1 Statement of Problem

Images are produced in order to record or display useful information. They are acquired in order to obtain two-dimensional (2-D) representation of a three-dimensional scene. Unfortunately, many images represent scenes in an unsatisfactory manner due to imperfections in the electronic or photographic medium because the conditions under which images are obtained are frequently less than ideal. Therefore, the recorded images often represent a degraded version of the original scene [1]. The imaging process, the atmosphere, and the recording medium all introduce degradations into the captured image so that the image that is actually recorded may fail to represent the scene adequately. The goal of image restoration is to manipulate an image in such a way that it will, in some sense, depict the scene more closely that it purports to represent [2].

The image restoration problem appears in many fields. Virtually all disciplines in which images are acquired under less than ideal conditions find restoration techniques useful – astronomy [3], medicine [4], military reconnaissance [5], to name a few. Photo-processing labs may also find restoration techniques a valuable tool in "touching up" special

photographs [6]. These fields have diverse aims for image restoration, but certain fundamentals are common to all image restoration problems.

The degradations may have many causes, but two types of degradations are often dominant: noise and blurring, each of which introduces peculiar problems for image restoration. The most basic of these is observation noise which can be caused by film-grain noise, quantization noise, or other random disturbances. For each of these causes, however, the process by which the degradation is introduced cannot be described deterministically, and information in the image may be lost [7].

The second source of image degradation is blurring. Blurring is a form of bandwidth reduction of the image due to the imperfect image formation process [8]. It can be caused by relative motion between the camera and the original scene, or by an optical system, which generates out of focus images. When aerial photographs are produced for remote sensing purposes, blurs are introduced by atmospheric turbulences, aberrations in the optical system, and relative motion between the camera and the ground [9]. Attempting to reverse or invert this blurring process introduces a number of problems. First, the inversion of this process often amplifies the noise in the image. Second, the process may be non-invertible, so that multiple solutions are possible. Third, the blurred image is typically a windowed version of the blurred scene, so that some of the boundary information necessary for reversing the blur is lost. Finally, the blur itself may be unknown or incompletely specified, as it is the case in most of the real situations. In each case, the image restoration process must deal with the fact that the information has been lost or obscured.

From the previous discussion, one can see that the fundamental hurdle in image restoration is lack of knowledge. If all the degradations suffered by an image were known,

then they could in general be removed. In some cases, the degradation actually destroys information in the image, and the knowledge of the degradation process is insufficient to counteract the degradation. In every case, however, the information no longer exists, or it is not easily accessible, or it is known only in a probabilistic sense. On the other hand, most image restoration algorithms generally require some *a priori* information in order to obtain a restored image. This information can be supplied in several ways. The most trustworthy source of information is knowledge about the image formation process itself. For example, light intensity is represented by a bounded range of numbers, and the restored image can be restricted to lie within these physically realistic boundaries. Another assumption often made is that the original scene is smooth, i.e. there is a degree of correlation (smoothness) among neighboring points in the original image [8]. This holds true for virtually every realistic image; however, the degree and type of smoothness may vary considerably from one image to another. Thus, the smoothness assumption requires further information in order to be applied accurately in restoration process.

Closely related to the smoothness assumption is the use of an autoregressive (AR) model for the image [10]. An AR process assumes a certain parametric model of the smoothness in the data. Images are typically formed by regions of near-constant intensity or texture with sharp transitions. This type of behavior makes AR models more suitable for images than moving-average (MA) models which are not appropriate as image models. Image blur can generally be modeled as an MA process. MA processes are ideal for modeling the intensity-averaging effect of blur. Once again, however, the choice of model does not supply all the needed information. The model, structure and parameters can be obtained by inspection of the degraded image. However, this is not true in general. The

image restoration process requires further assumptions to deal with the lack of accessible information.

Noise in the observed image presents a unique and difficult problem for image restoration. Typically, there is no way to reverse completely the effects of noise - the information is lost. It is possible, however, to make some assumptions that allow the image restoration. The noise may be considered as additive white Gaussian noise (AWGN); the restoration can then be designed to compensate for noise under this assumption [11]. Even this assumption requires knowledge that is not always immediately available. The variance of the noise must be supplied as well as the types of noise distribution.

Various constraints may be imposed in order to specify more accurately the path to a restored image. Often these constraints are nothing more than the educated guesses made to facilitate the restoration process. The image processing may supply a constraint which is actually a poor representation of reality. How can one know whether the constraint improves or deteriorates the restoration? Visual inspection is possible, but it is often slow, inaccurate, and otherwise undesirable. Therefore, it can not be included in image restoration algorithms. Lack of easily accessible knowledge of constraint validity presents a hurdle for image restoration algorithms.

The more severe problem of image restoration is blind image deconvolution which is the process of estimating both the true image and blur from the degraded image characteristics, using the partial information about the imaging system. There are several motivating factors behind the use of blind image deconvolution for image restoration applications [8]. In practice, it is often costly, dangerous, or physically impossible to obtain *a priori* information about degradation process and original scene.

The blind image deconvolution field clearly needs a method for testing the assumptions imposed on the simultaneous restoration of degraded image and identification of blurring process. If such a test were available, then assumptions could be validated. The neural networks are useful techniques in statistical data analysis. It has widely been used for different image processing applications. It has been used for image restoration, pattern classification, etc. The self-organization like structure of neural networks makes it possible to be used for blind image deconvolution. In this dissertation, a neural network based on ARMA models is extended to nonlinear ARMA models. The approach has also been extended to space-variant neural networks base on ARMA models. These models will provide a powerful tool for blind image deconvolution.

1.2 Contributions of the Dissertation

The first contribution of this research work is designing and implementation of blind image deconvolution of nonlinearly degraded images using ARMA based neural networks. The nonlinearity of the imaging systems is the one that compresses or enhances a certain range of intensities. Therefore, nonlinear MA process is assumed for degradation processes which are based on Volterra filters. However, the autoregressive processes may be assumed to be linear or nonlinear. The nonlinear AR processes have same form as that of Volterra filters.

The second and important contribution of this dissertation offers a new space-variant neural network approach to blind image deconvolution. This approach is based on the activities of the sub-regions of the image known as blocks. The blind deconvolution of these blocks is based upon the fact that blurring affects more the textured regions than smooth

regions, while noise is prominent and affects more the smoother regions. Therefore, activity based network is proposed to handle this problem along with the image restoration and space-variant blur identification.

The last and final contribution of this dissertation is the introduction of extended cost function based on human perception system. This extended cost function contains two new terms in order to match the second order statistics of the images. Therefore, the new cost function can improve the visual quality of the images in a better way.

1.3 Organization of the Dissertation

Chapter 2 provides an overview of the image restoration problem. The image formation process is described along with appropriate mathematical models. Several common PSF's are presented. The chapter reviews the most common restoration techniques for dealing with blurred and noisy images.

Chapter 3 describes the fundamental tool used in this dissertation - the neural networks and genetic algorithms. An overview of the feedforward neural network with back-propagation algorithm is presented. Finally the genetic algorithms are introduced along with their application areas.

Chapter 4 deals with the blind image deconvolution of the linearly degraded images by using artificial neural networks based on linear and space-invariant ARMA processes. This technique is developed for the specific integration of genetic algorithms for weight initialization of the neural network.

Chapter 5 contributes to the blind image deconvolution of nonlinearly degraded images by using artificial neural networks based on nonlinear degraded process or MA

process. This technique is particularly important to handle nonlinearity of the sensors along with sharp contrasts enhancement which may occur in natural scenes.

Chapter 6 develops a space-variant neural network model based on human visual perception system. This method first divides the image into small blocks and then it is assumed that the degradation is space-invariant within the block. Each block is then treated according to the activity inside the block. An extended cost function based on human visual system is developed for the neural network for better restoration of the degraded images.

Finally, Chapter 7 summarizes the material presented in this dissertation and draws conclusions from the advances made to the neural network approach aided by genetic algorithm to blind image restoration and blur identification. Some future research directions in this field are also suggested.

Chapter 2

Digital Image Restoration

This chapter describes a number of fundamentals relating to the image restoration problem. First, the image formation process is described for both continuous and discrete systems. Certain assumptions must be made to simplify the mathematical description of the image formation process, and these assumptions are stated explicitly. Second, a number of common PSF's are defined and mathematical models are presented to approximate various common physical causes of blur. Finally, this chapter provides a brief overview of the most popular restoration techniques.

2.1 Image Formation

The image formation process represents a 2-D mapping of a 3-D scene. The system that forms the image may introduce distortions into the mapping process. Furthermore, the process of recording the 2-D mapping may introduce the distortion as well. A general degraded image formation model is represented by the following equation [1]:

$$y(r,s) = U\left[\int_{-\infty}^{\infty}\int_{-\infty}^{\infty} h(r,s;f,g;x(f,g))\,df\,dg\right] \Theta v(r,s) \qquad (2.1.1)$$

where $y(r,s)$ is the degraded image, $x(f,g)$ is the true image and $v(r,s)$ is the noise process that affects the image formation at the time of recording. The point spread function

PSF that characterizes the entire blurring process is represented by the symbol $h(r,s;f,g;x(f,g))$. The symbol Θ corresponds to a point-by-point operation. The image formation process may be linear or nonlinear process, which is represented by $U[.]$.

Some assumptions are made about the degradation process to simplify the above equation. One of the important assumptions is that the degradation process is caused by a linear shift invariant PSF that acts on the true image. It will reduce the computational complexity of many image restoration algorithms. Another assumption is about the noise which is assumed to be purely additive in nature. These assumptions, due to their low computational complexity, are commonly used in practice for a variety of applications [7]. Therefore, these assumptions simplify the model to a convolution summation of the true image with the PSF as given below

$$y(r,s) = \int_{-\infty}^{\infty}\int_{-\infty}^{\infty} h(r-f,s-g)x(f,g)\,df\,dg + v(r,s) \tag{2.1.2}$$

Both the original image $x(f,g)$ and the observed image $y(r,s)$ represent real-valued intensity distributions and take nonnegative values only. As a result $h(r,s)$ is real valued and nonnegative as well. With uniform sampling, the degradation model can be reduced to the following superposition summation,

$$\begin{aligned} y(i,j) &= x(i,j) * h(i,j) + v(i,j) \\ &= \sum_{(m,n)} x(m,n)h(i-m,j-n) + v(i,j) \end{aligned} \tag{2.1.3}$$

where * denotes the two dimensional linear convolution operator, (i,j) represents the discrete pixel coordinates, $x(i,j)$ and $y(i,j)$ are the sampled values of the true image

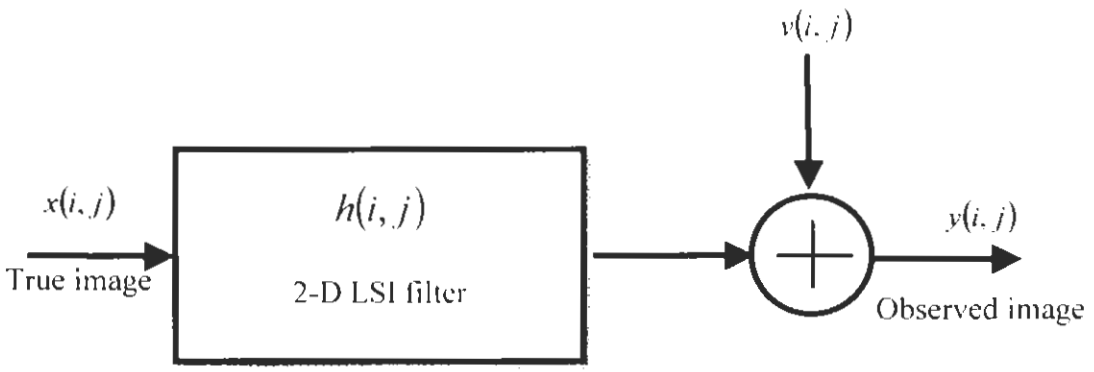

Figure 2.1 Linear Degradation Model

$x(r,s)$ and observed image $y(r,s)$, and $h(i,j)$is a linear shift-invariant blur of the sampled system, also known as the point-spread function (PSF). The purpose of image restoration can now be specified as the computation of an estimate $\hat{x}(i,j)$ of the original image $x(i,j)$ when $y(i,j)$ is observed. Figure 2.1 gives an overview of the discrete linear degradation model. Many image restoration methods make the use of *a priori* information about the characteristics of the degrading system and the noise. In practical situations, however, it is quite difficult to obtain this information directly from the image formation process. Therefore, in such image restoration methods, the properties of the imperfect imaging system are estimated directly from the observed degraded image itself, prior to the restoration process [8].

Another convenient shorthand notation of eq (2.1.3) is lexicographic representation in which image is scanned row-wise and storing the data in vector from.

$$y = Hx + v \tag{2.1.4}$$

where $\boldsymbol{y}$ and $\boldsymbol{x}$ are the lexicographically ordered vectors of size $MN \times 1$. If a circular convolution is assumed in the eq (2.1.4), the blurring matrix $\boldsymbol{H}$ becomes block circulant structure. The advantage of having the circular convolution in the above equation is that the eigenvalues and vectors of $\boldsymbol{H}$ can be computed easily and are, in fact, given by the coefficients of the discrete Fourier transform of $h(i,j)$ and the discrete Fourier basis functions, respectively. Therefore, the frequency domain model of degradation process is:

$$Y(w_1, w_2) = H(w_1, w_2) X(w_1, w_2) + V(w_1, w_2) \tag{2.1.5}$$

where w_1 and w_2 are the discrete vertical and horizontal frequency variables.

2.2 Blur Models

The blurring of images is modeled as the convolution of an ideal image with point-spread function (PSF), $h(i,j)$, as given in eq (2.1.3). It is worth noting that point-spread functions are assumed to be space-invariant which means that the image is blurred in exactly the same way at every spatial location. Point-spread functions, that do not follow this assumption are known as space-variant blurs, like rotational blurs (turning wheels) and local blurs (a person out of focus while the background is in focus). The modeling, restoration and identification of images degraded by spatially varying blurs is actually still a largely unsolved problem [12].

As the identification and restoration algorithms are always based on spatially discrete images, therefore, we present the blur models in their continuous forms, followed by their discrete (sampled) counterparts. It is also assumed that the sampling rate of the

images has been chosen high enough to minimize the (aliasing) errors involved in going from the continuous to discrete models.

The spatially continuous PSF $h(i,j)$ of any blur satisfies three constraints, namely non-negativity of PSF, real valued property of the PSF and conservation of energy of the degraded image. Therefore, $h(r,s)$ takes on non-negative values only because of the physics of the underlying image formation process. As we are dealing with real-valued images therefore the point-spread function $h(i,j)$ also should be a real-valued function. The imperfections in the image formation process should not absorb or generate "energy". Consequently, for spatially continuous blurs, the PSF is constrained to satisfy

$$\int_{-\infty}^{\infty}\int_{-\infty}^{\infty} h(r,s)drds = 1, \tag{2.2.1}$$

and for spatially discrete blurs:

$$\sum_{i=0}^{N-1}\sum_{j=0}^{M-1} h(i,j) = 1 \tag{2.2.2}$$

In the following, we will present five common point-spread functions (PSF), which are encountered regularly in practical situations of interest,

2.2.1 No Blur

In case the recorded image is imaged perfectly, no blur will be apparent in the discrete image. The spatially continuous PSF can then be modeled as a Dirac delta function:

$$h(r,s) = \delta(r,s) \tag{2.2.3}$$

and the spatially discrete PSF as a unit pulse:

$$h(i,j) = \delta(i,j) = \begin{cases} 1 & \text{if } (i = j = 0) \\ 0 & \text{elsewhere} \end{cases} \tag{2.2.4}$$

The eq (2.2.4) shows that the image will have no blur as long as the amount of "spreading" in the continuous image is smaller than the sampling grid applied to obtain the discrete image.

2.2.2 Linear Motion Blur

Linear motion blur is a commonly observed blur which is found in the images having relative motion between the recording device and the scene. This can be in the form of a translation, a rotation, a sudden change of scale, or some combinations of these. The most important case of a motion blur is global translation, in which the scene to be recorded translates relative to the camera at a constant velocity, $v_{relative}$, and an angle of ϕ radians with the horizontal axis during the exposure interval $[0,t_{exposure}]$. The blurring effect, caused by such distortion, will be in one-dimension and treated as linear motion blurring. Since the "length of motion" can be defined as $L = v_{relative}\ t_{exposure}$, therefore, PSF may be given by [13]:

$$h(r,s,L,\phi) = \begin{cases} \dfrac{1}{L} & \text{if } \sqrt{r^2+s^2} \le \dfrac{L}{2} \text{ and } \dfrac{r}{s} = -\tan(\phi) \\ 0 & \text{elsewhere} \end{cases} \tag{2.2.5}$$

The discrete version of the eq (2.2.5), can only be obtained in a close form expression, if linear motion blur is assumed along the horizontal axis i.e., $\phi = 0$. Therefore,

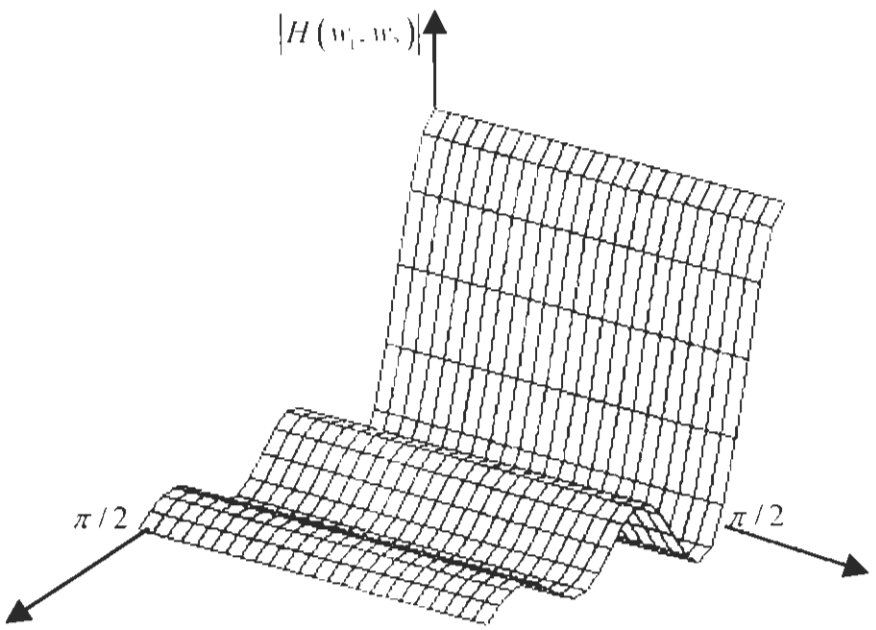

Figure 2.2 PSF of motion blur in the Fourier domain $|H(w_1, w_2)|$ for $L=25$ and $\phi=0$.

$$h(i,j;L)=\begin{cases}\dfrac{1}{L} & if\ \mathrm{i}=0, |\mathrm{j}| \le \left|\dfrac{L-1}{2}\right| \\ \dfrac{1}{2L}\left\{(L-1)-2\left\lfloor\dfrac{L-1}{2}\right\rfloor\right\} & if\ \mathrm{i}=0, |\mathrm{j}| = \left|\dfrac{L-1}{2}\right| \\ 0 & \text{elsewhere}\end{cases} \qquad (2.2.6)$$

Figure 2.2, shows the modulus of the Fourier transform of the PSF of motion blur with $L=25$ and $\phi=0$. This figure illustrates that the blur is effectively a horizontal low-pass filtering operation and that the blur has spectral zeros along characteristic lines.

2.2.3 Uniform Out-of-Focus Blur

A 3-D scene is imaged by a camera onto a 2-D imaging plane. Some parts of the scene are in focus while other parts are not. If the aperture of the camera is circular, the image of any point source is a small disk, known as the circle of confusion. The degree of

defocus depends on the focal length ζ and the aperture number of the lens η, and the distance between camera and object is s. However, if the degree of defocusing is large relative to the wavelengths considered, a geometrical approach can be followed resulting in a uniform intensity distribution within the circle of confusion [14]. The spatially continuous PSF of this uniform out-of-focus blur with radius R is given by:

$$h(r,s,R)=\begin{cases}\dfrac{1}{\pi R^2} & \text{if } \sqrt{r^2+s^2}\le R^2\\ 0 & \text{elsewhere}\end{cases} \tag{2.2.7}$$

Also for this PSF the discrete version $h(i,j)$ is not easily arrived at. A coarse approximation is the following spatially discrete PSF [14]:

$$h(i,j,R)=\begin{cases}\dfrac{1}{C} & \text{if } \sqrt{i^2+j^2}\le R^2\\ 0 & \text{elsewhere}\end{cases} \tag{2.2.8}$$

where C is a constant that must be chosen so that the above equation is satisfied. Again a low pass behavior can be observed (in this case both horizontally and vertically), as well as a characteristic pattern of spectral zeros as shown in Figure 2.3.

2.2.4 Atmospheric Turbulence Blur

Atmospheric turbulence is a severe limitation in remote sensing. Although the blur introduced by atmospheric turbulence depends on a variety of factors (such as temperature, wind speed, exposure time), for long-term exposures the point-spread function can be described reasonably well by a Gaussian function [15]:

$$h(r,s,\sigma_G)=C\exp\left(-\frac{r^2+s^2}{2\sigma_G^2}\right) \tag{2.2.9}$$

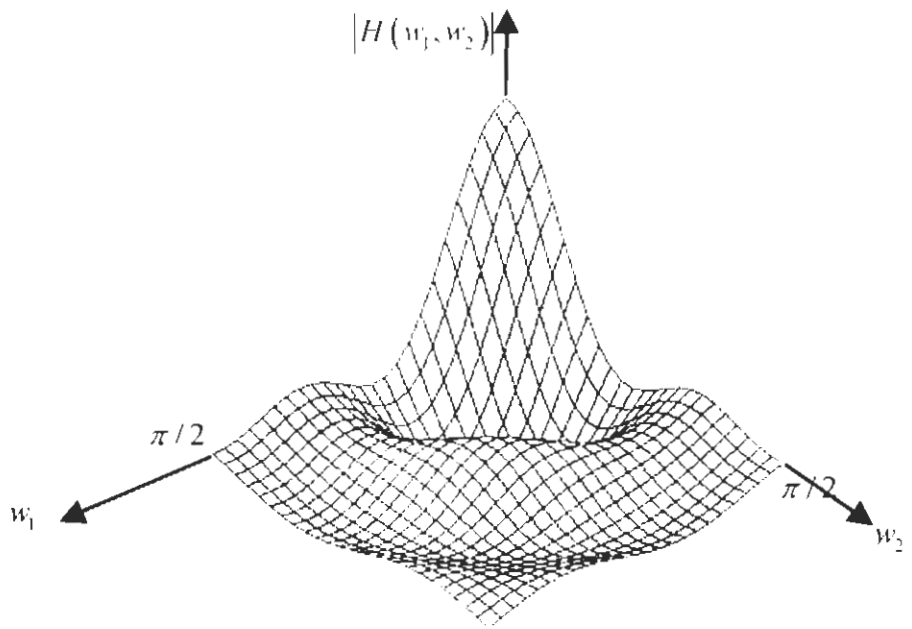

Figure 2.3 PSF of out of focus blur in the Fourier domain $|H(w_1, w_2)|$, for $R=2.5$

where σ_b determines the amount of spread of the blur, and C is a constant. The PSF given in eq (2.2.9) is separable in horizontal and vertical components. Therefore, its discrete version is obtained by first computing a 1-D discrete Gaussian PSF $\tilde{h}(i)$, which is found by a numerical discretization of the continuous PSF. For each PSF element $\tilde{h}(i)$, the 1-D continuous PSF is integrated over the area covered by the 1-D sampling grid, namely $\left[i-\frac{1}{2}, i+\frac{1}{2}\right]$:

$$\tilde{h}(i, \sigma_b) = C \int_{i-\frac{1}{2}}^{i+\frac{1}{2}} \exp\left(-\frac{x^2}{2\sigma_b^2}\right) dx \qquad (2.2.10)$$

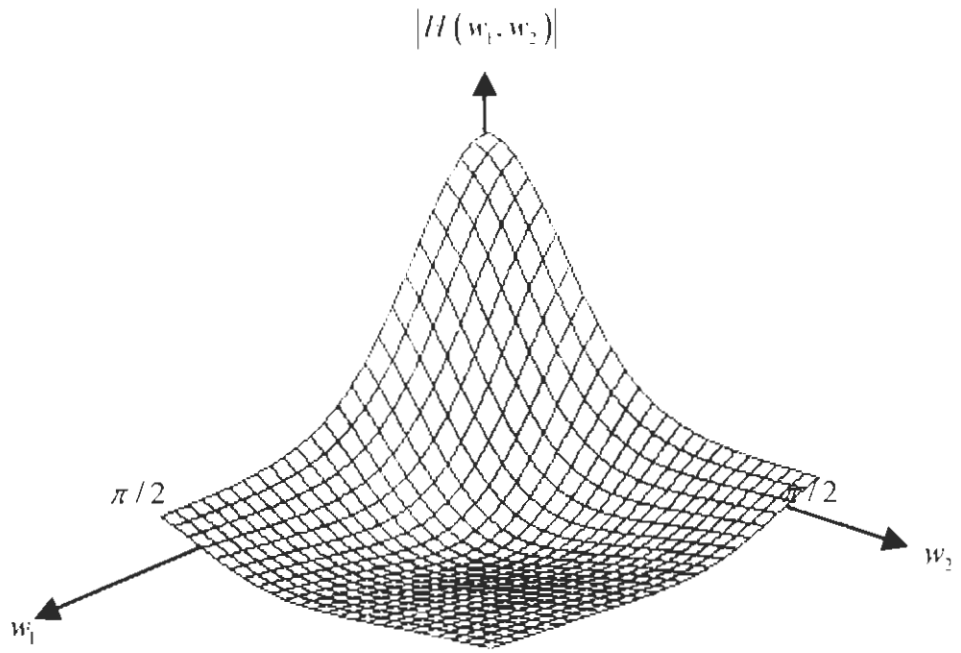

Figure 2.4 Gaussian PSF in the Fourier domain (σ_G=5.2).

Since the spatially continuous PSF does not have a finite support, it has to be truncated properly. The spatially discrete approximation is then given by:

$$h(i, j, \sigma_{t_i}) = \tilde{h}(i, \sigma_{t_i})\tilde{h}'(j, \sigma_{t_i}) \qquad (2.2.11)$$

Figure 2.4 shows this PSF in the spectral domain (σ_G=5.2). It has been observed that Gaussian blurs did not have exact spectral zeros.

2.2.5 Scatter Blur

The X-ray images show detail of different parts due to the varying amount of radiation, which is absorbed by the different parts, being radiated. Unfortunately, the X-ray quanta are scattered from their incident paths, resulting in a distribution of radiation about a point. Although there are many factors which influence the PSF resulting from this scatter,

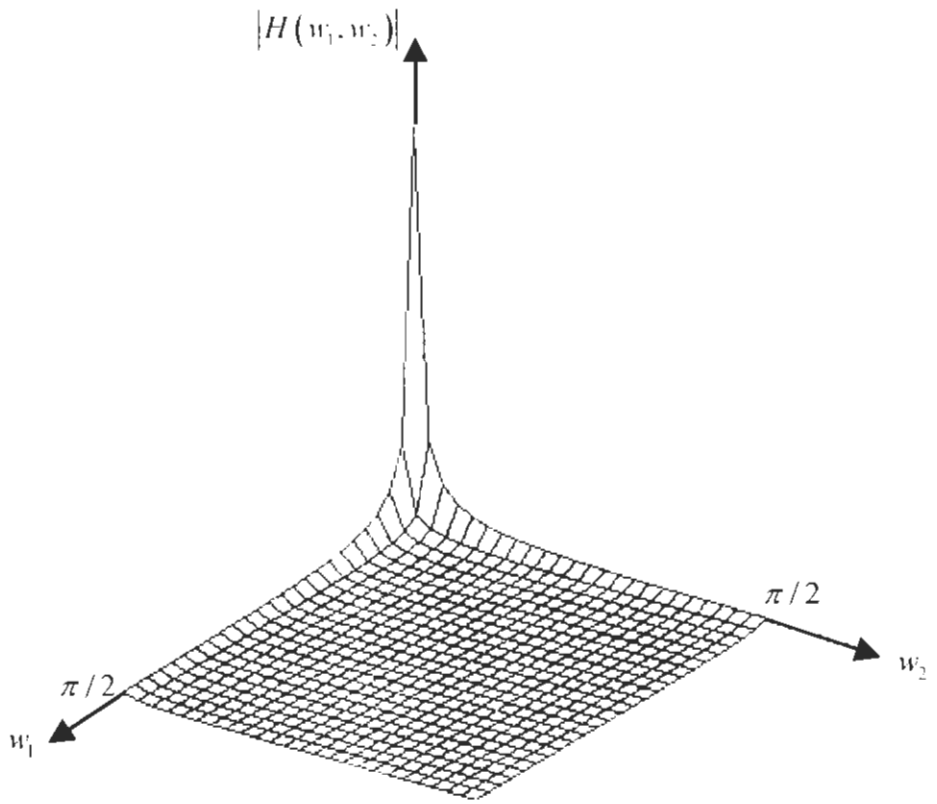

Figure 2.5 X-ray Scatter PSF in the Fourier domain (β=0.02).

but within diagnostic energy ranges the PSF may be described sufficiently accurately by the following radially symmetric PSF [16]:

$$h(r,s;\beta) = \frac{C}{\left(\beta^2 + \left(r^2 + s^2\right)\right)^{\frac{3}{2}}} \qquad (2.2.12)$$

Here β determines the severity of the blur, and is a function of the distance between the radiated object and the detector. Figure 2.5 shows the PSF of scatter blur in Fourier transform.

2.3 Types of Noises in Images

Noise is defined as the unwanted component of the image and may be additive or multiplicative in nature [17]. The noise which is assumed to be additive can be modeled as

$$y(i,j) = x(i,j) + v(i,j) \tag{2.3.1}$$

where $x(i,j)$ is a desired image component and $v(i,j)$ is the additive noise component of the image. Similarly, the multiplicative noises are represented as

$$y(i,j) = x(i,j).v(i,j) \tag{2.3.2}$$

The different types of noises in an image are Gaussian noise, heavy-tailed noise, salt and pepper noise, quantization and uniform noise and photographic noise.

2.3.1 Gaussian Noise

Probably the most frequently occurring noise is additive Gaussian noise. It is widely used to model thermal noise and, under some reasonable conditions, is the limiting behavior of other noises, e.g., photon counting noise and film grain noise. The density function of univariate Gaussian noise, v, with mean μ and variance σ^2 is

$$p_v(r) = \left(2\pi\sigma^2\right)^{-\frac{1}{2}} e^{-(r-\mu)^2/2\sigma^2} \tag{2.3.3}$$

for $-\infty < r < \infty$. Notice that r is infinite in both the positive and negative directions, therefore $p_v(r)$ also is nonzero for negative values of r.

The most significant property of the Gaussian distribution is called the Central Limit Theorem, which states that the distribution of a sum of a large number of independent, small

random variables has a Gaussian distribution. Note the individual random variables do not have to have a Gaussian distribution themselves, nor do they even have to have the similar distribution, [18][19].

2.3.2 Heavy-Tailed Noises

In many situations, the conditions of the Central Limit Theorem are not quite true as defined in Gaussian noise because of the lack of enough number of terms in the sum or it may also be due to insufficiently independent terms [20]. However, the noise may have the approximately Gaussian center of the density but not the tails. Therefore, such types of noises are treated as heavy tailed. "Heavy tails" means that the density $p_v(r)$ approaches to zero more slowly than the Gaussian for large values of r.

2.3.3 Salt and Pepper Noise

Salt and pepper noise is due to the occurrence of wide variety of processes that result in some basic image degradation in which only a few pixels are noisy, but they are very noisy. The effect is similar to sprinkling white and black dots (like - salt and pepper -) on an image [21]. Such noise may be removed by using simple mean or median filtering techniques.

2.3.4 Quantization and Uniform Noise

Quantization noise results when a continuous random variable is converted to a discrete one or when a discrete random variable is converted to one with fewer levels. In images, quantization noise often occurs in the acquisition process. When a continuous image is acquainted through a sensor and then converted into a digital representation. This

conversion requires two steps sampling and quantization. The quantization tries to quantize colors inside the image and assign each quantized level a binary number. The process introduces noise in the image, which is usually modeled as uniform.

2.3.5 Photographic Grain Noise

Photographic grain noise is a characteristic of photographic films. It limits the effective magnification if one can obtain a digital image from a photograph. A photographic film is made up from millions of tiny grains. Two important reasons of such a noise are that the grains are uniform in size, and that the probability that a grain changes, is proportional to the number of photons incident upon it.

2.4 Image Restoration Methods

There are two main approaches to the image restoration:

1. The PSF function is assumed to be known, and image restoration methods have been developed to restore the image. Such methods are known as ***Classical Methods for image restoration***. Although these methods are simple but in practical situations such PSF's are either not available or practically impossible to estimate at the time of capturing the images.

2. In the second approach, PSF and true image is estimated from the degraded image characteristics and partial information available about the imaging system. Such types of image restorations are known as ***blind image restoration***. There are two main types of the techniques used for blind image restoration.

a. Identifying the PSF separately from the true image, in order to use it later with one of the classical image restoration methods, which require *a priori* knowledge of PSF before attempting to restore the image. Therefore, estimation of PSF and the true image are disjoint procedures. This approach leads to computationally simple algorithms.

b. Incorporating the identification procedure with the restoration methods. This merger involves simultaneously estimating the PSF and the true image, using the statistics of the blurred image only. Such a problem is more difficult than the previous one and requires computationally complex algorithms, which are recently emerging in the literature. Therefore, such methods are known as ***Emergent Methods***. There are emergent blind image restoration methods in which perception motivated cost functions are used in order to have better image restoration, and are known as ***perception based methods.***

2.4.1 Classical Techniques

In classical image restoration techniques, it is assumed that the PSF of the blur is satisfactorily known and a number of methods are introduced, for removing the blur from the recorded image $x(i,j)$ using a linear filter. If the point-spread function of the linear restoration filter, denoted by $d(i,j)$, has been designed, the restored image is given by

$$\begin{aligned}\hat{x}(i,j) &= d(i,j) * y(i,j) \\ &= \sum_{k=0}^{N-1}\sum_{l=0}^{M-1} d(k,l)\, y(i-k, j-l)\end{aligned} \tag{2.4.1}$$

or in the spectral domain by

$$\hat{X}(w_1, w_2) = D(w_1, w_2) Y(w_1, w_2) \tag{2.4.2}$$

The objective of this section is to explore appropriate restoration filters $d(i, j)$ or $D(w_1, w_2)$ for use in above two equations. Therefore, there are two types of classical techniques - one that use Fourier transform and the second one that use algebraic equations.

2.4.1.1 Transform Related Techniques

In transform related techniques, the image is restored in the frequency domain where the problem of image restoration becomes simple because the convolution in time domain is converted into multiplication in the frequency domain.

a) Inverse Filter

An inverse filter is a linear filter whose point-spread function $h_{inv}(i, j)$ is the inverse of the blurring function $h(i, j)$ in the sense that:

$$h_{inv}(i, j) * h(i, j) = \sum_{k=0}^{N-1} \sum_{l=0}^{M-1} h_{inv}(k, l) * h(i-k, j-l) = \delta(i.j) \tag{2.4.3}$$

The inverse filters seem difficult to design according to eq (2.4.3). However, the spectral counterpart of eq (2.4.3) immediately shows the solution to this design problem [1]:

$$H_{inv}(w_1, w_2) H(w_1, w_2) = 1 \quad \Rightarrow \quad H_{inv}(w_1, w_2) = \frac{1}{H(w_1, w_2)} \tag{2.4.4}$$

The inverse filter requires PSF of blur as *a priori* knowledge, and it allows for perfect restoration if noise is absent. However, if noise is present then restoration process becomes:

$$\hat{X}(w_1, w_2) = H_{inv}(w_1, w_2) Y(w_1, w_2) = \frac{1}{H(w_1, w_2)} \{H(w_1, w_2) X(w_1, w_2) + V(w_1, w_2)\}$$
$$= X(w_1, w_2) + \frac{V(w_1, w_2)}{H(w_1, w_2)} \quad (2.4.5)$$

If the noise is absent, the second term in eq (2.4.5) disappears so that the restored image is identical to the ideal image. Unfortunately, several problems exist with eq (2.4.5). One of the major problem is that $H(w_1, w_2)$ is zero at certain selected frequencies(w_1, w_2), in case of linear motion blur and the out-of-focus blur. Second major problem is that even if the blurring function's spectral representation $H(w_1, w_2)$ does not actually become zero but becomes small, the second term in eq (2.4.5), known as the inverse filtered noise will become very large. Therefore, inverse filtered images are often dominated by excessively amplified noise.

b) Least-Squares Filters

To overcome the noise sensitivity of the inverse filter, a number of restoration filters have been developed that are collectively called least-squares filters. We describe the two most commonly used filters, namely the Wiener filter and the constrained least-squares filter.

i) Wiener Filter

The Wiener filter is a linear spatially invariant filter of the form given in eq (2.4.1), in which the point spread function $d(i, j)$ is chosen such that it minimizes the mean-squared error (MSE) between the ideal and the restored image. This criterion attempts to minimize the difference between the ideal image and the restored:

$$MSE = E\left[\left(x(i,j)-\hat{x}(i,j)\right)^2\right] \approx \sum_{i=0}^{N-1}\sum_{j=0}^{M-1}\left(x(i,j)-\hat{x}(i,j)\right)^2 \qquad (2.4.6)$$

The solution of this minimization problem is known as the Wiener filters, and is defined easily in the spectral domain:

$$D_{wiener}(w_1,w_2) = \frac{H^*(w_1,w_2)}{H^*(w_1,w_2)H(w_1,w_2) + \dfrac{S_v(w_1,w_2)}{S_x(w_1,w_2)}} \qquad (2.4.7)$$

where $H^*(w_1,w_2)$ is the complex conjugate of $H(w_1,w_2)$. $S_x(w_1,w_2)$ and $S_v(w_1,w_2)$ are the power spectrum of the ideal image and the noise, respectively. The power spectrum is a measure of the average signal power per spatial frequency (w_1,w_2) carried by the image. In the noiseless cases, the Wiener filter approximates to inverse filter given in eq (2.4.4).

When the recorded image is noisy, the Wiener filter trades-off restoration by inverse filtering and suppression of noise for those frequencies where $H(w_1,w_2) \to 0$. However, if we assume that the noise is uncorrelated, i.e. white noise, then $S_v(w_1,w_2) = \sigma_v^2$. Small values of σ_v^2 will yield a result close to the inverse filter, while large values will over-smooth the restored image. The estimation of $S_x(w_1,w_2)$ is somewhat more problematic. However, one can replace $S_x(w_1,w_2)$ by an estimate of the power spectrum of the blurred image $S_y(w_1,w_2)$ and compensate for the variance of the noise σ_v^2 [1]:

$$S_x(w_1,w_2) \approx S_y(w_1,w_2) - \sigma_v^2 \qquad (2.4.8)$$

In this approach, little *a priori* knowledge is required. Typical artifacts of the Wiener restoration are the residual blur in the image and the "ringing" or "halo" artifacts present near edges in the restored image.

ii) Constrained Least-Squares filter

The constrained least-squares filter [23] is another approach, for overcoming some of the difficulties of the inverse filter and of the Wiener filter, while still retaining the simplicity of a spatially invariant linear filter. If the restoration is a good one, the blurred version of the restored image should be approximately equal to the recorded distorted image, i.e. $h(i,j)*\hat{x}(i,j) \approx y(i,j)$. Therefore, a more reasonable expectation for the restored image is that it has to satisfy the following equation:

$$\left\| y(i,j) - h(i,j)*\hat{x}(i,j) \right\|^2 = \sum_{k=0}^{N-1}\sum_{l=0}^{M-1}\left(y(k,l) - h(k,l)*\hat{x}(k,l) \right)^2 \approx \sigma_v^2 \qquad (2.4.9)$$

There are potentially many solutions that satisfy the above relation. Therefore, a commonly used second criterion is to select the solution that is as "smooth" as possible. This is due to the fact that the inverse filter tends to amplify the noise $v(i,j)$, The solution to the above minimization problem is the constrained least-squares filter $D_{cls}(w_1, w_2)$ which can easily formulated in the discrete Fourier domain as:

$$D_{cls}(w_1, w_2) = \frac{H^*(w_1, w_2)}{H^*(w_1, w_2)H(w_1, w_2) + \alpha C^*(w_1, w_2)C(w_1, w_2)} \qquad (2.4.10)$$

Here α is a tuning or regularization parameter and C is frequency domain representation of second order derivative, also known as Laplacian operator. A 2-D discrete approximation of the Laplacian operator in spatial domain is given as:

	-1	
-1	4	-1
	-1	

It should be noted that although the motivations of Weiner filter and constrained least squares filter are quite different but their formulations are quite similar. Indeed these filters perform equally well, and they behave similarly in the case that the variance of the noise σ_v^2, approaches zero. A vast amount of literature exists on the usage of more complicated image models, especially the ones inspired by 2-D auto-regressive processes [24] and the Markov random field theory [25].

c) Homomorphic Filter Restoration

Homomorphic image restoration is based on the illumination-reflectance image model. This model represents an image in terms of its illumination and reflectance components by means of relation

$$y(i,j) = i_o(i,j)r_o(i,j) \tag{2.4.11}$$

where $i_o(i,j)$ and $r_o(i,j)$ in eq (2.4.11) represents illumination and reflectance components, respectively. The illumination component is generally characterized by slow spatial variations, while the reflectance component tends to vary abruptly, particularly at the junctions of dissimilar objects [2]. Therefore, low frequencies of the Fourier transform of the logarithm of an image can be associated with illumination and the high frequencies with reflectance. A good deal of control can be gained over the illumination and reflectance components with harmonic filter. This control requires specifications of a filter function

$H(w_1, w_2)$ that affects the low and high frequency components of the Fourier transform in different ways [26].

There are three major drawbacks of homomorphic filters [2]; firstly the associations between image components and frequencies are rough approximations. Secondly, the method can only be used where non-uniform illumination of the source and blurring are the major issues like in X-ray images. Thirdly, the implementation of homomorphic filters becomes unwieldy when dealing with large images.

2.4.1.2 Spatial Domain Techniques

Spatial domain techniques involve attempting to find a direct solution to the image degradations, without going to the frequency domain.

a) Iterative Filters

Iterative restoration filters are spatial domain filters. They are used, when the dimensions of the image to be restored are very large or additional knowledge is available about the restored image [27], [28], [29]. The basic form of iterative restoration filters is the one that iteratively approaches the solution of the inverse filter, and is given by:

$$\hat{x}_{n+1}(i,j) = \hat{x}_n(i,j) + \beta\left(y(i,j) - h(i,j) * \hat{x}_n(i,j)\right) \qquad (2.4.12)$$

where $\hat{x}_n(i,j)$ is the restoration result after n iterations. Usually in the first iteration $\hat{x}_0(i,j)$ is chosen to be identical to zero or identical to $y(i,j)$. The iterations in eq (2.4.12) are independently run many times, and are referred to as the van Cittert, Bially, or Landweber iterations. Now, during these iterations the blurred version of the current

restoration result $\hat{x}_n(i,j)$ is compared to the recorded image $y(i,j)$. The difference between the two is scaled and added to the current restoration result to give the next restoration result.

The iterative scheme has several advantages like it does not require the convolution of images with 2-D PSF's, containing many coefficients, no Fourier transforms are required, the iterations can be continued indefinitely, and the scheme can be extended to include all types of *a priori* knowledge. On the negative side, the iterative scheme has many disadvantages, like the condition $H(w_1, w_2) > 0$ is not satisfied by many blurs, scheme does not include any knowledge about the spectral behavior of the noise and the ideal image, and its convergence is slow [29].

b) Boundary Value Problem

The blurred images always have finite spatial extent and are obtained by the convolution of the ideal image with the PSF of the blur which may be extended beyond the borders of the observed degraded image. Therefore, a part of the information that is necessary to restore the border pixels is not available to the restoration process. This problem is known as the boundary value problem, and poses a severe problem to restoration filters. Although at first glance, the boundary value problem seems to have a negligible effect because it affects only border pixels, but this is not at all true [30].

The point-spread function of the restoration filter has a very large support, typically as large as the image itself. Consequently, the effect of missing information at the borders of the image propagates throughout the image deteriorating the entire image. Two types of solutions to the boundary value problem are used based on spatial domain and Fourier

domain. In a spatial domain filter, missing image information outside the observed image can be estimated by extrapolating the available image data [30].

2.4.2 Blind Image Restoration

There are two main approaches to blind image deconvolution. In the first approach, the blur is estimated from the degraded image using the available partial information about the image and degrading system. Such methods are known as *a priori* blur identification methods. Then a classical image restoration algorithm is applied on the degraded image to restore the original image. In the second approach blur identification procedure is embedded in the restoration process, in order to identify blur and restore original image simultaneously. These techniques are categorized as Emergent techniques.

2.4.2.1 *A Priori* Blur identification Methods

A priori blur identification methods perform blind deconvolution by identifying the PSF prior to restoration. This general class of techniques makes assumptions on the characteristics of the PSF such as symmetry and availability of a known parametric form of the blur. Based on these assumptions, an attempt is made to completely characterize the PSF using special features of the true/blurred image [31].

Popular parametric models include PSF's resulting from linear camera motion or an out-of-focus lens system which are explained earlier. Once the PSF has been completely identified, one of the classical restoration techniques is used to estimate the true image. A *priori* blur identification techniques are the simplest class of blind deconvolution methods to implement and have low computational requirements. They are applicable to situations in

which the true image is known to possess special features, and/or when the PSF is known to be of a special parametric form.

2.4.2.2 Emergent Techniques

A number of new image restoration methodologies have been developed in recent years to address the problem of blind image restoration. These techniques can estimate the PSF and restore the degraded image, simultaneously, using the statistics of the degraded image only. The emergent techniques are based on different computing tools like neural networks, genetic algorithms and wavelets.

a) Image Restoration using Neural Networks

Motivated by the biological neural network in which the processing lies in a large number of neurons linked with synaptic weights, artificial neural network models attempt to achieve good performance via dense interconnections of simple computational elements. Neural net models have great potential in areas where many hypothesis are pursued in parallel, high computation rates are required, and the current best systems are far from equaling human performance.

Image restoration was first implemented using the Hopfield neural networks for binary images in late 80's. This neural network contained the huge amount of redundant neurons making it computationally heavy for gray scale images [32]. Later, a joint blur identification and image restoration using multilayered neural network based on ARMA model was studied for binary level images [33]. The advantage of the method was low computations and less *a priori* information required for the image restoration and blur identification process. The method has problems of convergence. The method was later

modified for gray level images, as well. Although the technique was fault tolerant but it was computationally complex. It was also difficult to remove the ringing effects and noise in smooth background [34]. The method was then restudied to improve its performance by modifying the upper and lower bounds in the cost function of the neural network [35]. Later a new approach was investigated to consider the effects of the edges in the image by improving the cost function of the neural network [36].

Model based neural networks are also reported for image restoration, in which the weights of a conventional neural network were coupled with small number of parameters [37]. These parameters which include a regularization parameter as well, serve as a basis to make the solution stable and to remove ill-posed nature of the problem. The model based neural network treated the edge and texture regions as equivalent but the noise masking capabilities of these two types of regions are different. Later, new methods were developed to make the regularization parameters adaptive according to the local statistics of the region using fuzzy model-based neural networks and hierarchical neural networks [38][39].

Recently a recursive soft decision approach to blind image deconvolution is reported which contains a modified cost function which consists of data fidelity measure, image and blur domain regularization terms and soft blur estimation error. This cost function is implemented for hierarchical neural networks which contains regularization parameters as well in order to convert the ill posed restoration problem into well posed problem [40].

b) Image Restoration using Wavelets

All the previous adaptive techniques examined the problem in spatial domain, using various local measures to describe the type of activity near a pixel. The use of wavelets for

the task of image enhancement and restoration has been thoroughly studied in recent years from the multiresolution/subband perspective [41][42]. A matrix formulation was studied for wavelet based subband decomposition which allows for the computation of the decomposition of both the signal and the convolution operator in the wavelet domain. Therefore, this approach can be used to restore single channel image with some multichannel image restoration routine [43].

The wavelet concept has also been used with Kalman filtering technique which uses a multiscale Kalman smoothing. The filter is directly applied to the wavelet coefficients of noisy image ordered onto a quadtree structure in order to obtain noisy wavelet coefficients [44]. The wavelet domain approaches provide a useful method for image restoration with preservation of edges in the scene. It is achieved due to the local adaptivity of the wavelet coefficients having details. Although this approach is efficient to implement but still requires reasonable computational complexity [45].

c) Image Restoration using Genetic Algorithms

Genetic algorithms are stochastic search techniques based on natural selection and genetics. GA's differ from conventional optimization techniques in that they are parallel, probabilistic, and use only the objective function. They are superior to gradient descent techniques, which are biased toward local optima. Although no formal proof exists for the convergence of GA's, they are usually able to locate the neighborhood of the optimum quickly. However, they are not well suited for fine tuning of solutions. Furthermore, GA's are difficult to apply to large scale optimization problems because of the large memory requirements [46].

In order to work with GA's a population of individuals is created in which each individual has certain fitness. The particular traits of an individual are encoded in the chromosome, which consists of a string of parameters or genes. All GA's perform three basic operations- selection, crossover, and mutation. From the parent generation, individuals with high fitness are selected for reproduction of next generation. Recombination occurs through crossover and mutation. This process continues till you reach a certain optimization criteria.

Different types of blind deconvolution algorithms are proposed in literature depending upon the use and location of use of GA's. GA's are used in combination with neural networks to find optimized weight of the neural network implemented for image deconvolution. In neural networks the cost function usually has local minima problem. This problem is resolved by the use of GA's that go straight for global minimum [46].

In blind deconvolution of linearly degraded images simulated annealing technique was first proposed by McMallum [47]. If a system is in thermal equilibrium at temperature T, then the probability that the system is in particular configuration is $P(E) = \exp(-E/kT)$, where E is energy of the system and k is Boltzmann's constant. Simulated annealing attempts to reach the minimum energy state through a series of atomic reconfigurations (local perturbations) which are accepted if energy is decreased with probability $P(\Delta E) = \exp(-\Delta E/kT)$ [48][49]. Therefore, such a method is named as simulated annealing genetic algorithms (SAGA). Blind deconvolution of nonlinearly degraded images, using SAGA, has been reported in literature [50].

d) Multichannel Blind Image Restoration

There are many applications of image restoration which are processed as a multichannel nature problem i.e., there are several image planes available called channels with redundant, as well as, complete information. The different channels may correspond to different frequencies, different sensors, or different time frames. Specific applications of multichannel image restoration are carried out where multiple blurred and noisy copies of the same scene are available. Multichannel blind deconvolution of images is much more complicated problem than single channel images, due to the higher dimensionality of the problem along with other problems [51][52]. However, relevant information present in a given channel can be taken into account when processing the others, providing therefore, more accurate restoration results. In order to effectively deconvolve the observed image, this joint processing of the different channels is particularly essential when cross-channel blurring is present. However, even in the absence of cross-channel blurring, more precise restorations can be obtained by combining information from the various channels [53] [54].

Various approaches for the restoration of noisy and blurred multichannel images are reported using Wiener filtering [55][56], set theoretic and constrained least squares [57][58], Bayesian methods [59][60][61] and Total Variation methods [62].

e) ARMA Parameter Estimation Methods

Blind deconvolution using ARMA parameter estimation is a technique which involves modeling the true image as a two-dimensional autoregressive (AR) process and the PSF as a two-dimensional moving average (MA) process. Therefore, the resulting blurred image is represented as an autoregressive moving average (ARMA) process.

The true image is modeled as a two-dimensional autoregressive (AR) process represented by:

$$x(i,j) = \sum_{k,l \in S_a} a_{kl} x(i-k, j-l) + v_1(i,j) \qquad (2.4.13)$$

where a_{kl} are the image model coefficients , $x(i,j)$ is the true image, and $v_1(i,j)$ is the zero-mean homogeneous noise process with covariance matrix which is statistically independent of $x(i,j)$. The AR model coefficients a_{kl} of support, S_a, are chosen to minimize the variance of $v_1(i,j)$ denoted by $\sigma_{v_1}^2$ [63]. The model of the true image is valid in applications such as photography where the true images are generally smooth and homogeneous [64]. The model is also appropriate for texture images, but model order selection is required to estimate the number of AR coefficients. The AR model is not valid for situations in which the true image has abrupt changes in local image characteristics, such as for edges.

In most practical situations, the PSF is of finite extent and its effect on the true image can be modeled as that of a two-dimensional FIR filter. From the linear degradation model of eq (2.1.3), the degraded image $y(i,j)$ can be expressed as:

$$y(i,j) = \sum_{m,n \in S_h} h_{m,n} x(i-m, j-n) + v_2(i,j) \qquad (2.4.14)$$

where S_h is the finite support of the PSF $h_{m,n}$, and $v_2(i,j)$ is the additive noise of the imaging system assumed to be zero-mean Gaussian noise. The identification of ARMA parameters allows us to identify the true image and PSF. The existing methods of this class are generalized cross-validation (GCV) [65], and neural networks [33].

i) The Generalized Cross-Validation Approach

General cross-validation (GCV) is a widely recognized technique in the field of data analysis. It is sometimes known as "leave-one-out" or predictive sample reuse. Historically, it has been used as a criterion for estimating the optimal regularization parameter in smoothing problems. The principle behind GCV is straightforward. The data is divided into two sets - an estimation set and a validation set. The estimation set is used to obtain a model or estimate based on a particular parameter value or assumption. The validation set is then used to validate the performance of the model or estimate and thus the assumption. Therefore, many competing parameter values may be tested to find the most appropriate parameter values. The difficulty with dividing the data into two sets is that it is necessary to use as much of the data as possible to obtain a reliable estimate. At the same time it is also desirable to test the estimate on as much of the data that was excluded from the estimation process as possible. The data is divided into M sets. The assumption being tested is imposed on all the sets but one, and a validation error measure is computed for the omitted set. The process is repeated, selecting a different set each time, until all the sets have been exhausted. The validation error measured for each set is averaged to produce the validation error for the particular parameter value or assumption. Thus, all the data is used for both estimation and validation [66].

Different methods have been proposed to solve the problem of blind image restoration and even computationally simpler algorithm has also been introduced with a slight loss in the quality of restoration [67].

ii) Neural Networks

A joint blur identification and image restoration using multilayered neural network based on ARMA model was studied, where auto-regressive (AR) part determines the image model coefficients and the moving average (MA) part determines the blur function of the system as shown in eqs (2.4.13) and (2.4.14), respectively. The structured neural network was decomposed into two adaptive associative networks. The operation between the first and second layer was auto-associative excited by random Gaussian noise while between second and third layer is hetero-associative. The output of third layer is the estimate of the observed image [33]. The weights can be updated using different methods like gradients method and genetic algorithms or any combination of the two. The cost function or fitness criteria may be taken as the square of the error between the observed and the estimate of the blurred image [64][68]. The output of the second layer was the estimated true image while the weights between second and third layer were the estimate of the blurring function.

Chapter 3

Hybrid Computing Tools – Artificial Neural Networks and Genetic Algorithms

In this chapter we will study two basic computing tools i.e. Artificial Neural Networks and Genetic Algorithms. The combination of these two tools is treated as hybrid computing. The Artificial Neural Networks are physical cellular systems which can acquire, store and utilized experimental knowledge like human brain. The most popular representation of Artificial Neural Networks is Feedforward multilayer perceptron.

3.1 Feedforward Multilayer Perceptron

Standard multilayer feedforward networks contain neurons arranged in layers. The neurons are generally connected to all the neurons in the adjacent layers through uni-directional links called synaptic weights. The first layer in such networks is called input layer and the last layer is called output layer. The intermediate layers are called hidden layers. There is no limit on the number of hidden layers. However, one or two hidden layers are sufficient to solve any problem [70]. Generally, the multilayer perceptron has different number of neurons and different synaptic weights for different layers. Let $u_j^{[s]}$ denote the value of internal potential (signal) of the j^{th} neuron located in the s^{th} layer (s=1,2,3). The weighted sum of the inputs is computed by the neuron according to the formula:

$$u_j^{[s]} = \sum_{i=0}^{n_{s-1}} w_{ji}^{[s]} o_i^{[s-1]} \qquad (3.1.1)$$

$$s = 1,2,3; j = 1,2,...,n_s$$

where $w_{ji}^{[s]}$ are the synaptic weights of j^{th} neuron of s^{th} layer. $o_i^{[s]}$ is the input vector of the s^{th} layer. These inputs can also be represented as $x_i^{[s]} = o_i^{[s-1]}, o^{[0]} = x_i, o_i^{[3]} = y_i$. The number of neurons, in the s^{th} layer, are represented by symbol n_s. The neuron output is computed by passing the weighted sum of its input (i.e. the internal potential $u_j^{[s]}$) by a nonlinear bounded activation function $\psi_j^{[s]}$ as shown in Figure 3.1. This operation can be described as:

$$o_i^{[s]} = \psi_j^{[s]}(u_j^{[s]}) = \psi_j^{[s]}\left[\sum_{i=0}^{n_s-1} w_{j_i}^{[s]} o_i^{[s-1]}\right] \qquad (3.1.2)$$

There are two major classes of optimization algorithms in order to find optimum weights of this network called learning of the neural networks. The first one is Calculus based technique that employs gradient-directed searching mechanism to solve the error surface or differential surface of the objective function. The back-propagation algorithm is based on this technique. The second one is evolutionary computing technique that employs the concept of natural selection i.e., genetic algorithms.

3.1.1 Back-propagation Algorithm

Let us consider a multilayer perceptron of three layers, i.e. input layer, hidden layer and output layer, having n_1, n_2 and n_3 neurons, respectively. The standard back-propagation algorithm uses the steepest descent gradient approach to minimize the mean square error function [71]. Such a local error function for any p^{th} learning example can be written as

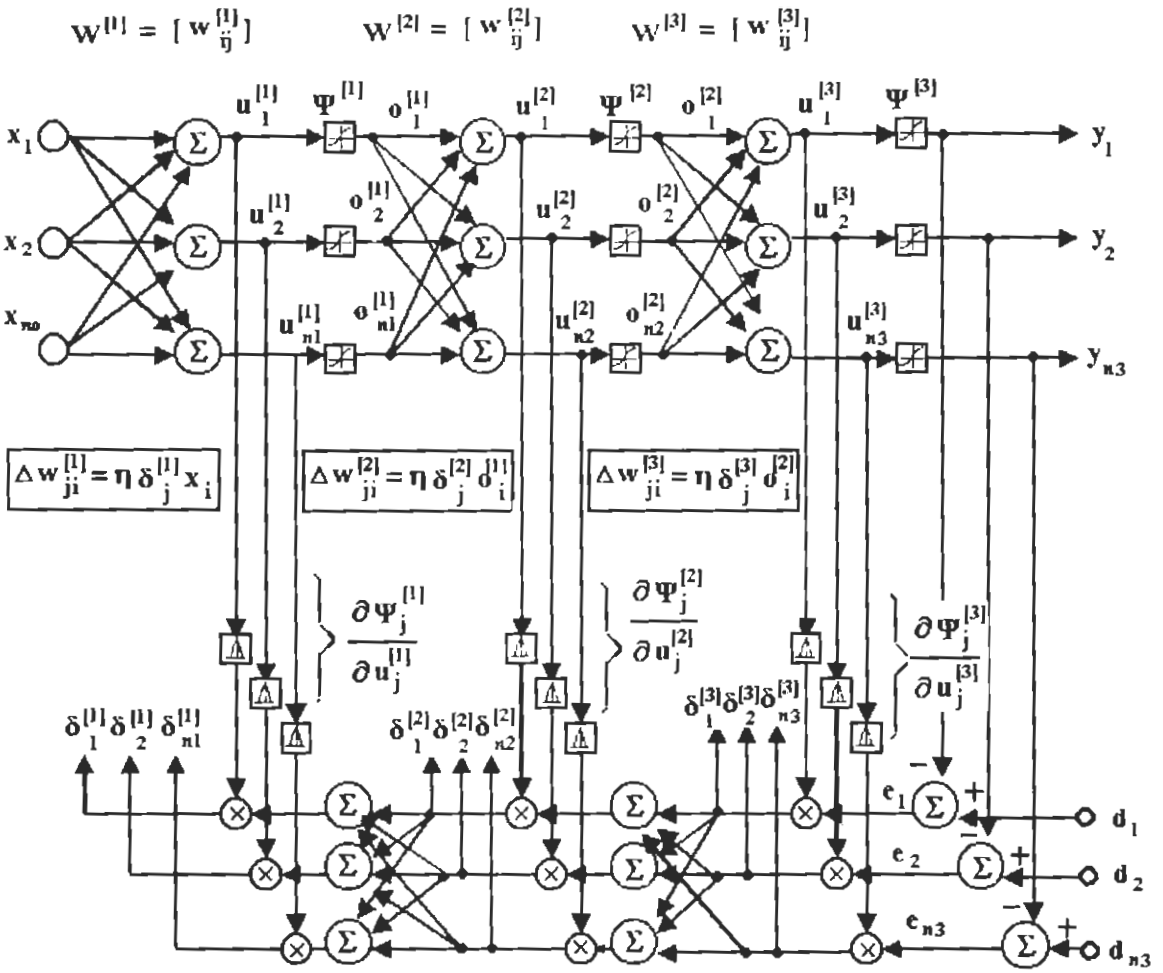

Figure 3.1 Neural network architecture of a three layer perceptron with standard back-propagation algorithm.

$$E_p = \frac{1}{2}\sum_{j-1}^{n3}(d_{jp} - y_{jp})^2 = \frac{1}{2}\sum_{j-1}^{n3} e_{jp}^2 \tag{3.1.3}$$

Now the global error function may be written as

$$E = \sum_p E_p = \frac{1}{2}\sum_p \sum_j (d_{jp} - y_{jp})^2 \tag{3.1.4}$$

Where d_{jp} and y_{jp} are the desired and actual output signals of the j^{th} output neuron for the p^{th} pattern. There are two basic approaches to find the minimum of global error function E. The first techniquc is the on-line or per example learning in which the training patterns are presented sequentially, usually in random order. The second approach is batch learning in which total error function E is minimized in such a way that the weight changes are accumulated over all learning examples before the weights are actually changed.

Now here we will discuss the on-line learning approach in which the gradient search in the synaptic weight space is carried out on the basis of a local error function E_p which can be written as:

$$\Delta w_{ji}^{[s]} = -\eta \frac{\partial E_p}{\partial w_{ji}^{[s]}} \tag{3.1.5}$$

First determine an updating formula for the synaptic weights $w_{ji}^{[s]}$ for $(s = 3)$ of the output layer. Using the chain rule for eq (3.1.5), we can write

$$\Delta w_{ji}^{[3]} = -\eta \frac{\partial E_p}{\partial w_{ji}^{[3]}} = -\eta \frac{\partial E_p}{\partial u_j^{[3]}} \frac{\partial u_j^{[3]}}{\partial w_{ji}^{[3]}} \tag{3.1.6}$$

where $u_j^{[3]}$ can be written as

$$u_j^{[3]} = \sum_{i=1}^{n3} w_{ji}^{[3]} x_i^{[3]} = \sum_{i=1}^{n3} w_{ji}^{[3]} o_i^{[2]} \tag{3.1.7}$$

and local error, called delta $\delta_j^{[3]}$ is defined as

$$\delta_j^{[3]} = \frac{\partial E_p}{\partial u_j^{[3]}} = \frac{\partial E_p}{\partial e_{jp}} \frac{\partial e_{jp}}{\partial u_j^{[3]}} = e_{jp} \frac{\partial \psi_j^{[3]}}{\partial u_j^{[3]}} \tag{3.1.8}$$

We obtained a general formula for updating the weights in the output layer as

$$\Delta w_{ji}^{[3]} = \eta \delta_j^{[3]} x_i^{[3]} = \eta \delta_j^{[3]} o_i^{[2]} \tag{3.1.9}$$

where

$$\delta_j^{[3]} = e_{jp} (\psi_j^{[3]})' = (d_{jp} - y_{jp}) \frac{\partial \psi_j^{[3]}}{\partial u_j^{[3]}} \tag{3.1.10}$$

Updating the synaptic weights in the hidden layers is a little more complicated. For the second hidden layer we can still write

$$\Delta w_{ji}^{[2]} = -\eta \frac{\partial E_p}{\partial w_{ji}^{[2]}} = -\eta \frac{\partial E_p}{\partial u_j^{[2]}} = \eta \delta_{j^{[2]}} x_i^{[2]} = \eta \delta_j^{[2]} o_i^{[1]} \tag{3.1.11}$$

where this local error cannot be directly evaluated as is done for the local errors in the output layer. Using the chain rule we can write

$$\delta_j^{[2]} = -\frac{\partial E_p}{\partial u_j^{[2]}} (j = 1, 2, 3..., n_2) \tag{3.1.12}$$

However, this local error cannot be directly evaluated as is done for the local errors in the output layer. Using the chain rule we can write

$$\delta_j^{[2]} = -\frac{\partial E_p}{\partial u_j^{[2]}} = -\frac{\partial E_p}{\partial o_j^{[2]}} \frac{\partial o_j^{[2]}}{\partial u_j^{[2]}} \tag{3.1.13}$$

As we know that

$$\delta_j^{[2]} = \psi_j^{[2]}(u_j^{[2]}) \tag{3.1.14}$$

we have

$$\delta_j^{[2]} = -\frac{\partial E_p}{\partial o_j^{[2]}} \frac{\partial \psi^{[2]}}{\partial u_j^{[2]}} \tag{3.1.15}$$

The factor $-\frac{\partial E_p}{\partial o_j^{[2]}}$ can be evaluated as

$$-\frac{\partial E_p}{\partial o_j^{[2]}} = \sum_{i-1}^{n3} \delta_j^{[3]} \frac{\partial}{\partial o_j^{[2]}} \left[\sum_{i=1}^{n3} w_{ik}^{[3]} o_k^{[2]} \right] = \sum_{i-1}^{n3} \delta_j^{[3]} w_{ij}^{[3]} \tag{3.1.16}$$

The local error in the second layer can be evaluated as

$$\delta_j^{[2]} = \frac{\partial \Psi^{[2]}}{\partial u_j^{[2]}} \sum_{i-1}^{n3} \delta_i^{[3]} w_{ij}^{[3]} \tag{3.1.17}$$

Analogously,

$$\Delta w_{ji}^{[1]} = \eta \delta_j^{[1]} x_i^{[1]} = \eta \delta_j^{[1]} o_i^{[0]} = \eta \delta_j^{[1]} x_i \tag{3.1.18}$$

The basic back-propagation algorithm can be performed by realizing the following steps:

1. Initialize all synaptic weights $w_{ij}^{[s]}$ to small random values.

2. Present input for the class of learning examples and calculate the actual output of all neurons using the present values of $w_{ij}^{[s]}$ and the pattern.

3. Specify the desired output and evaluate the local errors $\delta_i^{[s]}$ for all layers.

4. Adjust the synaptic weights according to the iterative formula given in eq (3.1.18), i.e.,

$$\Delta w_{ji}^{[s]} = \eta \delta_j^{[s]} x_i^{[s]} \tag{3.1.19}$$

5. Present another input pattern corresponding to the next learning example and go back to step 2.

All the training examples are presented cyclically until the synaptic weights are stabilized, i.e. until the error of the entire set is acceptably low and the network converges. The behavior of the network is also explained in Figure, 3.1. After training a multilayer perceptron usually has the feature of generalization, i.e. it has the ability for proper response to input patterns not presented during the learning process.

3.1.2 Extended Back-Propagation Algorithm

This learning algorithm has some drawbacks. First learning parameter η should be chosen small to provide minimization of the total error function E. For a small η the learning process becomes very slow. On the other hand, large values of η correspond to rapid learning, but lead to parasitic oscillation which prevent the algorithm from converging to desired solution. Moreover, if the error function contains many local minima, the network might get trapped in some local minima, or get stuck on very flat plateau. A simple way to improve the standard back-propagation learning algorithm is to smooth the weight changes by adding the momentum term

$$\Delta w_{ji}^{[s]}(k) = \eta \delta_j^{[s]} o_i^{[s-1]} + a \Delta w_{ji}^{[s]}(k-1), \qquad (3.1.20)$$

where

$$\eta > 0, \qquad 0 \le a < 1, \qquad \text{and } s = 1, 2, 3$$

The type of the neural network presented in this dissertation is extended form of feedforward neural network with back-propagation algorithm. The main difference is in the connection weights. In standard multilayer feedforward network one neuron is connected to all the input neurons but the neurons in neural network used for image restoration are connected to the adjacent neurons. The second major difference lies in their cost functions.

3.2 Genetic Algorithms

Genetic algorithms provide a mechanism that mimics the process observed in natural evolution and is known as the GA. This technique of optimization is similar to its associated algorithms: simulated annealing, evolutionary strategies, and evolutionary programming, which are classified as guided random techniques [72][73]. The GA operates as an entirely different optimization procedure and provides further flexibility and robustness that are unique for neural networks. Because of its simple implementation procedure, the GA can be used as an optimization tool for designing neural network-hybrid systems for real-world applications. Therefore, the potential use of the GA in neural networks is immeasurably wide.

The GA is a searching process based on the laws of natural selection and genetics. Usually, a simple GA consists of three operations: selection, cross-over, mutation and replacement. The population comprises a group of chromosomes from which candidates can

be selected for the solution of a problem. Initially, a population is generated randomly. The fitness values of the all chromosomes are evaluated by calculating the objective function in a decoded form (phenotype). A particular group of chromosomes (parents) is selected from the population to generate the offspring by the defined genetic operations. The fitness of the offspring is evaluated in a similar fashion to their parents. The chromosomes in the current population are then replaced by their offspring, based on a certain replacement strategy. Such a GA cycle is repeated until a desired termination criterion is reached (for example, a predefined number of generations is produced). If all goes well throughout this process of simulated evolution, the best chromosome in the final population can become a highly evolved solution to the problem.

3.2.1 Encoding Scheme

The encoding scheme is a key issue in any GA because it can severely limit the window of information that is observed from the system. To enhance the performance of the algorithm, a chromosome representation that stores problem specific information is desired. In general, the GA evolves a multiset of chromosomes. It should be noted that each chromosome should represent a trial solution to the problem setting. The chromosome is usually expressed in a string of variables, each element of which is called a gene. The variable can be represented by binary, real number, or other forms and its range is usually defined by the problem specified. Bit-string encoding is the most classic approach used by GA researchers due to its simplicity and traceability. However, a string-based representation may pose difficulties for and sometimes unnatural obstacles to some optimization problems, e.g., the graph coloring problem.

3.2.2 Fitness Techniques

The objective function (or evaluation function) is a main source to providing the mechanism for evaluating the status of each chromosome. This is an important link between the GA and the system. It takes a chromosome (or phenotype) as input and produces a number or list of numbers (objective value) as a measure to the performance of the chromosome. However, its range of values varies from problem to problem. To maintain uniformity over various problem domains, a fitness function is needed to map the objective value to a fitness value.

3.2.3 Parent Selection

Parent selection emulates the survival-of-the-fittest mechanism in nature. It is expected that a fitter chromosome receives a higher number of offspring and thus has a higher chance of surviving in the subsequent generation. There are many ways to achieve effective selection, including ranking, tournament, and proportionate schemes but the key assumption is to give preference to fitter individuals.

The most important types of selection are roulette wheel selection and tournament selection. In roulette wheel selection, individuals are given a probability of being selected that is directly proportionate to their fitness. Two individuals are then chosen randomly from the populated based on these probabilities and are allowed to produce offspring. The tournament selection is a popular strategy for the selection of parents. In this strategy, a subpopulation of N individuals is chosen at random from population. The individuals of this subpopulation then compete on the basis of their fitness. The individual in the subpopulation with highest fitness wins the tournament and becomes the selected

individual. All of the subpopulation members are then placed back into the general population and the process is repeated.

3.2.4 Crossover

Crossover is a recombination operator that combines subparts of two parent chromosomes to produce offspring that contain some parts of both parents' genetic material. A probability term, p_c, is set to determine the operation rate. Many GA practitioners consider the crossover operator to be the determining factor that distinguishes the GA from all other optimization algorithms.

Different kinds of crossover have been reported. The most common type is single point crossover and multipoint crossover. In single point crossover, a crossover point is randomly selected and the portions of the two chromosomes beyond this point are exchanged to form the offspring. Multipoint crossover is similar to single-point crossover, except that m crossover positions are chosen at random with no duplication.

Single- and multipoint crossover define cross points where the chromosome can be split. Uniform crossover generalizes the scheme to make every locus a potential crossover point. A random binary string with the same length as the chromosome indicates which parent will supply the child with the associated bit. At each location, the corresponding bits of the parents are exchanged if the random string contains a '1" at that location. If the random bit is "0', no exchange takes place.

3.2.5 Mutation

Mutation is an operator that introduces variations into the chromosome. This variation can be global or local. The operation occurs occasionally (usually with small

probability) but randomly alters the value of a string position. Each bit of a bitstring is replaced by a randomly generated bit if a probability test is passed. Some GA practitioners use standard mutation to flip bits. Using this variant, "1" is replaced by a "0" or vice versa if the probability test is passed. This approach results in an effective rate of mutation that is twice as high as the previous one.

3.2.6 Replacement Strategies

After generating the subpopulation (offspring), two representative strategies can be proposed for old generation replacement:

Generational Replacement: Each population of size n generates an equal number of new chromosomes to replace the entire old population. This strategy may make the best member of the population fail to reproduce offspring in the next generation. So the method is usually combined with an elitist strategy where one chromosome or a few of the best chromosomes are copied into the succeeding generation. The elitist strategy may increase the speed of domination of a population by a super chromosome, but on balance it appears to improve the performance

Steady-State Replacement: This strategy means that only a few chromosomes are replaced once in the population to produce the succeeding generation. Usually the worst chromosomes are replaced when new chromosomes are inserted into the population. The number of new chromosomes is to be determined by this strategy. In practice, only one to two new chromosomes are being used by steady-state reproduction.

Although the GA is a powerful optimization tool but it does have certain weaknesses in comparison to other optimization techniques. A number of barriers have yet to be

overcome before it can be applied to some real-world implementations. Due to the randomness of the GA operation, it is difficult to predict its performance, a factor that is crucial for hard-deadline, real-time applications. The source of the problem lies in the diversity of the chromosomes that cause the on-line system performance to be unpredictable. However, there are large classes of problems that appear to be more amenable to solution by GAs than by any other available optimization techniques. These tasks often involve multiple objectives. Moreover, since the GA can jump out of local optima because they are search techniques, it is more desirable for multimodal problems. Perhaps the most encouraging areas of application are the impending neural network-hybrid systems. The use of GAs with neural networks (NN) and fuzzy logic is expected to receive more attention in the future.

Chapter 4

Blind Deconvolution of Linearly Degraded Images using Artificial Neural Networks

The first step in image restoration is identification of *a priori* information about the imaging system and the type of degradations that the image has suffered. This information is used to model the system. These models depend upon the physical nature of the problem and often describe the degradation process. However, in most real life situations a sufficient *a priori* information about point spread function (PSF) of the blurring system is rarely available. Therefore, we have to estimate both the true image and the blur from the degraded image characteristics, using partial information about the imaging system. This type of image restoration is referred to as blind image restoration or blind image deconvolution.

4.1 Image and Degradation Models

The *a priori* information is used to design two types of imaging models, i.e. image models and degradation models which are given below:

4.1.1 Image Models

Image models express our prior knowledge about the structure of the original image. The development of a suitable model for discrete images requires a trade-off between the accuracy of representation and its utility in image identification and restoration. The incorporation of *a priori* information into the restoration process is essential in order to obtain acceptable solutions or regularizing the ill-posed image restoration.

The image models can be distinguished into two broad categories i.e., deterministic and statistical (stochastic). In stochastic model, an image is considered to be a sample function of an array of random variables called random fields. A random field model can provide complete statistical characterization for a given class of images—all statistical properties of the images can, in principle, be derived from this random field model. Different random field have been proposed [74]. Firstly, the Gauss Markov random fields (GMRF) in which $\{x(i,j)\}$ is assumed Gaussian and the field is characterized explicitly in terms of expectations rather than probability densities. Secondly, the Gibbs random fields (GRF) in which energy is associated with each possible field $\{x(i,j)\}$ and probability density is then constructed implicitly from $E(\{x(i,j)\})$. Thirdly, the multiscale random fields consist of Gauss Markov random fields (GMRF) extended in the form of trees, using the concept of multiresolution. In this dissertation, the image is assumed to be a realization of Gauss Markov random process. Then it can be modeled as a noncausal minimum variance representation (NMVR) with nonsymmetric model support. The state space representation of this model is given as:

$$x(i,j) = \sum_{(k,l)\in S_a} a_{k,l}\, x(i-k, j-l) + v_1(i,j) \tag{4.1.1}$$

where $a_{k,l}$ are the image model coefficients and this model is also named as autoregressive(AR) model because it represent an autoregressive process as well. This model can have different models supports S_a. Some common choices for the model support are:

$$S_a = \begin{cases} \{(k,l):(k \geq 0, l \geq 0) \cap (k+l > 0)\}, & \text{quarter plane} \\ \{(k,l):(k > 0, l \leq 0) \cap (k \geq 0, l > 0)\}, & \text{nonsymmetric halfplane} \\ \{(k,l):(k > 0, l \leq 0) \cap (k \geq 0, l > 0)\}, & \text{semi-causal} \\ \{(k,l):\forall (k,l) \neq (0,0)\}, & \text{noncasual} \end{cases} \tag{4.1.2}$$

The model supports are also shown in the Figure 4.1

4.1.2 Degradation Model

Random fluctuations in the intensity, color, texture, object boundary or shape can be seen in most of the real world images. The causes for these fluctuations are diverse and complex, and they often due to factors such as non-uniform lightening, random fluctuations in object surface orientation and texture, complex scene geometry and noise. Consequently, processing of such images becomes a problem of statistical inference which requires the definition of statistical model corresponding to the image pixel. A more general approach which can be addressed in this problem is also random fields and the degraded image also assumed to be the realization of Gauss Markov random process and the degradation suffered during the image formation process modeled as a convolution summation having a noncausal support and additive white noise. Thus, the noisy blurred image is described by the following state-space model [33]:

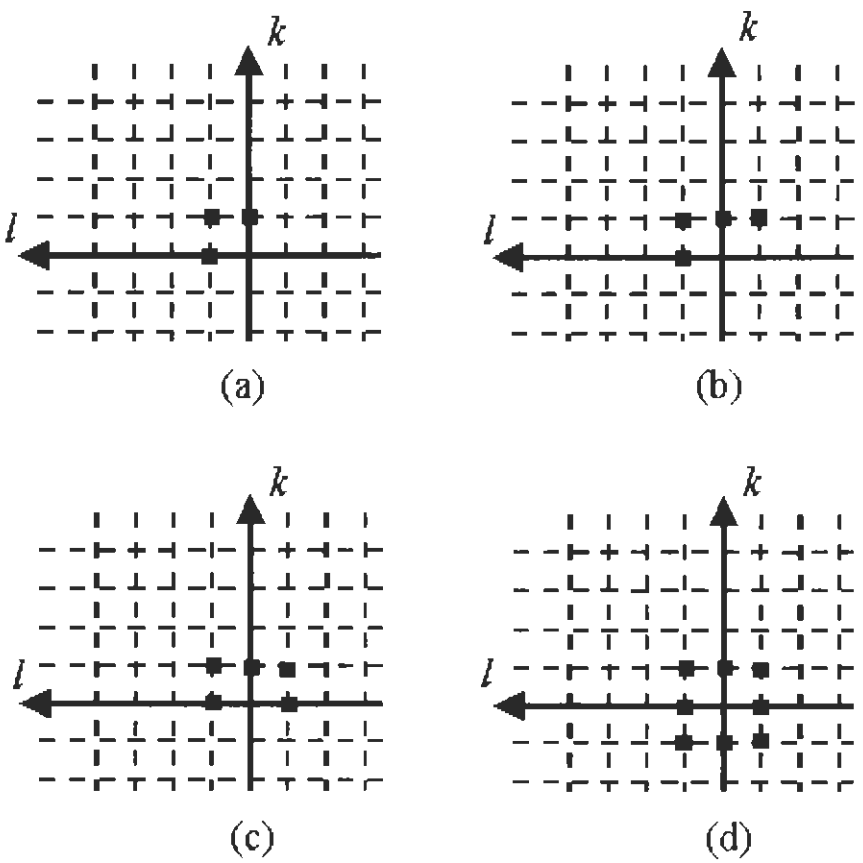

Figure 4.1 Model support for various first order image models (a) quarter plane model, (b) nonsymmetric halfplane model, (c) semi-causal model, (d) noncasual model.

$$y(i,j) = \sum_{(m,n)\in S_h} h_{m,n} x(i-m, j-n) + v_2(i,j) \qquad (4.1.3)$$

where $y(i,j)$ is the observed image distorted by a blurring function or point spread function (PSF) $h_{m,n}$. $v_2(i,j)$ is additive white Gaussian noises with zero mean and variances $\sigma_{v_2}^2$. This model is also named as moving average (MA) model because it represents the moving average process.

This project identifies the blurring function $h_{m,n}$ and restores the degraded image, simultaneously, using a multilayer neural network structure which is based on image and degradation models, i.e. a combination of AR and MA processes. Therefore, the overall operation of multilayer neural network is based upon the ARMA process. The self-organization like structure of the neural network is used to solve the ARMA parameter estimation problem. The problem of blind image restoration is difficult in the sense that there is no *a priori* information about the blur and image. Image degradation process may be linear or nonlinear process. It may also be either space-invariant or a space-variant process. The image degradation is normally nonlinear and space-variant process. However, for algorithmic simplicity, we have assumed the degradation process to be linear and space-invariant. This model can identify the non-causal blur function and restores the original image at the same time.

4.2 Blind Image Deconvolution of Linearly Degraded Images

The artificial neural network is based upon the image and degradation models represented by the eqs. (4.1.1) and (4.1.3), respectively. These equations represent the auto-regressive moving average (ARMA) process for blur identification and restoration of

linearly and space-invariant degraded images. The weights of the neural network, i.e. image model coefficients and blurring function, were updated through feedbacks using gradient method, where cost function was the square of the error between observed and the estimate of the blurred image [33]. There are many local minima in the error performance surface, and it is unavoidable for the algorithm to get stuck in a local minima and the flat plateau. Although different methods like Brains method and adding momentum terms, have been proposed in order to get out of local minima but still these methods have not produced satisfactory results. As a result, one usually runs the algorithm several times with different random initial configuration and chooses the configuration with lowest stress. Therefore, we have proposed to use evolutionary computing methods like genetic algorithm to find the global minima of the error performance surface. Then the gradient-based algorithms should be applied to converge to the solution which is the main motivation of this chapter.

There are practical difficulties in estimating $a_{k,l}$, and $h_{m,n}$ due to high computational complexity of PSF's with large support, instability of the algorithm, and non-unique solution. These problems can be overcome by using the following assumptions [8]:

1. The coefficients $h_{m,n}$, are positive, symmetric and have zero phase. These constraints are used for stability and uniqueness of the solution.
2. The PSF has known parametric form consisting of only few parameters. This lowers the computational complexity.
3. The image formation system is assumed not to absorb or generate energy so that, the total energy in the object is equal to that of the observed image i.e.,

$$\sum_{(m,n)\in S_h} h_{m,n} = 1 \qquad (4.2.1)$$

4.2.1 Neural Network for Image Restoration

A feed-forward three-layer neural network structure can be presented to simultaneously identify the blur function and restore the degraded image. This structured network was decomposed into two adaptive associative networks [33].

1. The operation between the first layer L_1 and the second layer L_2 was assumed to be equivalent to that of an auto-associative network, which is excited by a random Gaussian process.
2. The information then passes forward from the second layer L_2 to the third layer L_3 by hetero-associative process.
3. The output of the third layer L_3 is the estimate of the observed blurred image.

The weights of the two associative networks were initialized using the genetic algorithm and then updated using gradient based algorithm. When the networks have converged to stable states, weights of the hetero-associative network equal to the coefficients of unknown blur function and second layer L_2 represents the restored image.

4.2.1.1 Procedure for Neural Network

This artificial neural network consists of three 2-D structured layers L_1, L_2 and L_3 with same number of neurons, i.e. $M \times N$, as shown in Figure 4.2. Initially, the inputs to the first layer L_1 are assumed to be a random Gaussian process image with no information about the original image. $a_{k,l}$ are weights of connection between layers L_1 and L_2 which are initiated using genetic algorithm and then updated to optimize the solution. The operation

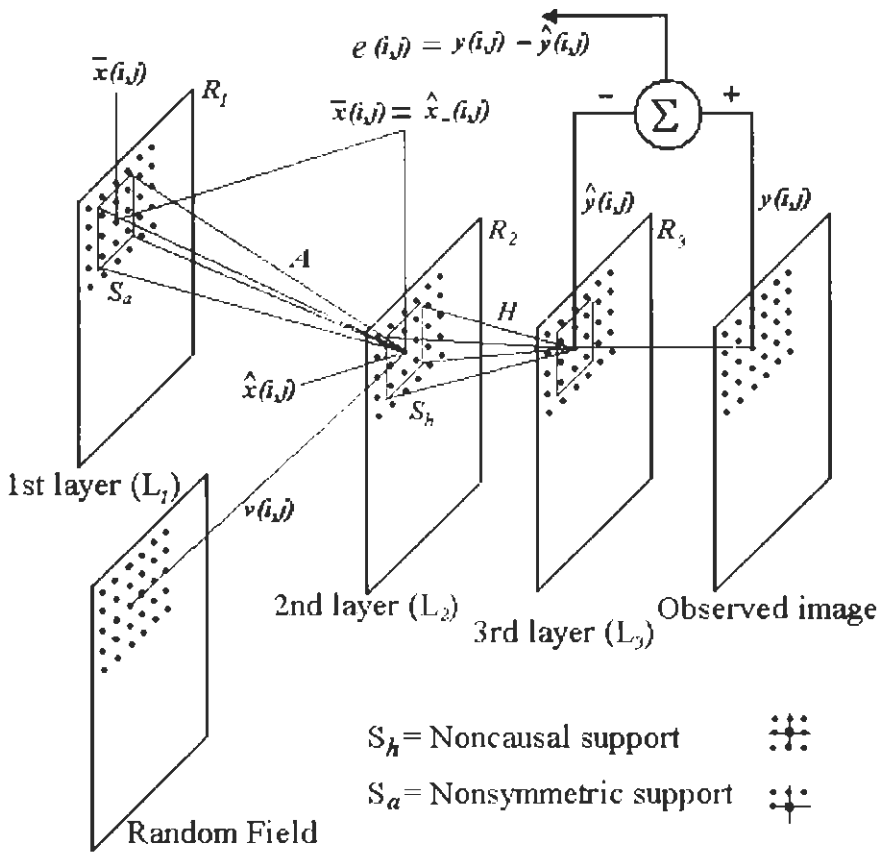

Figure 4.2 The structure of the artificial neural network based on linear ARMA model.

between the first and the second layer is given below:

$$\hat{x}(i,j) = \sum_{(k,l)\in S_a} a_{k,l}\bar{x}(i-k, j-l) + v_1(i,j) \tag{4.2.2}$$

The neuron values of the second layer L_2, i.e. $\hat{x}(i,j)$, are then feedback to the corresponding neurons of the first layer L_1, i.e. $\bar{x}(i,j)$, for the next iteration, according to the following equation.

$$\bar{x}(i,j) = \hat{x}\_(i,j) \tag{4.2.3}$$

The operation between second layer L_2 and third layer L_3 defines the hetero-associative operation or MA process. The output of the $(i,j)^{th}$ neuron of the third layer will be calculated according to eq (4.2.4).

$$\hat{y}(i,j) = \sum_{(m,n)\in S_h} h_{m,n}\hat{x}(i-m, j-n) + v_2(i,j) \tag{4.2.4}$$

where A is assumed to be $a_{k,l}$ and H is assumed to be $h_{m,n}$. Once the convergence of the algorithm will be achieved, the layer L_2 will represent the restored image.

4.2.1.2 The Cost Function

The identification and restoration processes are implemented simultaneously by using a dynamic iterative algorithm to minimize the error function of the neural network. The error function or cost function consists of two terms the hetero-associative errors which is fed from layer L_3 and an auto associative error which comes from L_1 and L_2. The hetero-associative error is given as

$$E_y(w) = \frac{1}{M \times N} \sum_{(i,j)\in R_3} \{y(i,j) - \hat{y}(i,j)\}^2 \tag{4.2.5}$$

and the auto-associative error is

$$E_x(w) = \frac{1}{M \times N} \sum_{(i,j) \in R_2} \{\bar{x}(i,j) - \hat{x}(i,j)\}^2 \tag{4.2.6}$$

4.2.1.3 Genetic Algorithm

One main desire is to find out optimized synaptic weights that will give better restored image and exact or close point spread function. In order to avoid local minima problem, G.A are used to search for global minimum. The G.A are being used to find weights of the feedforward neural network, which are close to the desired solution. Our proposed neural network consists of two layers and each layer contains a set of weights $a_{k,l}$ and $h_{m,n}$. Therefore, a set of these weights W was treated as a chromosome which is given as:

$$\begin{aligned} W &= W_x, W_y \\ W_x &= [a_{k,l}] \\ W_x &= [h_{m,n}] \end{aligned} \tag{4.2.7}$$

where W_x and W_y are sets of floating point numbers. The ordinary rule of thumb for choosing the population size is to choose it five to six times the length of a chromosome.

a) Initialization

The genes representing weights were produced by using a pseudo-random generator. The values of the genes were floating between 0 and 1 but the sum of all weights in a layer must be equal to one according to the third assumption of image models otherwise layer would generate energy [75].

b) Fitness Criterion

The fitness criterion in genetic algorithm is always taken between zero and one. The individual having fitness equal to one is assumed to be the fit while the one having zero fitness is treated as worst fit. Therefore, we have to chose a fitness function F in such a way that when it equal to one the errors between different layers should be zero, which is taken as

$$F = \frac{F_x + F_y}{2} \tag{4.2.8}$$

where

$$F_x = \frac{1}{1+E_x}$$
$$F_y = \frac{1}{1+E_y} \tag{4.2.9}$$

c) Cross-over, Reproduction and Next Generation

The population in a generation is sorted out according to the fitness criterion in a descending order. The top one third was given a chance to produce five children per pair. The next one third was given a chance to produce 3 children per pair. They were similar to child 1, child 2 and child 3 as given above. The last one third was given a chance to produce only one child per pair, which is similar to child 1.

For selection of a new generation, the rule for survival of the fittest is being used. All the parents and children are sorted in a descending order of fitness after calculating the fitness of the children. The ones equal to the number of population were chosen for the next generation. So the new population was a blending and overlap of the previous and the present with no fixed percentage for either generation [76].

d) Mutation

Mutation is the process in which genes are randomly mutated (changed). Mutation plays an important role when every new generation does not seem to improve the fitness.

e) Termination Criterion

When the fitness of the best chromosome in the new population was almost the same as that of the best chromosome in the previous population, the program was terminated. Quantitatively the criterion for termination was;

$$\left|F_{new} - F_{prev}\right| < 0.01 \tag{4.2.10}$$

If we chose a very low value it is possible that GA may not reach to it and may become an infinite loop. On the other hand, if we take a higher value the GA may terminate before convergence.

4.2.1.4 Learning Algorithm

A gradient-based algorithm was used to train and optimize the network by minimizing the squares of errors. Specifically the weights between L_2 and L_3, which only depend on E_y, were updated as

$$h_{p,q}^{new} = h_{p,q}^{old} - \alpha \frac{\partial E_y(w)}{\partial h_{p,q}} \tag{4.2.11}$$

The updating equation for linear part of the blur coefficients

$$h_{p,q}^{new} = h_{p,q}^{old} + \frac{2\alpha_1}{M \times N} \sum_{(i,j)\in R_3} \{y(i,j) - \hat{y}(i,j)\}\hat{x}(i-p, j-q) \tag{4.2.12}$$

The weights of the auto-associative network are related to E_x in L_2 and E_y propagated form L_3. Therefore, the coefficients of the linear part of the auto-associative network are iteratively updated by eq (4.2.13)

$$a_{u,v}^{new} = a_{u,v}^{old} - \beta \frac{\partial\{E_y(w) + E_x(w)\}}{\partial a_{u,v}} \tag{4.2.13}$$

We find the following updating equation for $a_{u,v}$,

$$a_{u,v}^{new} = a_{u,v}^{old} + \beta \sum_{(i,j)\in R_2} \left[\delta(m,n) + \frac{2}{M \times N} \{\bar{x}(i,j) - \hat{x}(i,j)\} \right] \bar{x}(i-u, j-v) \tag{4.2.14}$$

where

$$\delta(k,l) = \frac{2}{M \times N} \sum_{(m,n)\in R_3} h_{m-k,n-l} \{y(i,j) - \hat{y}(i,j)\} \tag{4.2.15}$$

4.3 Simulation Studies

A three layered neural network model was implemented for space-invariant blur identification and restoration of linearly degraded images. The operation between first and second layer of the neural network assumed to be linear space-invariant autoregressive (AR) process, as given in eq (4.2.2). The operation between second and third layer was assumed to be linear space-invariant moving average (MA) process, which represents the degradation process and was given in eq (4.2.4). A genetic algorithm based method was proposed to be used for fast searching of optimum weights for the neural network because genetic algorithms have capability for searching for the global minimum of the error performance

(a) 'Lena' image (b) 'Cameraman' image

Figure 4.3 Original undistorted images

surface of the cost function which is represented by eq (4.2.5) and (4.2.6). Once global minimum is detected, a gradient based method was also used for fast convergence to the global minima. Therefore, the weights of the neural network were updated using eq (4.2.12) and (4.2.14).

The artificial neural network was applied to the image 'Lena' and 'Cameraman'. The original images of 'Lena' and 'Cameraman' had the dimensions 256×256 with 256 grey levels as shown in Figure 4.3(a) and 4.3(b), respectively. These pictures were particularly relevant for testing the efficiency of the current schemes because they exhibit a combination of smooth background together with a wide variety of textural patterns. The image 'Lena' contains smooth background and face with contrasts of relatively fine textures in the feathers on the hat. We would be testing the ability of the algorithms to sharpen those fine features in the images while suppressing of ringing effects and noises in the smooth regions.

The image 'Cameraman' contains a variety of textural changes, e.g., Cameraman is in the picture is quite close than the buildings. This feature would be interesting in space-variant image restoration where atmospheric turbulence may degrade images more to the distant objects.

In order to check performance of the neural network for blind image deconvolution, the best improvement measure of the quality of the restored images is the human inspection. However, two meaningful measures called the improvement in the signal to noise ratio (ISNR) of the image and normalized mean square-error (NMSE) of the identified blur were assumed. The improvement in the signal to noise ratio (ISNR) of the image is ratio of two important quantities known as the percentage mean square error of degraded image to the percentage mean square error of the restored image [8]. Therefore, ISNR was defined as follows:

$$ISNR = \frac{MSE(\{v(i,j)\})}{MSE(\{\hat{x}(i,j)\})} \tag{4.3.1}$$

where MSE was given as:

$$\{MSE(\hat{x}(i,j))\} = 100\frac{\sum_{s,t}\{c\hat{x}(s,t) - x(s,t)\}^2}{\sum_{s,t} x^2(s,t)} \tag{4.3.2}$$

The value of c can be calculated using the following relation:

$$c = \frac{\sum_{i,j} x(i,j)\hat{x}(i,j)}{\sum_{i,j} x^2(i,j)} \tag{4.3.3}$$

where $y(i,j)$ is the given blurred image and $\hat{x}(i,j)$ is the restored image. The second evolution criteria, i.e. normalized mean square-error (NMSE) of the identified blur is defined as [77]:

$$NMSE = \frac{\sqrt{\sum_{m,n}\left\{h_{m,n} - \hat{h}_{m,n}\right\}^2}}{\sum_{m,n} h_{m,n}} \tag{4.3.4}$$

where $h_{m,n}$ and $\hat{h}_{m,n}$ are the true and estimated blur. These performance measures can only be evaluated for controlled experiments where undistorted image $x(i,j)$ and true blur $h_{m,n}$ are available.

The artificial neural network was applied on images degraded by linear space-invariant Gaussian blur with noise. The images given in Figure 4.3, were degraded with two different 5×5 Gaussian space-invariant masks in order to produce degraded images with SNR of 30dB, termed as having high SNR, and SNR of 20dB, named as degraded images with low SNR. The quantization noise or Gaussian noise was also added in the images in order to study the performance of neural network model in noisy environment. In the light of assumption about the blurring function $h_{m,n}$, its form will be:

l_6	l_5	l_4	l_5	l_6
l_5	l_3	l_2	l_3	l_5
l_4	l_2	l_1	l_2	l_4
l_5	l_3	l_2	l_3	l_5
l_6	l_5	l_4	l_5	l_6

The computational complexity of the genetic algorithm was calculated and it was found that one chromosome requires $51\times256\times256$ multiplication and additions in order to complete one cycle. Similarly, the gradient descent algorithm requires $700\times256\times256$

multiplication and $725\times256\times256$ additions in order to complete one iteration. The algorithm was implemented and the results are given in the subsequent sections.

4.3.1 Blind Deconvolution of the Image Degraded by Space-Invariant Gaussian Blur with Uniform Quantization Noise

The two blurred images were obtained by using two different 5×5 linear Gaussian blurring functions with SNR of 30db and 20db which represents the degraded images with high SNR and low SNR, respectively. Then a small quantization noise was also added to check the performance of the neural network in the presence of this noise.

Figure 4.4 shows the degraded images with high SNR containing quantization noise and images restored with the linear space-invariant neural network model. Table 4.1 shows the blurring functions used to degrade the images, estimated blurring function obtained from the neural network and SNR in the restored images. It is observed that space-invariant estimated blur is quite close to the blurring function and restored image has also better quality than degraded image in terms of ISNR.

Figure 4.5 shows the degraded images with low SNR and images restored with the neural network model. Table 4.2 shows the blurring functions used to degrade the images, estimated blurring function obtained form the neural network and ISNR in the restored images. The estimated blur is quite accurately estimated along with the restored image. The quality of the degraded image has been significantly improved for the degraded images with low SNR.

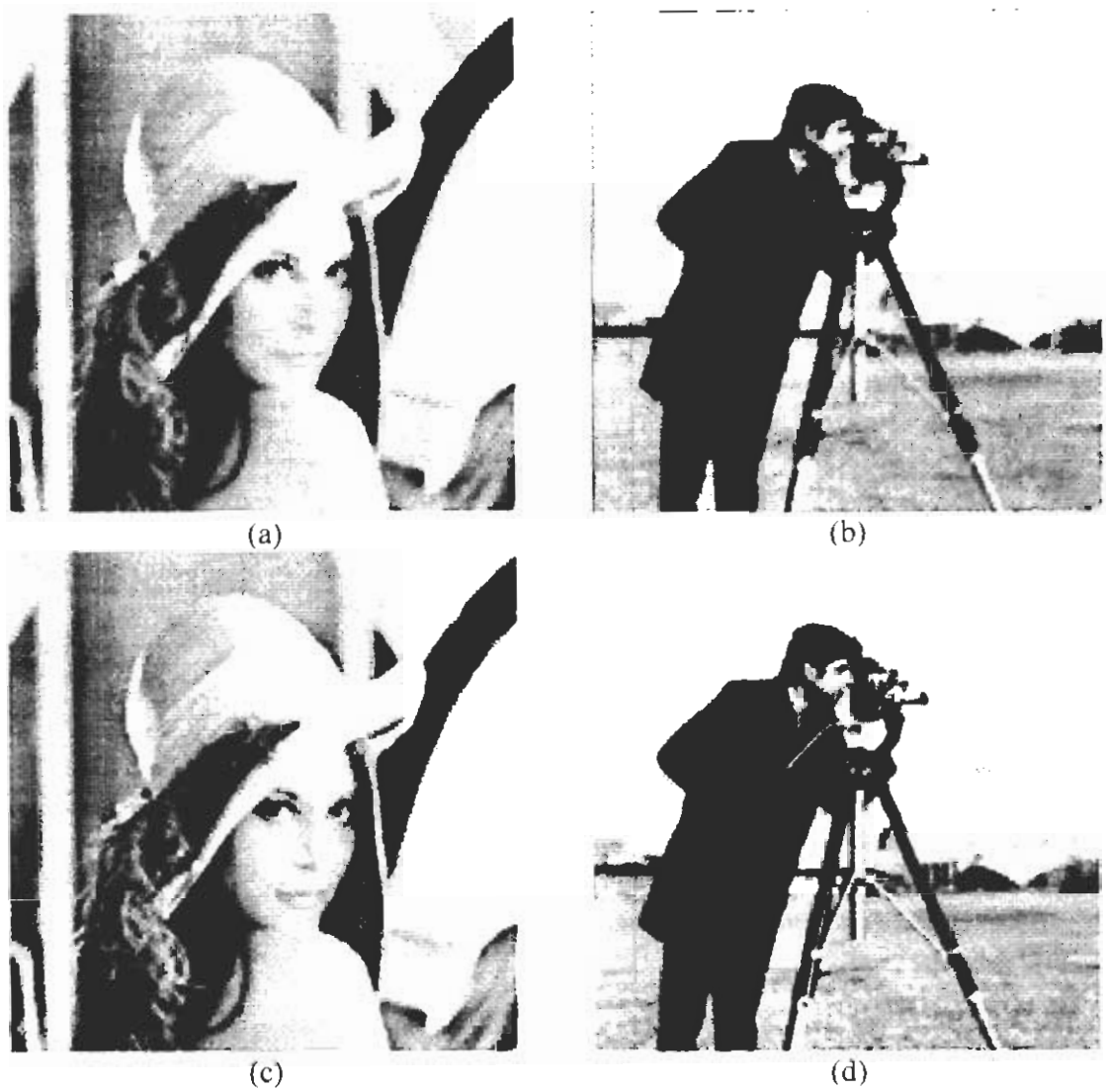

Figure 4.4 Blind image deconvolution degraded images with 30db SNR using neural networks based on linear ARMA model. a) Degraded 'Lena' image with quantization noise, b) Degraded 'Cameraman' image with quantization noise. c) Restored 'Lena' image, and d) Restored 'Cameraman' image.

Table 4.1 Real and estimated blur parameters along with ISNR of restored images after blind image deconvolution of degraded images with quantization noise having 30db SNR using neural networks based on linear ARMA model.

'Lena' Image		
	Real $h_{m,n}$	Estimated $h_{m,n}$
l_1	0.2	0.2575170
l_2	0.055	0.0540297
l_3	0.05	0.0472861
l_4	0.035	0.0337941
l_5	0.035	0.0337897
l_6	0.03	0.0304147
ISNR	2.166638	

'Cameraman' Image		
	Real $h_{m,n}$	Estimated $h_{m,n}$
l_1	0.2	0.2675411
l_2	0.055	0.0540457
l_3	0.05	0.0472983
l_4	0.035	0.0337970
l_5	0.035	0.0337920
l_6	0.03	0.0304168
ISNR	2.327335	

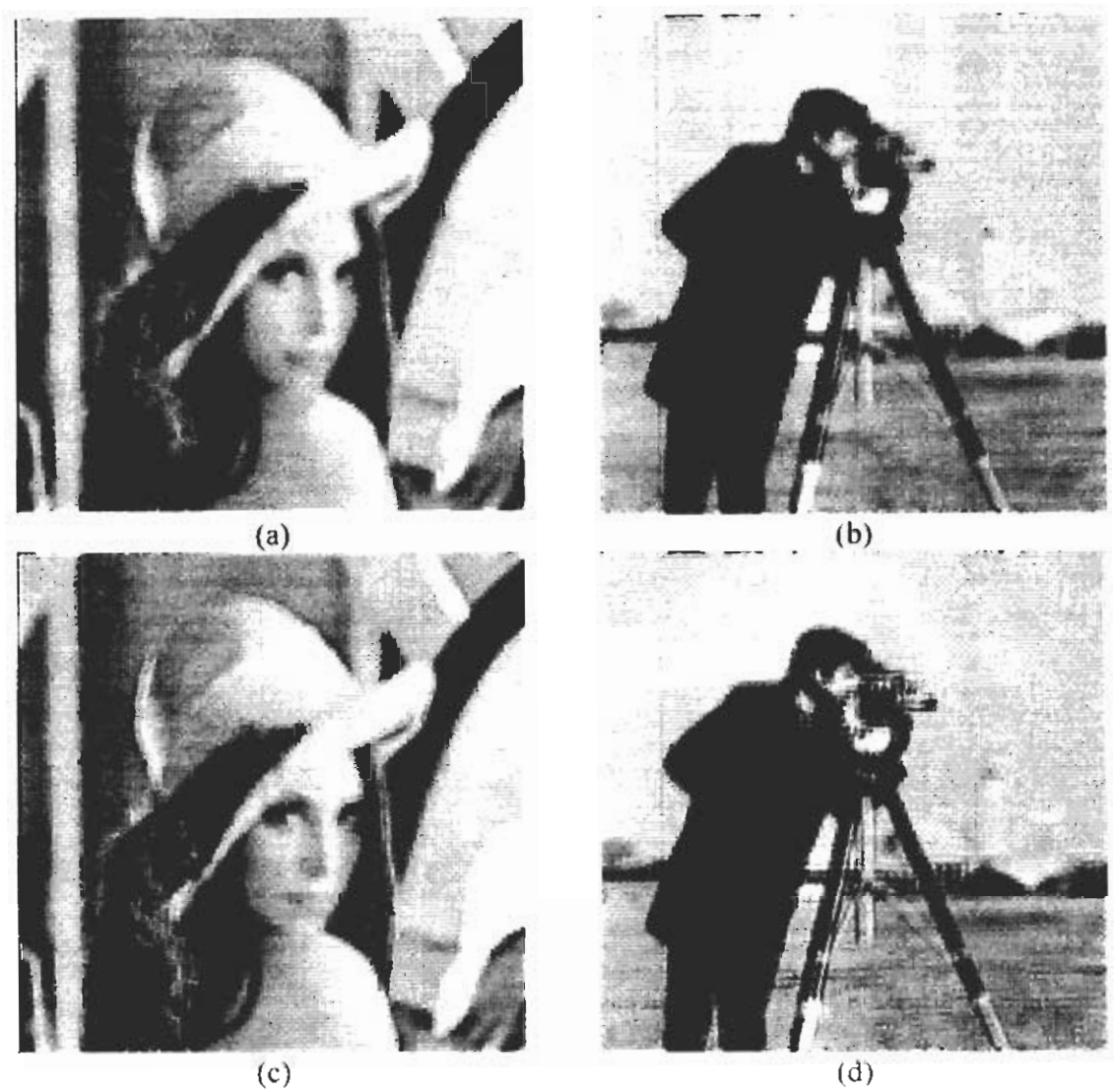

Figure 4.5 Blind image deconvolution degraded images with 20db SNR using neural networks based on linear ARMA model. a) Degraded 'Lena' image with quantization noise, b) Degraded 'Cameraman' image with quantization noise, c) Restored 'Lena' image, and d) Restored 'Cameraman' image.

Table 4.2 Real and estimated blur parameters along with ISNR of restored images after blind image deconvolution of degraded images with quantization noise having 20 db SNR using neural networks based on linear ARMA model.

'Lena' Image		
	Real $h_{m,n}$	Estimated $h_{m,n}$
l_1	0.006	0.006755
l_2	0.01	0.015404
l_3	0.0187	0.014729
l_4	0.05	0.033789
l_5	0.05	0.033782
l_6	0.04	0.030406
ISNR	1.83984	

'Cameraman' Image		
	Real $h_{m,n}$	Estimated $h_{m,n}$
l_1	0.006	0.006758
l_2	0.01	0.015405
l_3	0.0187	0.014728
l_4	0.05	0.033787
l_5	0.05	0.033779
l_6	0.04	0.030397
ISNR	1.977105	

4.3.2 Blind Deconvolution of the Image Degraded by Space-Invariant Gaussian Blur with AWGN

The two types of blurred images were obtained by using two different 5×5 linear Gaussian blurring functions with SNR of 30db and 20db which represents the degraded images with high SNR and low SNR, respectively. Then 30db AWGN noise was also added to check the performance of the neural network in the presence of this noise.

Figure 4.6 shows the degraded images with high SNR and images restored with the neural network model. Table 4.3 shows the blurring functions used to degrade the images, estimated blurring function obtained form the neural network and ISNR in the restored images.

Figure 4.7 shows the degraded images with low SNR and images restored with the neural network model. Table 4.4 shows the blurring functions used to degrade the images, estimated blurring function obtained form the neural network and ISNR in the restored images. Results show that the AWGN causes more damage to the degraded image. The degraded images with AWGN noise produce less clear restored images as compared to the results obtained with small quantization noise. However, the restored images from degraded images with high SNR provided better results that the restored images obtained from the degraded images with low SNR. It is obvious from the ISNR of the restored images as well. However, the blurring functions are estimated with the same accuracy which shows that that the blurring function can be estimated with similar accuracy with or without AWGN.

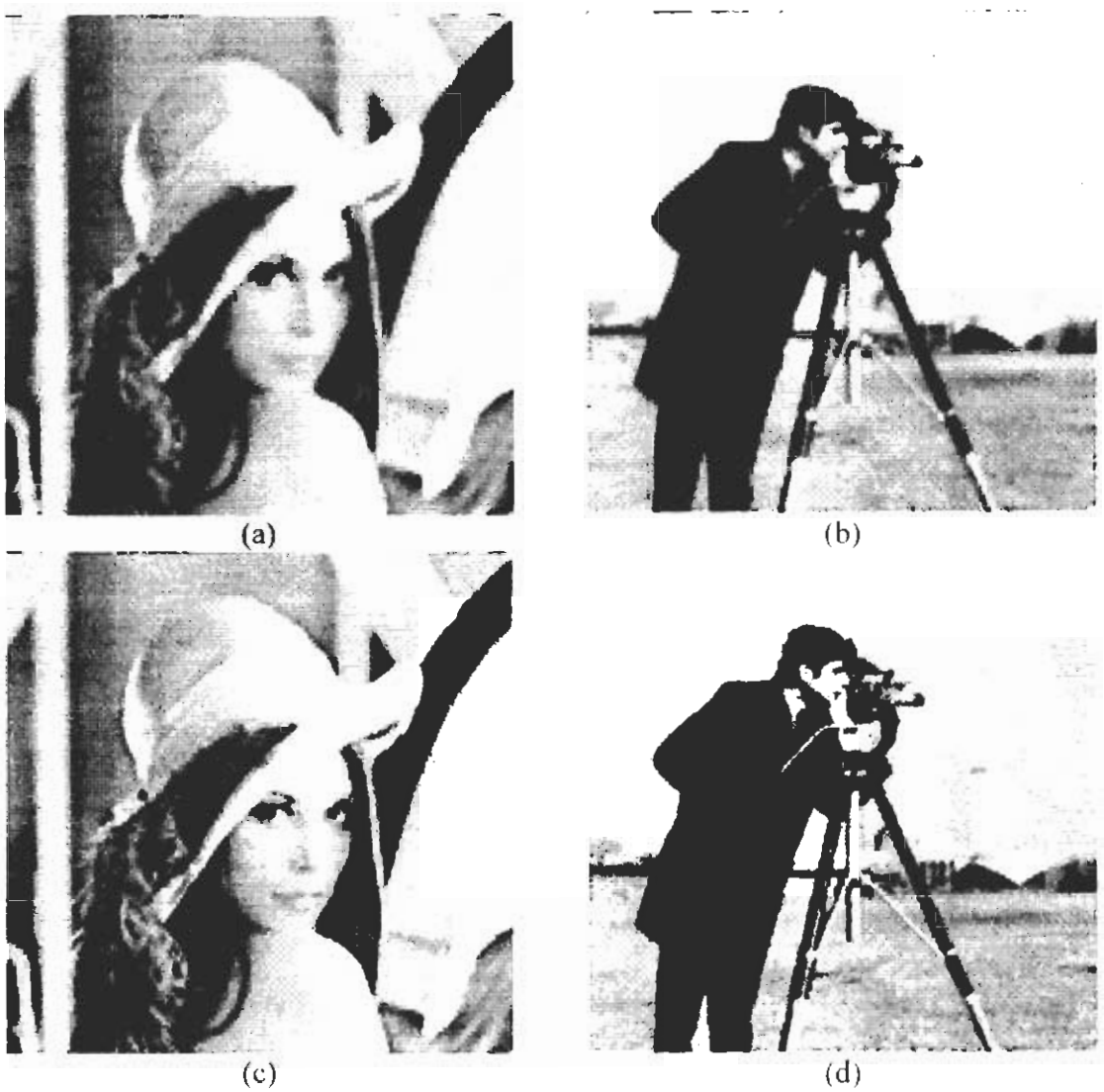

Figure 4.6 Blind image deconvolution of degraded images having 30db SNR using neural networks based on linear ARMA model. a) 'Lena' image degraded with AWGN, b) 'Cameraman' image degraded with AWGN. c) Restored 'Lena' image. and d) Restored 'Cameraman' image.

Table 4.3 Real and estimated blur parameters along with ISNR of restored images after blind image deconvolution of degraded images with AWGN having 30 db SNR using neural networks based on linear ARMA model.

'Lena' Image		
	Real $h_{m,n}$	Estimated $h_{m,n}$
l_1	0.2	0.2675235
l_2	0.055	0.0540259
l_3	0.05	0.0472884
l_4	0.035	0.0337958
l_5	0.035	0.0337912
l_6	0.03	0.0304172
ISNR	2.06782	

'Cameraman' Image		
	Real $h_{m,n}$	Estimated $h_{m,n}$
l_1	0.2	0.2675331
l_2	0.055	0.0540340
l_3	0.05	0.0472920
l_4	0.035	0.0337976
l_5	0.035	0.0337978
l_6	0.03	0.0304201
ISNR	2.269680	

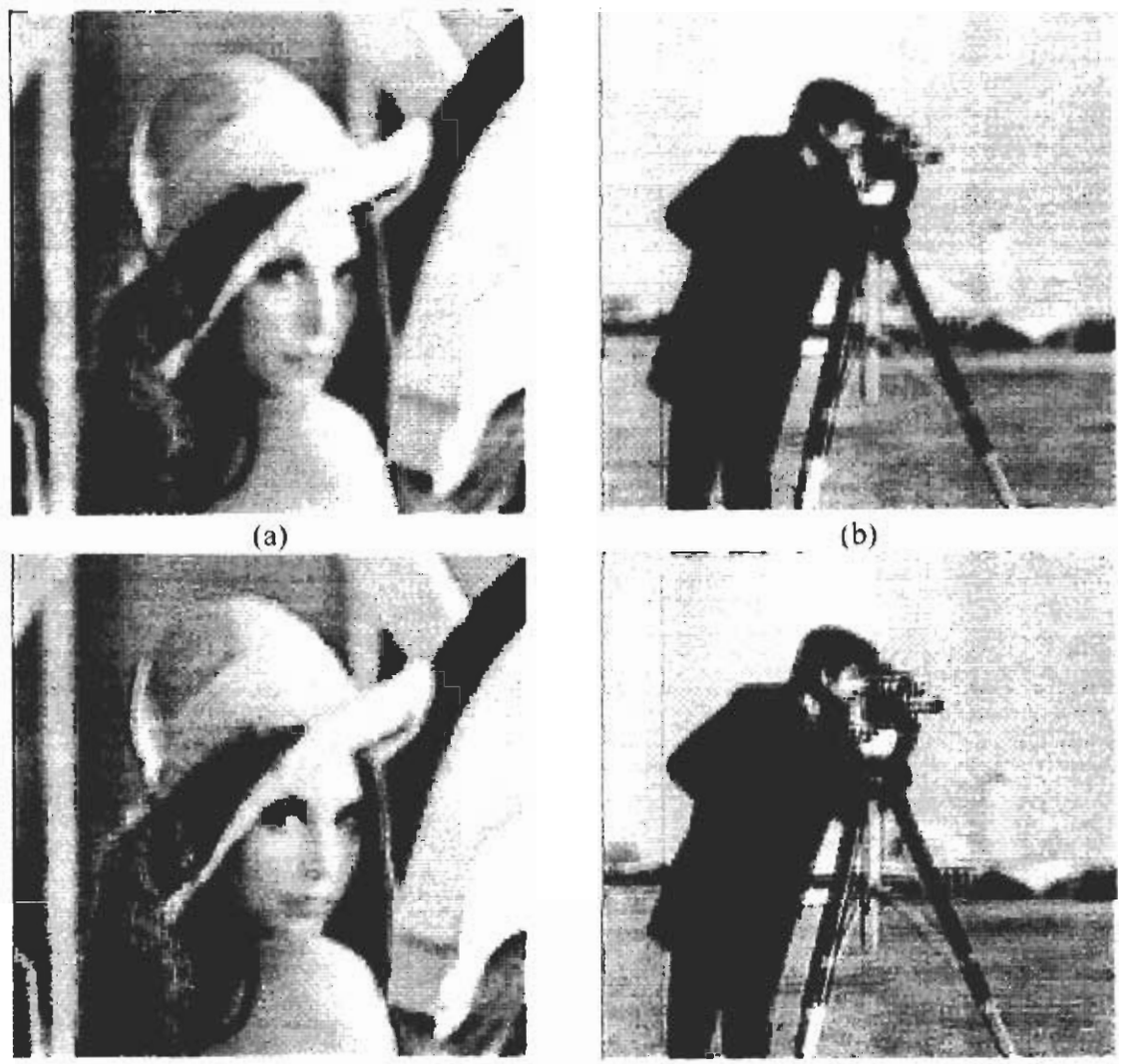

Figure 4.7 Blind image deconvolution of degraded images having 20db SNR using neural networks based on linear ARMA model. a) 'Lena' image degraded with AWGN, b) 'Cameraman' image degraded with AWGN, c) Restored 'Lena' image, and d) Restored 'Cameraman' image.

Table 4.4 Real and estimated blur parameters along with ISNR of restored images after blind image deconvolution of degraded images with AWGN having 20 db SNR using neural networks based on linear ARMA model.

'Lena' Image		
	Real $h_{m,n}$	Estimated $h_{m,n}$
l_1	0.006	0.006755
l_2	0.01	0.015403
l_3	0.0187	0.147286
l_4	0.05	0.055337
l_5	0.05	0.043784
l_6	0.04	0.030410
ISNR	1.898794	

'Cameraman' Image		
	Real $h_{m,n}$	Estimated $h_{m,n}$
l_1	0.006	0.006758
l_2	0.01	0.015405
l_3	0.0187	0.014728
l_4	0.05	0.053779
l_5	0.05	0.044776
l_6	0.04	0.030401
ISNR	2.0391431	

Chapter 5

Blind Deconvolution of Nonlinearly Degraded Images using Artificial Neural Networks

Degradations, which are usually caused by relative motion between object and camera, or wrong focus or defects of optical lens, may be a linear or nonlinear process [73]. For linear degradation process, enough work has already been done. However, blind deconvolution of nonlinearly degraded image is difficult, having more computational complexity. It includes the nonlinearity in the imaging processes which normally occurs in images of interest introducing nonlinear degradation in the images. This is the main motivation of this chapter. A structured neural network was proposed which resembles the network explained in the previous chapter. It is decomposed into two adaptive associative networks. The operation between the first and second layer is also assumed to be auto-associative excited by random Gaussian noise while between second and third layer is hetero-associative. The output of third layer was the estimate of the observed image [33]. The weights were updated through feedback using gradients method, where cost function was the square of the error between observed and the estimate of the blurred image.

5.1 Neural Network for Blind Deconvolution of Nonlinearly Degraded Images using Linear AR Process

The true image model is represented as a linear autoregressive process which is given in eq (4.1.1). However, the blurred image model is assumed to be a nonlinear process in order to handle nonlinearities of the imaging sensor which may enhance or compress certain intensity range of an image. Therefore, the degradation process is modeled according to the Volterra filters [73] concept with the following state space relationship:

$$y(i,j) = \sum_{(m,n)\in S_h} h_{m,n}x(i-m,j-n) + \sum_{(m_1,n_1,m_2,n_2)\in S_h} h_{m_1,n_1,m_2,n_2} < x(i-m_1,j-n_1)x(i-m_2,j-n_2) >_{255} + v_1(i,j) \tag{5.1.1}$$

where $<\ldots>_{255}$ represents modulo 255. There are also practical difficulties in estimating $h_{m,n}$ and h_{m_1,n_1,m_2,n_2} due to high computational complexity of PSF's with large support, instability of the algorithm, and non-unique solution. Therefore, in order to avoid these problems, the linear PSF $h_{m,n}$ is assumed to be positive, symmetric and has zero phase. However, the nonlinear part of PSF, i.e. h_{m_1,n_1,m_2,n_2}, should be negative. This constraint is for particular cases in which the sensor compresses certain intensity range of the image [50][73]. In general, the image formation system is also assumed not to absorb or generate energy. Therefore, the total energy in the object is equal to that of the observed image.

$$\sum_{(m,n)\in S_h} h_{m,n} + \sum_{(m_1,n_1,m_2,n_2)\in S_h} h_{m_1,n_1,m_2,n_2} = 1 \tag{5.1.2}$$

5.1.1 Neural Network for Blurred Image Representation

This artificial neural network consists of three 2-D structured layers L_1, L_2 and L_3. Each layer contains $M \times N$ neurons. The inputs to the first layer L_1 are assumed to be a random Gaussian process image with no information about the original image. $a_{k,l}$ are weights of connection which are initiated according to some criteria like GA's and then updated to optimize the solution. $a_{k,l}$ is space-invariant and hence is independent of i and j. The operation between the first and the second layer is given in eq (4.2.2). The neuron values of the second layer i.e., $\hat{x}(i,j)$, are then fedback to the corresponding neurons of the first layer, i.e. $\overline{x}(i,j) = \hat{x}\_(i,j)$, for the next iteration.

The operation between second and third layer defines the hetero-associative operation or MA process. The output of the $(i,j)^{th}$ neuron of the third layer will be calculated as follows

$$\hat{y}(i,j) = \sum_{(m,n)\in S_h} h_{m,n}\hat{x}(i-m, j-n) + \sum_{(m_1,n_1,m_2,n_2)\in S_h} h_{m_1,n_1,m_2,n_2} < \hat{x}(i-m_1, j-n_1)\hat{x}(i-m_2, j-n_2) >_{255} \tag{5.1.3}$$

where $h_{m,n}$ and h_{m_1,n_1,m_2,n_2} are the connection weights, also called as coefficients of the PSF. It is assumed that the PSF is space-invariant, therefore, $h_{m,n}$ and h_{m_1,n_1,m_2,n_2} are also independent of i and j. The structure of the proposed neural network is also shown in Figure 4.2 where A consists of image model coefficients $a_{k,l}$ and H consists of nonlinear blurring function having blurring parameters $h_{m,n}$ and h_{m_1,n_1,m_2,n_2}.

5.1.2 Learning Algorithm

The identification and restoration processes are implemented simultaneously by using a dynamic iterative algorithm to minimize the same hetero-associative errors given in eq (4.2.5) and the auto-associative error given in eq (4.2.6). A gradient-based algorithm was used to train and optimize the network by minimizing the squares of errors. Specifically the weights between L_2 and L_3, which only depend on E_y, were updated as

$$h_{p,q}^{new} = h_{p,q}^{old} - \alpha_l \frac{\partial E_y(w)}{\partial h_{p,q}} \tag{5.1.4}$$

and

$$h_{p_1,q_1,p_2,q_2}^{new} = h_{p_1,q_1,p_2,q_2}^{old} - \alpha_n \frac{\partial E_y(w)}{\partial h_{p_1,q_1,p_2,q_2}} \tag{5.1.5}$$

The updating equation for linear part of the blur coefficients

$$h_{p,q}^{new} = h_{p,q}^{old} + \frac{2\alpha_l}{M \times N} \sum_{(i,j)\in R_3} \{y(i,j) - \hat{y}(i,j)\}\hat{x}(i-p, j-q) \tag{5.1.6}$$

The updating equation for the nonlinear part of the blur coefficients

$$h_{p_1,q_1,p_2,q_2}^{new} = h_{p_1,q_1,p_2,q_2}^{old} + \frac{2\alpha_n}{M \times N} \sum_{(i,j)\in R_3} \{y(i,j) - \hat{y}(i,j)\}\hat{x}(i-p_1, j-q_1)\hat{x}(i-p_2, j-q_2) \tag{5.1.7}$$

The weights of the auto-associative network are related to E_x in L_2 and E_y propagated form L_3. Therefore, the coefficients of the auto-associative network are iteratively updated by

$$a_{u,v}^{new} = a_{u,v}^{old} - \beta \frac{\partial\{E_y(w) + E_x(w)\}}{\partial a_{u,v}} \tag{5.1.8}$$

We find the following updating equation for $a_{u,v}$,

$$
\begin{aligned}
& a_{u,v}^{new} \\
& = a_{u,v}^{old} + \beta \sum_{(i,j)\in R_2} \left[\frac{2}{M \times N} \{\bar{x}(i,j) - \hat{x}(i,j)\} \bar{x}(i-u, j-v) \right. \\
& + \frac{2}{M \times N} \{y(i,j) - \hat{y}(i,j)\} \left\{ \sum_{(m,n)\in S_h} h_{m,n} \bar{x}(i-u-m, j-v-n) \right. \\
& + \sum_{(m_1,n_1,m_2,n_2)\in S_h} h_{m_1,n_1,m_2,n_2} \left(\bar{x}(i-m_1-u, j-n_1-v) \sum_{(r,s)\in S_a} \bar{x}(i-m_2-r, j-n_2-s) \right. \\
& \left. \left. \left. + \bar{x}(i-m_2-u, j-n_2-v) \sum_{(k,l)\in S_a} \bar{x}(i-m_1-k, j-n_1-l) \right) \right\} \right]
\end{aligned}
\tag{5.1.9}
$$

5.1.3 Simulation Studies

The proposed three layer neural network was implemented for blind image restoration. The form of the nonlinear blurring function is given in Table 5.1. The weights of the neural network were initialized using GA's and then updated using eqs. (5.1.6), (5.1.7), and (5.1.9). The momentum term and a little noise were added in the learning process in order to get out of the local minima and flat plateau. Branin's method [78] was also employed, which changes the sign of the learning parameter if the error becomes greater than the previous one thus improving the convergence of the algorithm.

The algorithm has been applied on linear motion blur or de-focused images in which nonlinearity of the imaging sensor was also considered. The performance of the network was evaluated for Gaussian blur function with two types of noises, i.e. quantization noise and AWGN.

Table 5.1 The form of nonlinear blurring function.

a) The form of linear part of the blurring function, i.e. $h_{m,n}$, is given as

l_6	l_5	l_4	l_5	l_6
l_5	l_3	l_2	l_3	l_5
l_4	l_2	l_1	l_2	l_4
l_5	l_3	l_2	l_3	l_5
l_6	l_5	l_4	l_5	l_6

b) The form of nonlinear part of the blurring function, i.e . h_{m_1,n_1,m_2,n_2} , is given as

q12	q11	q10	q11	q12	q11	q10	q9	q10	q11	q10	q9	q8	q9	q10	q11	q10	q9	q10	q11	q12	q11	q10	q11	q12
q11	q9	q8	q9	q11	q10	q8	q7	q8	q10	q9	q7	q6	q7	q9	q10	q8	q7	q8	q10	q11	q9	q8	q9	q11
q10	q8	q6	q8	q10	q9	q7	q6	q7	q9	q8	q6	q4	q6	q8	q9	q7	q6	q7	q9	q10	q8	q6	q8	q10
q11	q9	q8	q9	q11	q10	q8	q7	q8	q10	q9	q7	q6	q7	q9	q10	q8	q7	q8	q10	q11	q9	q8	q9	q11
q12	q11	q10	q11	q12	q11	q10	q9	q10	q11	q10	q9	q8	q9	q10	q11	q10	q9	q10	q11	q12	q11	q10	q11	q12
q11	q10	q9	q10	q11	q9	q8	q7	q8	q9	q8	q7	q6	q7	q8	q9	q8	q7	q8	q9	q11	q10	q9	q10	q11
q10	q8	q7	q8	q10	q8	q6	q5	q6	q8	q7	q5	q4	q5	q7	q8	q6	q5	q6	q8	q10	q8	q7	q8	q10
q9	q7	q5	q7	q9	q7	q5	q4	q5	q7	q6	q4	q2	q4	q6	q7	q5	q4	q5	q7	q9	q7	q5	q7	q9
q10	q8	q7	q8	q10	q8	q6	q5	q6	q8	q7	q5	q4	q5	q7	q8	q6	q5	q6	q8	q10	q8	q7	q8	q10
q11	q10	q9	q10	q11	q9	q8	q7	q8	q9	q8	q7	q6	q7	q8	q9	q8	q7	q8	q9	q11	q10	q9	q10	q11
q10	q9	q8	q9	q10	q8	q7	q5	q7	q8	q6	q5	q4	q5	q6	q8	q7	q5	q7	q8	q10	q9	q8	q9	q10
q9	q7	q6	q7	q9	q7	q5	q3	q5	q7	q5	q3	q2	q3	q5	q7	q5	q3	q5	q7	q9	q7	q6	q7	q9
q8	q6	q4	q6	q8	q6	q4	q2	q4	q6	q4	q2	q1	q2	q4	q6	q4	q2	q4	q6	q8	q6	q4	q6	q8
q9	q7	q6	q7	q9	q7	q5	q3	q5	q7	q5	q3	q2	q3	q5	q7	q5	q3	q5	q7	q9	q7	q6	q7	q9
q10	q9	q8	q9	q10	q8	q7	q5	q7	q8	q6	q5	q4	q5	q6	q8	q7	q5	q7	q8	q10	q9	q8	q9	q10
q11	q10	q9	q10	q11	q9	q8	q7	q8	q9	q8	q7	q6	q7	q8	q9	q8	q7	q8	q9	q11	q10	q9	q10	q11
q10	q8	q7	q8	q10	q8	q6	q5	q6	q8	q7	q5	q4	q5	q7	q8	q6	q5	q6	q8	q10	q8	q7	q8	q10
q9	q7	q5	q7	q9	q7	q5	q4	q5	q7	q6	q4	q2	q4	q6	q7	q5	q4	q5	q7	q9	q7	q5	q7	q9
q10	q8	q7	q8	q10	q8	q6	q5	q6	q8	q7	q5	q4	q5	q7	q8	q6	q5	q6	q8	q10	q8	q7	q8	q10
q11	q10	q9	q10	q11	q9	q8	q7	q8	q9	q8	q7	q6	q7	q8	q9	q8	q7	q8	q9	q11	q10	q9	q10	q11
q12	q11	q10	q11	q12	q11	q10	q9	q10	q11	q10	q9	q8	q9	q10	q11	q10	q9	q10	q11	q12	q11	q10	q11	q12
q11	q9	q8	q9	q11	q10	q8	q7	q8	q10	q9	q7	q6	q7	q9	q10	q8	q7	q8	q10	q11	q9	q8	q9	q11
q10	q8	q6	q8	q10	q9	q7	q6	q7	q9	q8	q6	q4	q6	q8	q9	q7	q6	q7	q9	q10	q8	q6	q8	q10
q11	q9	q8	q9	q11	q10	q8	q7	q8	q10	q9	q7	q6	q7	q9	q10	q8	q7	q8	q10	q11	q9	q8	q9	q11

5.1.3.1 Blind Image Deconvolution of Nonlinearly Degraded Images with Uniform Quantization Noise

The two types of blurred images were obtained by using two different 5×5 nonlinear Gaussian blurring functions to produce degraded image having SNR of 30db and 20db which represents the degraded images with high SNR and low SNR, respectively. Then a small quantization noise was also added to check the performance of the neural network in the presence of this noise.

Figure 5.1 shows the degraded images with high SNR and images restored with the neural network model. The restored images show that feather on the hat of 'Lena' image are more sharp and clear than the restored images obtained using neural network based on linear ARMA model as shown in Figure 4.4. However, the proposed method provides comparable estimation of blurring parameters as shown by the NMSE of estimated blur in Table 5.2.

Figure 5.2 shows the degraded images with low SNR and images restored with the neural network model. The proposed network produced significant restoration even when the degraded images had low SNR. The blur was also estimated with comparable accuracy to the results of neural network based on linear ARMA model as shown by the NMSE of estimated blur which is indicated in Table 5.2.

5.1.3.2 Blind Image Deconvolution of Nonlinearly Degraded Images with AWGN

The two types of blurred images were obtained by using two different 5×5 nonlinear Gaussian blurring functions with high SNR and low SNR along with 30db AWGN noise.

(a) (b)

Figure 5.1 Blind image deconvolution of nonlinearly degraded images small quantization noise having SNR of 30db using neural networks based on linear AR model. a) Degraded image of 'Lena'. b) 'Lena' image restored using neural network.

(a) (b)

Figure 5.2 Blind image deconvolution of nonlinearly degraded images with small quantization noise having SNR of 20db using neural networks based on linear AR process. a) Degraded image of 'Lena'. b) 'Lena' image restored using neural network.

Table 5.2 NMSE of estimated blur and ISNR of restored images after blind image deconvolution of nonlinearly degraded images with quantization noise having 20 db and 30db SNR using neural networks based on linear AR model.

Performance measure	SNR of 30db	SNR of 20db
ISNR	3.016127	2.8512
NMSE	0.116847	0.004589

(a) (b)

Figure 5.3 Blind image deconvolution of nonlinearly degraded images with AWGN having SNR of 30db using neural networks based on linear AR model. a) Degraded image of 'Lena', b) 'Lena' image restored using neural network.

(a) (b)

Figure 5.4 Blind image deconvolution of nonlinearly degraded images with AWGN having SNR of 20db using neural networks based on linear AR model. a) Degraded image of 'Lena', b) 'Lena' image restored using neural network.

Table 5.3 NMSE of estimated blur and ISNR of restored images after blind image deconvolution of nonlinearly degraded images with AWGN having 20 db and 30db SNR using neural networks based on linear AR model.

Performance measure	SNR of 30db	SNR of 20db
ISNR	2.46068	2.185799
NMSE	0.115554	0.00456

The performance of the neural network was evaluated in terms of ISNR of the restored image and NMSE of the identified blur. The restored images show quite promising results in terms of image quality and blur estimation. Figure 5.3 shows the degraded images with high SNR along with images restored using neural network model based on nonlinear MA model and linear AR model. Table 5.3 shows the ISNR of the restored image and NMSE of the identified blur.

Figure 5.4 shows the degraded images with low SNR and images restored with the proposed neural network model. In case of degraded image with low SNR having AWGN, slight noise amplification has also been observed along with the restoration of the blurred images. However, quality of the restored images is still better than the linear model.

5.2 Neural Network for Blind Deconvolution of Nonlinearly Degraded Images using Nonlinear ARMA Model

In this section, a nonlinear ARMA model is proposed to solve the blind image deconvolution of nonlinearly degraded images. The linear image model was used, which assumes that the images should be smooth in nature, as represented by eq (4.1.1). In fact images can contain sharp contrasts in certain parts of images. Therefore, in this section, we have proposed a nonlinear image model in order to cater for the sharp contrasts that occur in the natural images. It is this nonlinear image model which is the main motivation of this chapter. The nonlinear image model is also model similar to the Volterra filters and it is given as

$$x(i,j) = \sum_{(k,l)\in S_a} a_{k,l}x(i-k,j-l) + \sum_{(k_1,l_1,k_2,l_2)\subset S_a} a_{k_1,l_1,k_2,l_2} < x(i-k_1,j-l_1)x(i-k_2,j-l_2) >_{255} + v_1(i,j) \quad (5.2.1)$$

However, the blurred image was modeled as a nonlinear process using 2nd order Volterra filter as represented in eq (5.1.1). The same assumptions like positive, symmetric and zero phase PSF, are also made in order to avoid the problems of the estimating $a_{k,l}$, a_{k_1,l_1,k_2,l_2}, $h_{m,n}$ and h_{m_1,n_1,m_2,n_2} due to high computational complexity of point spread functions with large support, instability of the algorithm, and non-unique solution.

5.2.1 Neural network for Blurred Image Representation

This artificial neural network resembles the network explained in the previous section. The structure of the network also consists of three 2-D structured layers L_1, L_2 and L_3 with $M \times N$ neurons. The operation between the first layer L_1 and the second layer L_2 was assumed to be equivalent to that of a nonlinear auto-associative network, which is excited by a random Gaussian process. The information then passes forward from the second layer L_2 to the third layer L_3 by a nonlinear hetero-associative process. The output of the third layer L_3 is the estimate of the observed blurred image. Initially, the inputs to the first layer L_1 are assumed to be a random Gaussian process image with no information about the original image. $a_{k,l}$ and a_{k_1,l_1,k_2,l_2}, are weights of connection between layers L_1 and L_2 which are initiated according to some criteria, i.e. GA's, and then updated to optimize the solution. The operation between the first and the second layer will be

$$\hat{x}(i,j) = \sum_{(k,l)\in S_a} a_{k,l}\bar{x}(i-k,j-l) + \sum_{(k_1,l_1,k_2,l_2)\in S_a} a_{k_1,l_1,k_2,l_2} < \bar{x}(i-k_1,j-l_1)\bar{x}(i-k_2,j-l_2) >_{255} + v_1(i,j) \tag{5.2.2}$$

The neuron values of the second layer L_2, i.e. $\hat{x}(i,j)$, are then fedback to the corresponding neurons of the first layer L_1 i.e., $\bar{x}(i,j) = \hat{x}\_(i,j)$, for the next iteration. The operation between second layer L_2 and third layer L_3 defines the nonlinear hetero-associative operation or MA process. The output of the *(i,j)th* neuron of the third layer will be calculated using eq (5.1.3). The structure of the proposed neural network is same as shown in Figure 4.2 where the image model coefficients $a_{k,l}$ and a_{k_1,l_1,k_2,l_2} are represented by A. However, H is the same nonlinear blurring function having blurring parameters $h_{m,n}$ and h_{m_1,n_1,m_2,n_2}.

5.2.2 Learning Algorithm

A gradient-based algorithm was used to train and optimize the network by minimizing the same hetero-associative errors given in eq (4.2.5) and the auto-associative error given in eq (4.2.6). The updating expressions for the weights between L_2 and L_3, which only depend on E_y, were calculated using eqs (5.1.4) and (5.1.5). However, same updating expressions were obtained as given in eq (5.1.6) and (5.1.7).

The weights of the auto-associative network are related to E_x in L_2 and E_y propagated form L_3. Therefore, the coefficients of the linear part of the auto-associative network are iteratively updated by using eq (5.1.8) and the coefficients of the nonlinear part of the auto-associative network are updated using the following expression

$$a_{u_1,v_1,u_2,v_2}^{new} = a_{u_1,v_1,u_2,v_2}^{old} - \beta \frac{\partial\{E_y(w) + E_x(w)\}}{\partial a_{u_1,v_1,u_2,v_2}} \tag{5.2.3}$$

We find the following updating equation for $a_{u,v}$,

$$\begin{aligned} a_{u,v}^{new} = a_{u,v}^{old} + \beta \sum_{(i,j)\in R_2} \Bigg[& \frac{2}{M\times N}\{\bar{x}(i,j) - \hat{x}(i,j)\}\bar{x}(i-u, j-v) \\ & + \frac{2}{M\times N}\{y(i,j) - \hat{y}(i,j)\}\Bigg\{ \sum_{(m,n)\in S_h} h_{m,n}\bar{x}(i-u-m, j-v-n) \\ & + \sum_{(m_1,n_1,m_2,n_2)\in S_h} h_{m_1,n_1,m_2,n_2}\big(\bar{x}(i-m_1-u, j-n_1-v)\hat{x}(i-m_2, j-n_2) \\ & + \bar{x}(i-m_2-u, j-n_2-v)\hat{x}(i-m_1, j-n_1)\big)\Bigg\}\Bigg] \end{aligned} \tag{5.2.4}$$

and for a_{k_1,l_1,k_2,l_2}

$$\begin{aligned} & a_{u_1,v_1,u_2,v_2}^{new} \\ & = a_{u_1,v_1,u_2,v_2}^{old} + \alpha_{a_2} \sum_{(m,n)\in R_2} \Bigg[\frac{2}{M\times N}\{\bar{x}(m,n) - \hat{x}(m,n)\}\bar{x}(m-u_1, n-v_1)\bar{x}(m-u_1, n-v_1) \\ & + \frac{2}{M\times N}\{y(m,n) - \hat{y}(m,n)\}\Bigg[\sum_{(i,j)\in S_h} h_{i,j}\bar{x}(m-i-u_1, n-j-v_1)\bar{x}(m-i-u_2, n-j-v_2) \\ & + \sum_{(i_1,j_1,i_2,j_2)\in S_h} h_{i_1,j_1,i_2,j_2}\{\hat{x}(m-i_1, n-j_1)\bar{x}(m-i_2-u_1, n-j_2-v_1)\bar{x}(m-i_2-u_2, n-j_2-v_2) \\ & + \hat{x}(m-i_2, n-j_2)\bar{x}(m-i_1-u_1, n-j_1-v_1)\bar{x}(m-i_1-u_2, n-j_1-v_2)\}\Bigg]\Bigg] \end{aligned} \tag{5.2.5}$$

5.2.3 Simulation Studies

The algorithm has been applied on nonlinear motion blur or de-focused images in which nonlinearity of the imaging sensor was also considered. The results were tested on degraded images with both high SNR and low SNR. The neural network was based on the

nonlinear, image and degradation models. The form of the $h_{m,n}$ and h_{m_1,n_1,m_2,n_2} assumed in the view of the assumptions is shown in Table 5.1.

5.2.3.1 Blind Deconvolution of Nonlinear Degraded Images with Uniform Quantization Noise

The two blurred images were obtained by using two different 5×5 nonlinear Gaussian blurring functions with SNR of 30db and 20db which represents the degraded images with high SNR and low SNR, respectively. Then a small quantization noise was also added to check the performance of the neural network in the presence of this noise.

Figure 5.5 shows the nonlinearly degraded image with small quantization noise, having high SNR, and image restored with the neural network based on nonlinear ARMA model. The network provided better performance as compared with the results of nonlinearly degraded image restored using neural network based on linear AR model. Table 5.4 gives NMSE of the estimated nonlinear blur and ISNR in the restored images.

Figure 5.6 shows the nonlinearly degraded image with low SNR and image restored with the neural network based on nonlinear ARMA model. The NMSE of the estimated nonlinear blur and ISNR in the restored images of degraded images with low SNR is also shown in Table 5.4.

(a) (b)

Figure 5.5 Blind image deconvolution degraded images with quantization noise, having SNR of 30db, using neural networks based on nonlinear ARMA model. a) Degraded image of 'Lena' , b) Restored 'Lena' image.

(a) (b)

Figure 5.6 Blind image deconvolution degraded images with quantization noise, having SNR of 20db, using neural networks based on nonlinear ARMA model. a) Degraded image of 'Lena' , b) Restored 'Lena' image.

Table 5.4 NMSE of estimated blur and ISNR of restored images after blind image deconvolution of nonlinearly degraded images with quantization noise having 20 db and 30db SNR using neural networks based on nonlinear ARMA model.

Performance measure	SNR of 30db	SNR of 20db
ISNR	3.01055	2.8
NMSE	0.084016	0.006948

5.2.3.2 Blind Image Deconvolution of Nonlinearly Degraded Images with AWGN

The two types of blurred images were obtained by using two different 5×5 linear Gaussian blurring functions with SNR of 30db and 20db which represents the degraded images with high SNR and low SNR, respectively. Then 30db AWGN noise was also added to check the performance of the neural network in the presence of this noise.

Figure 5.7 shows the nonlinearly degraded images with AWGN, having high SNR, and images restored with the neural network model. Table 4.3 shows the blurring functions used to degrade the images, estimated blurring function obtained from the neural network and ISNR in the restored images.

Figure 5.8 shows the degraded images with low SNR and images restored with the neural network model. Table 5.5 shows the NMSE of estimated blur and ISNR of restored images after blind image deconvolution of nonlinearly degraded images with AWGN having SNR of 20 db and 30db using neural networks based on nonlinear ARMA model.

(a) (b)

Figure 5.7 Blind image deconvolution of nonlinearly degraded images with AWGN, having SNR of 30db, using neural network based on nonlinear ARMA model. a) Degraded image of 'Lena', b) Restored image of 'Lena'

(a) (b)

Figure 5.8 Blind image deconvolution of nonlinearly degraded images with AWGN, having 20db SNR, using neural networks based on nonlinear ARMA model. a) Degraded image of 'Lena', b) Restored image of 'Lena'.

Table 5.5 NMSE of estimated blur and ISNR of restored images after blind image deconvolution of nonlinearly degraded images with AWGN having 20 db and 30db SNR using neural networks based on nonlinear ARMA model.

Performance measure	SNR of 30db	SNR of 20db
ISNR	2.865799	2.288236
NMSE	0.089488	0.03233

Chapter 6

A New Space-Variant Neural Network Approach to Blind Image Deconvolution

The spatially variant blurs occur in variety of applications e.g. when two or more objects moving with different velocities relative to a recording device produce spatially variant motion blurs. Spatially variant blurs also occur when the object and image coordinates are tilted relative to each other, as well as in X-ray projection imaging, lens distortions, wave aberrations, and spatially varying Gaussian type blurs [79][80]. The early methods, for restoring image degraded by spatially variant blurs, are geometrical transformation techniques [81], but are not practical for complicated blurs. Another approach, which can treat a more general class of blurs, is based on the assumption that the blur is approximately spatially invariant in small sub-regions of image domain. These sectioning methods [82][83] partition the image, restoring each local region using its corresponding spatially invariant PSF, and results are then sewn together to obtain the restored image.

The goal of space-variant blind image restoration algorithms is described concisely as identification of useful *a priori* information such as the variant features of input images, integration of extracted knowledge into the schemes without compromising their flexibility, and development of appropriate computational techniques to optimize the cost function. In this section, we will develop an algorithm that addresses these requirements for systematic

image restoration, intelligent information integration using neural networks with massive parallel computing architectures, and effective optimization techniques. The proposed neural network-based scheme for image restoration can identify not only the space-variant noncausal blur function but can also cater for sharp contrasts that occur in the natural images along with the additive noise suppression in smooth backgrounds and restoration of severely blurred images. The structure of the proposed network is divided into small sub-regions, and autoregressive (AR) and moving average (MA) processes are implemented in view of the activity of the sub-regions.

A cost function, motivated by the human perception system is also assumed which consists of five parts i.e. data fidelity measure, image regularization error, blur domain regularization errors, local standard deviation mean square error (LSMSE) between degraded and an estimate of degraded image, and local standard deviation mean square error (LSMSE) between restored and degraded image. The first three terms are widely reported in literature while the last two terms are new, and are one of the motivations of this chapter. The structure of the neural network model is a combination of two adaptive associative networks and a random Gaussian process, to estimate the coefficients of the space-variant blur model and image model. The nonlinear estimation and restoration procedures are implemented using a dynamic iterative algorithm to minimize the error functions of the network. It provides a self-organization like structure to solve the problems without original undistorted data and blur information.

6.1 Image and Degradation Models

We have used linear image and degradation model for simplicity in the space-variant blind image restoration algorithm. Therefore, the state space representation of these models is given below:

$$x(i,j) = \sum_{(k,l)\in S_a} a_{k,l}^{\Lambda(A)} x(i-k, j-l) + v_1(i,j) \tag{6.1.1}$$

$$y(i,j) = \sum_{(m,n)\in S_h} h_{m,n}^{\Lambda(A)} x(i-m, j-n) + v_2(i,j) \tag{6.1.2}$$

where $x(i,j)$ is the undegraded image value at (i,j) and $y(i,j)$ is the observed image distorted by a space-variant blurring function or point spread function (PSF) $h_{m,n}^{\Lambda(A)}$. $v_1(i,j)$ and $v_2(i,j)$ are additive white Gaussian noises which are mutually independent with zero mean and variances $\sigma_{v_1}^2$ and $\sigma_{v_2}^2$, respectively. The $\{a_{k,l}^{\Lambda(A)}\}$ are noncausal minimum variance representation (NMVR) coefficients and S_a is the support of this noncausal model. There are practical difficulties in estimating $a_{k,l}$ and $h_{m,n}$ due to instable and non-unique solution. Therefore, in order to avoid these situations, the PSF $h_{m,n}^{\Lambda(A)}$ is assumed to be positive, symmetric and has zero phase [73]. As the image formation system is assumed not to absorb or generate energy. Therefore, the total energy in the object is equal to that of the observed image [8]

$$\sum_{(m,n)\in S_h} h_{m,n}^{\Lambda(A)} = 1 \tag{6.1.3}$$

6.2 Neural Network for Blurred Image Representation

A 2-D, three-layer feed-forward neural network structure can be presented to identify the space-variant noncausal blur function and restore the degraded image, simultaneously. This structured network was decomposed into two space-variant adaptive associative networks [33] where each layer of the neural network is sub divided into small region called blocks. The operation between the first layer L_1 and the second layer L_2 was assumed to be equivalent to that of a space-variant auto-associative network which is excited by a random Gaussian process. The information then passes forward from the second layer L_2 to the third layer L_3 by a space-variant hetero-associative process. The output of the third layer L_3 is the estimate of the observed blurred image. The weights of the two associative networks were updated in parallel according to the error functions. When the networks have converged to stable states, weights of the hetero-associative network equal the coefficients of unknown blur function and the undegraded image is obtained from the second layer.

6.2.1 Activity

It has been observed that degradation effects are more severe in the region with high texture of activity and noise does not contribute much as for as the visual quality of the image is concerned. However, the effect of the degradation is not severe in the smooth or low activity regions but the effect of noise in smooth regions will affect the visual quality of the image badly. Therefore, in order to suppress noise in the smooth regions and to enhance the sharpness in high activity region, we have proposed to use activity as one the measure

along with the cost functions. All the three, 2-D structured, layers L_1, L_2 and L_3 having same number of $(M \times N)$ neurons, were divided into small blocks of reasonable sizes. The activity $\Lambda(A)$ of each block of the degraded image was calculated, using the following relation [71]:

$$\Lambda(A) = \sum_{\text{even } i,j} \sum_{s=-1}^{1} \sum_{t=-1}^{1} \{y_A(i,j) - y_A(i+s, j+t)\}^2 \qquad (6.2.1)$$

According to the activity $\Lambda(A)$, these blocks were then categorized to belong to one of the four categories i.e., very high (VH) activity, high (H) activity, low (L) activity and very low (VL) activity. This information was then used by the neural network to treat the block accordingly.

6.2.2 Identification and Restoration

Initially, the inputs to the first layer L_1, which is converted into small block, are assumed to be a random Gaussian process image with degraded image information $y(i,j)$. $a_{k,l}^{\Lambda(A)}$ are four different types of weights of connection between the blocks of layers L_1 and L_2 according to the activity $\Lambda(A)$ of the blocks. These weights are also named as image model coefficients and are initiated according to some criterion and are then updated to optimize the solution. The space-variant auto-associative operation between the first and the second layer, of any block A, will be given as:

$$\hat{x}_A(i,j) = \sum_{(k,l) \in S_a} a_{k,l}^{\Lambda(A)} \overline{x}_A(i-k, j-l) + v_1(i,j) \qquad (6.2.2)$$

where $\hat{x}_A(i,j)$ represents output of the $(i,j)^{th}$ neuron, in A^{th} block of the second layer L_2 and $v_1(i,j)$ is the white Gaussian noise with zero mean and variance $\sigma_{v_1}^2$. S_a is the subset

of the whole region R_1 $(M \times N$ matrix$)$in L_1. This structure is similar to the AR model in the noncausal system. The $(i,j)^{th}$ neuron in L_2 is computed from neighboring neuron of its corresponding $\bar{x}_A(i,j)$ in L_1 except $\bar{x}_A(i,j)$. The dependence of the second layer outputs on the weights of different neurons is the same if the weights in this layer correspond to the same coefficients of the image NMVR model. This autoassociative network between L_1 and L_2 is an indirect generalization of the Hopfield circuit model [71], which is itself a special case of the Cohen-Grossberg theorem [84]. Moreover, the data processed in this associative model are interval valued and hence depict fuzzy set which is excited by random Gaussian noise [33]. The model adjusts its connection weights to reach an equilibrium state in which its associative error and the error propagated from L_3 are minimized. Once the equilibrium is reached, this model is equivalent to the NMVR model of the image.

The operation between second layer L_2 and third layer L_3 defines the space-variant hetero-associative operation or MA process. The output of the $(i,j)^{th}$ neuron in A^{th} block of the third layer will be calculated as follows

$$\hat{y}_A(i,j) = \sum_{(m,n)\in S_h} h_{m,n}^{\Lambda(A)} \hat{x}_A(i-m, j-n) \tag{6.2.3}$$

where $h_{m,n}^{\Lambda(A)}$ are the connection weights, also called as estimates of coefficients of the space-variant PSF. It is assumed that the point spread function $h_{m,n}^{\Lambda(A)}$, is space-invariant inside a block but also depends upon the activity of the block. S_h is a subset of the whole region R_2

$(M \times N \text{ matrix})$ in L_2. The size of the window S_h determines the order of the eq (6.2.3) .The structure of the proposed neural network is shown in Figure 6.1.

6.2.3 The Cost Function

The identification and restoration processes are implemented simultaneously by using a dynamic iterative algorithm to minimize the error function $E_y(w)$ and $E_x(w)$ of the neural network. The hetero-associative errors $E_y(w)$ consists of data fidelity measure $E_I(w)$ in the layer L_3, image regularization error $E_{II}(w)$, blur domain regularization error $E_{III}(w)$, local standard deviation mean square error (LSMSE) of degraded with an estimate of degraded image $E_{IV}(w)$, and local standard deviation mean square error (LSMSE) of restored and degraded image $E_V(w)$ i.e., [85][86]

$$E_y(w) = E_I(w) + E_{II}(w) + E_{III}(w) + E_{IV}(w) + E_V(w) \tag{6.2.4}$$

where weight vector w consists of $\{h_{m,n}\}$ and $\{a_{k,l}\}$ for all m,n,k,l. The first three terms involved in hetero associative error are given below:

$$E_I(w) = \frac{1}{MN} \sum_{(i,j)\in R_3} \{y_A(i,j) - \hat{y}_A(i,j)\}^2 \tag{6.2.5}$$

$$E_{II}(w) = \frac{\lambda_{A(A)}}{MN} \sum_{(i,j)\in R_3} \sum_{(m,n)} \{d_{m,n}\hat{x}_A(i-m, j-n)\}^2 \tag{6.2.6}$$

$$E_{III}(w) = \frac{\varphi}{MN} \sum_{(m,n)} \sum_{(q,r)} \{\phi_{q,r} h_{m-q,n-r}\}^2 \tag{6.2.7}$$

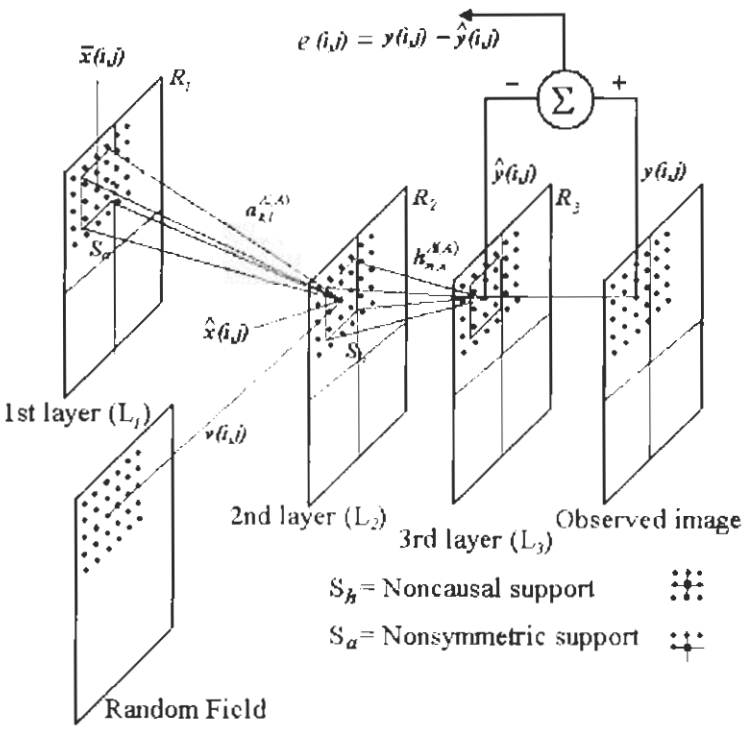

Figure 6.1 The structure of the proposed artificial neural network based on linear space-variant ARMA model.

where φ is the learning parameter and $\phi_{q,r}$ is the high pass filter. Three terms in hetero associative error, which are given in eq (6.2.5), (6.2.6) and (6.2.7), are widely reported in literature. The fist term in eq (6.2.4) is data fidelity measure and is minimized when $\hat{x}(i,j)$ is equal to the original image, where as second term in (6.2.4) increases in the presence of noise. Therefore, $\lambda_{\Lambda(A)}$ should be taken higher for smooth blocks and low for textured blocks, in order to regularize image more in smooth regions than the textured ones. Likewise, the third term in (6.2.4) is blur domain regularization term which is used to render piece-wise smoothness in the blur.

The last two terms are proposed from the motivation of human perception system because the terms presented in eq (6.2.5), (6.2.6) and (6.2.7), favour slow variations in the image and bear very little relationship to the manner in which humans view the differences between two images. Humans tend to pay more attention to sharp differences in intensity within an image e.g., edges and noise in background regions. Hence an error measure should take into account the concept that low variance regions in original image should remain low variance regions in the enhanced image, and high variance regions in the original image likewise remain high variance regions. Therefore, we have included two error measures which attempts to quantify the statistical differences between regions in an image rather than the differences between individual pixels which are given below:

$$E_{IV}(w) = \frac{1}{MN} \sum_{(i,j)\in R_3} \left\{ \sigma_A^2\left(\hat{y}_A(i,j)\right) - \sigma_A^2\left(y_A(i,j)\right) \right\}^2 \qquad (6.2.8)$$

$$E_V(w) = MN \sum_{(i,j)\in R_3} \left\{ \sigma_A^2\left(\hat{x}_A(i,j)\right) - \sigma_A^2\left(y_A(i,j)\right) \right\}^{-2} \qquad (6.2.9)$$

where the local standard deviation $\sigma_A^2\left(y_A(i,j)\right)$ is defined as

$$\sigma_A^2\left(y_A(i,j)\right)=\sum_{s=i-\frac{B}{2}}^{i+\frac{B}{2}}\sum_{t=j-\frac{B}{2}}^{j+\frac{B}{2}}\left[\frac{y_A(s,t)-M_B\left\{y_A(s,t)\right\}}{B^2}\right]^2 \tag{6.2.10}$$

where the local mean $M_B\left\{y_A(s,t)\right\}$ of the $B\times B$ neighborhood of pixel $y_A(i,j)$ in the image is defined as

$$M_B\left\{y_A(i,j)\right\}=\sum_{s=i-\frac{B}{2}}^{i+\frac{B}{2}}\sum_{t=j-\frac{B}{2}}^{j+\frac{B}{2}}\left[\frac{y_A(s,t)}{B^2}\right] \tag{6.2.11}$$

Therefore, the error $E_{IV}(w)$ given in eq (6.2.8) is termed as local standard deviation mean square error (LSMSE) of degraded with an estimate of degraded image. It is important because the mean square error between the two standard deviations gives an indication of the degree of similarity between the two images. The proposed LSMSE error between degraded image and an estimate of degraded image should be minimized in order to obtain homogeneous statistical regions.

However, the last term in the (6.2.4) shows local standard deviation mean square error (LSMSE) of restored and degraded image as shown in eq (6.2.9). As degradation is more severe in highly textured regions, which in turn causes decrease in corresponding local variance, therefore the error $E_{IV}(w)$ takes care of this decrease in local variance in degraded images. Hence the two proposed errors will cause smooth regions to remain noise free as much as possible and highly textured regions to be enhanced accordingly.

The second important error for the neural network is autoassociative error $E_x(w)$, which consist of only data fidelity measure between the layer L_1 and L_2 is given as

$$E_x(w) = \frac{1}{MN} \sum_{(i,j)\in R_2} \{\bar{x}_A(i,j) - \hat{x}_A(i,j)\}^2 \tag{6.2.12}$$

The next subsection will represent how errors have been minimized for the neural network.

6.2.4 Learning Algorithm

A gradient-based algorithm was used to train and optimize the network by minimizing the squares of errors. According to Figure 6.1 and its associated discussions, there is special requirement for the identification and restoration process in this neural network. The weights of different neurons which represent the same NMVR coefficient in L_2 and same PSF coefficients in L_3 must be updated in the same fashions in order for network's output to satisfy eq (6.2.2) and eq (6.2.3) Specifically the weights between L_2 and L_3, only depends upon heteroassociative error $E_y(w)$. Therefore, the PSF will be updated as follows:

$$h_{m,n}^{\Lambda(A)}(new) = h_{m,n}^{\Lambda(A)}(old) - \alpha \frac{\partial E_y(w)}{\partial h_{m,n}^{\Lambda(A)}}$$

$$\frac{\partial E_y(w)}{\partial h_{m,n}^{\Lambda(A)}} = \left\{ \frac{\partial E_I(w)}{\partial h_{m,n}^{\Lambda(A)}} + \frac{\partial E_{II}(w)}{\partial h_{m,n}^{\Lambda(A)}} + \frac{\partial E_{III}(w)}{\partial h_{m,n}^{\Lambda(A)}} + \frac{\partial E_{IV}(w)}{\partial h_{m,n}^{\Lambda(A)}} + \frac{\partial E_V(w)}{\partial h_{m,n}^{\Lambda(A)}} \right\} \tag{6.2.13}$$

where α is an adaptive convergence factor while partial derivatives given in eq (6.2.13) were evaluated and are given below:

$$\frac{\partial E_I(w)}{\partial h_{m,n}^{\Lambda(A)}} = \frac{-2}{MN} \sum_{(i,j)\subset R_3} \left\{ y_A(i,j) - \hat{y}(i,j) \right\} \hat{x}_A(i-m, j-n)$$

$$\frac{\partial E_{II}(w)}{\partial h_{m,n}^{\Lambda(A)}} = 0$$

$$\frac{\partial E_{III}(w)}{\partial h_{m,n}^{\Lambda(A)}} = \left(\frac{4}{A^6 MN} \right) \sum_{(i,j)\in R_3} \left[\left\{ \sigma_A^2\left(\hat{y}_A(i,j)\right) - \sigma_A^2\left(y_A(i,j)\right) \right\} \right.$$
$$\times \left\{ \sum_{p=i-\frac{A}{2}, q=j-\frac{A}{2}}^{i+\frac{A}{2}, j+\frac{A}{2}} \left\{ A^2 \hat{y}_A(p,q) - \sum_{s=i-\frac{A}{2}, t=j-\frac{A}{2}}^{i+\frac{A}{2}, j+\frac{A}{2}} \hat{y}_A(s,t) \right\} \right.$$
$$\left. \left. \times \left\{ A^2 \hat{x}_A(p-m, q-n) - \sum_{s-i-\frac{A}{2}, t=j-\frac{A}{2}}^{i+\frac{A}{2}, j+\frac{A}{2}} \hat{x}_A(s-m, t-n) \right\} \right\} \right]$$

$$\frac{\partial E_{IV}(w)}{\partial h_{m,n}^{\Lambda(A)}} = 0$$

$$\frac{\partial E_V(w)}{\partial h_{m,n}^{\Lambda(A)}} = \frac{2\varphi}{MN} \sum_{k,l} \sum_{s,t} \phi_{s,t} h_{k-s,l-t}^{\Lambda(A)} \phi_{k-m,l-n} \qquad (6.2.14)$$

Therefore, the weights between the layers L_2 and L_3 should be updated using (6.2.13) and (6.2.14). However, The weights of the auto-associative network are related to $E_x(w)$ in L_2 and $E_y(w)$ which propagates form the layer L_3. Therefore, the coefficients of the linear part of the auto-associative network are iteratively updated as

$$a_{k,l}^{\Lambda(A)}(new) = a_{k,l}^{\Lambda(A)}(old) - \beta \frac{\partial\{E_y(w) + E_x(w)\}}{\partial a_{k,l}^{\Lambda(A)}} \tag{6.2.15}$$

where $$\frac{\partial\{E_y(w) + E_x(w)\}}{\partial a_{k,l}^{\Lambda(A)}} = \frac{\partial\{E_I(w) + E_{II}(w) + E_{III}(w) + E_{IV}(w) + E_V(w) + E_x(w)\}}{\partial a_{k,l}^{\Lambda(A)}}$$

where β is also a convergence factor while partial derivatives given in eq (6.2.15) were evaluated and are given below:

$$\frac{\partial E_I(w)}{\partial a_{k,l}^{\Lambda(A)}} = \frac{-2}{MN} \sum_{(i,j)\in R_3} \{y_A(i,j) - \hat{y}_A(i,j)\} \sum_{m,n} h_{m,n}^{\Lambda(A)} \bar{x}_A(i-m-k, j-n-l)$$

$$\frac{\partial E_{II}(w)}{\partial a_{k,l}^{\Lambda(A)}} = \frac{\lambda_{\Lambda(A)}}{MN} \sum_{i,j} \sum_{u,v} \sum_{p,q} d_{u,v} d_{p,q} \hat{x}_A(i-u, j-v) \bar{x}_A(i-p-k, j-q-l)$$

$$\frac{\partial E_{III}(w)}{\partial a_{k,l}^{\Lambda(A)}} = \frac{4}{MNA^6} \sum_{(i,j)\in R_3} \Bigg[\{\sigma_A^2(\hat{y}_A(i,j)) - \sigma_A^2(y_A(i,j))\}$$
$$\times \Bigg\{ \sum_{p=i-\frac{A}{2}, q=j-\frac{A}{2}}^{i+\frac{A}{2}, j+\frac{A}{2}} \Bigg\{ A^2 \hat{y}_A(p,q) - \sum_{s=i-\frac{A}{2}, t=j-\frac{A}{2}}^{i+\frac{A}{2}, j+\frac{A}{2}} \hat{y}_A(s,t) \Bigg\}$$
$$\times \Bigg\{ A^2 \sum_{s,t} h_{s,t}^{\Lambda(A)} \bar{x}_A(p-s-k, q-t-l) - \sum_{s=i-\frac{A}{2}, t=j-\frac{A}{2}}^{i+\frac{A}{2}, j+\frac{A}{2}} \sum_{m,n} h_{m,n}^{\Lambda(A)} \bar{x}_A(s-m-k, t-n-l) \Bigg\} \Bigg\} \Bigg]$$

$$\frac{\partial E_{IV}(w)}{\partial a_{k,l}^{\Lambda(A)}} = \frac{-4MN}{A^2} \sum_{(i,j)\in R_3} \Bigg[\{\sigma_A^2(\hat{x}_A(i,j)) - \sigma_A^2(y_A(i,j))\}^{-3}$$
$$\times \sum_{p=i-\frac{A}{2}, q=j-\frac{A}{2}}^{i+\frac{A}{2}, j+\frac{A}{2}} \Bigg\{ \Big(\hat{x}_A(p,q) - \hat{\bar{x}}_A(i,j)\Big) \Bigg(\bar{x}_A(p-k, q-l) - \frac{1}{A^2} \sum_{s=i-\frac{A}{2}, t=j-\frac{A}{2}}^{i+\frac{A}{2}, j+\frac{A}{2}} \bar{x}_A(s-k, t-l) \Bigg) \Bigg\} \Bigg]$$

$$\frac{\partial E_V(w)}{\partial a_{k,l}^{\Lambda(A)}} = 0$$

$$\frac{\partial E_x(w)}{\partial a_{k,l}^{\Lambda(A)}} = \frac{-2}{MN} \sum_{(i,j)\in R_2} \{\bar{x}_A(i,j) - \hat{x}_A(i,j)\} \bar{x}_A(i-k, j-l)$$

Therefore, the weights between the layers L_1 and L_2 should be updated using (6.2.15).

6.3 Simulation Studies

Therefore, we have implemented a three layer neural network, in each layer, including the given degraded image, was subdivided into smaller block of sizes 16×16 and it was assumed that the blur is space-invariant in each block. Activity of each block of the degraded image was then calculated in order to categorize each. The operation between first two layers was assumed to the space-variant auto-associative process. Therefore, the block with VH activity were treated with one type of $\{a_{k,l}^{VH}\}$ NMVR coefficients, the blocks with H activity were treated with second type of $\{a_{k,l}^{H}\}$ NMVR coefficients, the block with L activity were treated with third type of $\{a_{k,l}^{L}\}$ NMVR coefficients and the blocks with VL activity were treated with last type of $\{a_{k,l}^{VL}\}$ NMVR coefficients. Similarly, second and third layer of the neural network represented the space-variant heteroassociative process containing $h_{m,n}^{\Lambda(A)}$ blurring coefficients for the blocks having activity $\Lambda(A)$ [71]. The momentum term and a little noise were added in the learning process in order to get out of the local minima and flat plateau. Branin's method [78] was also employed, which changes the sign of the learning parameter if the error becomes greater than the previous one and hence improve the convergence of the algorithm.

6.3.1 Blind Deconvolution of the Images Degraded by Space-invariant Gaussian Blur with Uniform Quantization Noise

The blind deconvolution, using space-invariant neural network, of an image degraded by space-invariant Gaussian blur with uniform quantization noise is illustrated in Figure 6.2 and Figure 6.3. The original "Lena" image has dimension of 256×256 with 256 grey levels as shown in Figure. 4.3(a). It was degraded by two different types of 5×5 Gaussian space-invariant masks with some quantization noise to form Figure 6.2(a) and 6.3(a). The blurring coefficients are given in Table 4.1 and 4.2. These degraded images represent the linear motion blur or de-focused image with space-invariant blur having high SNR and low SNR. The proposed algorithm was applied to these degraded images. The final restore images are given in Figure 6.2(b) and Figure 6.3(b). We observed that the restored image recover the fine details near the feather of the hat. In addition it suppresses the quantization noise in the smooth backgrounds effectively.

Our proposed method produces better ISNR of 6.69dB for high SNR (30db) as compared to ISNR of 2.1666db given in Table 4.1 and 4.966db for low SNR (20db) as compared to 1.839db given in Table 4.2. Similarly we have carried out comparison with two other models given in the literature - hierarchical model based neural network by Yap [85] and Hopfield type neural network method by Zhou [32], as shown in Table 6.1. NMSE of our proposed method and hierarchical model based neural network by Yap are 0.0268 and 0.048, respectively. The smaller NMSE value of our method shows that it produces more accurate blurring function estimates than the other one's.

(a) (b)

Figure 6.2 Blind deconvolution of images degraded with linear and space-invariant process, having SNR of 30db, using neural networks based on space-variant linear ARMA model. a) Degraded image of 'Lena' with 30db SNR and small quantization noise, b) Restored image of 'Lena'

(a) (b)

Figure 6.3 Blind deconvolution of images degraded with linear and space-invariant process, having SNR of 20db, using neural networks based on space-variant linear ARMA model. a) Degraded image of 'Lena' with 20db SNR and small quantization noise, b) Restored image of 'Lena'.

Table 6.1 ISNR restored images degraded by Gaussian blur and quantization noise having SNR of 20db with different image restoration methods.

Method	Space-variant neural network	Hierarchical model based NN by Yap	Hopfield NN method by Zhou	
			$\lambda = 10^{-3}$	$\lambda = 10^{-6}$
ISNR (dB)	4.966	4.75	3.39	4.6
NMSE	0.0268	0.048	-	-

6.3.2 Blind Deconvolution of the Images Degraded by Space-Invariant Gaussian Blur with AWGN

This subsection presents the blind deconvolution of an image degraded by space-invariant Gaussian blur with additive white Gaussian noise (AWGN) in order to demonstrate the flexibility of the proposed algorithm. The original image in Figure 4.3(a) was degraded by two different 5×5 Gaussian blurs with standard deviation of 2.0, followed by a 30-dB additive white noise to form noisy and blurred image having high and low SNR as shown in Figure 6.4(a) and 6.5(a). We have applied the same approach as before, to deconvolve the degraded images. The restored images in Figure 6.4(b) and 6.5(b) show that the overall sharpness of the image has been recovered, especially in highly textured regions of the recovered image.

Our proposed method produces ISNR of 4.325dB for high SNR (30db) as compared to ISNR of 2.1666db given in Table 4.1 and 3.465db for low SNR (20db) as compared to 1.839db given in Table 4.2. This is due to the ringing effects and noise amplification in smooth background regions in the algorithm given in chapter 4. The Table 6.2 shows a comparison of ISNR, for low SNR images, of the restored images and NMSE of identified blurs with hierarchical model based neural network by Yap [85]. The identified blur using the proposed method and by Yap [85] produces an NMSE of 0.03599 and 0.032, respectively. As these values are quite close therefore, NMSE value of the two algorithms show equal capacity to achieve accurate blurring function in the presence of AWGN.

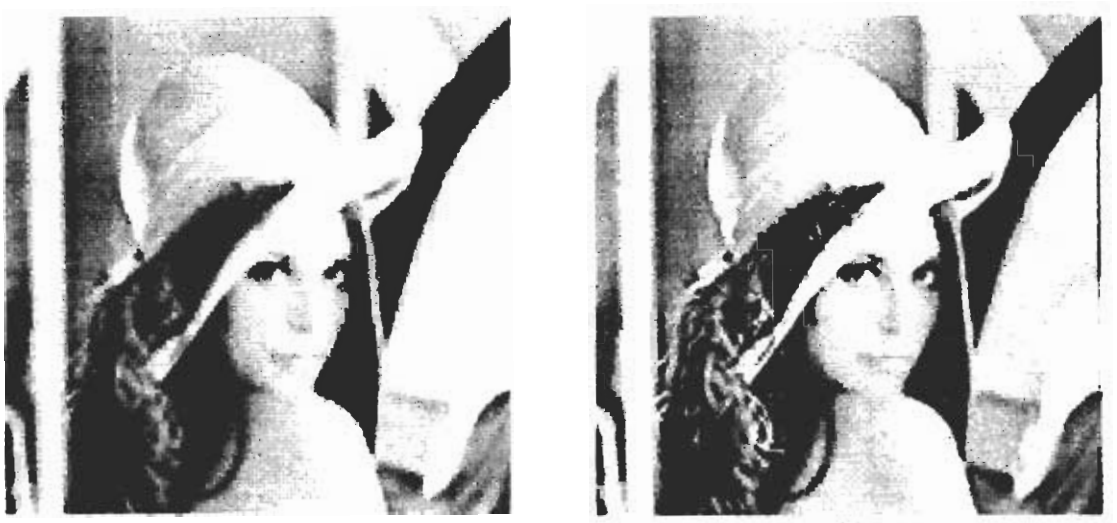

(a) (b)

Figure 6.4 Blind image deconvolution of degraded images with AWGN having 30db SNR using neural networks based on space-variant linear ARMA model. a) Degraded image of 'Lena', b) restored Image.

(a) (b)

Figure 6.5 Blind image deconvolution of degraded images with AWGN having 20db SNR using neural networks based on space-variant linear ARMA model. a) Degraded image of 'Lena', b) Restored image of 'Lena'.

Table 6.2 ISNR of restored images degraded by space-invariant Gaussian blur and AWGN noise having SNR of 20db with different space-invariant image restoration methods

Method	Our proposed algorithm	Hierarchical model based NN by Yap	Hopfield NN method by Zhou	
			$\lambda = 10^{-3}$	$\lambda = 10^{-6}$
ISNR (dB)	3.465	2.95	2.59	0.44
NMSE	0.03599	0.032	-	-

6.3.3 Blind Deconvolution of the Image Degraded by Space-Variant Gaussian Blur

Many real images contain degradations which are space-variant in nature. This could be due to motion of the object localized to a specific region, or relative motion of more than two objects having different velocities, or different types of severe degradations in different parts of the images, etc. Such degradations can however be modeled as space-invariant in the small sub-regions of the image because different regions of the images suffer different types of degradations. The current neural network may be extended to handle such degradations by restoring all the small sub-regions of the degraded image independently. But in order to illustrate the capability of the current algorithm to handle space-variant degradations, we have assumed a specific type of the degraded image in which degradations are subject to the activity of the regions.

The proposed space-variant neural network approach to blind image deconvolution was also evaluated to illustrate its capability to handle a specific type of space-variant Gaussian blur in the presence of quantization noise and AWGN in which space-variant Gaussian blur affects the images according to the activity of the region. In order to obtain degraded images having 30db SNR, we have used a set of four 5×5 Gaussian blurs. The form of these blurs is same as shown in Table 4.3. These blurs were applied to the original image given in Figure 4.3(a) according to the activity of the sub-regions of the image. The small quantization noise or 30db AWGN was also added into the image. Similar procedure was applied to get the degraded image having 20db SNR using another set of four 5×5 Gaussian blurs followed by small quantization noise or 30db AWGN.

(a) (b)

Figure 6.6 Blind deconvolution of images degraded by a linear and space-variant process with quantization noise using space-variant neural network approach. a) Degraded image of 'Lena' having SNR= 30db, b) Restored image of 'Lena'

(a) (b)

Figure 6.7 Blind deconvolution of images degraded by a linear and space-variant process with AWGN using space-variant neural network approach. a) Degraded image of 'Lena' having SNR= 30db, b) Restored image of 'Lena'

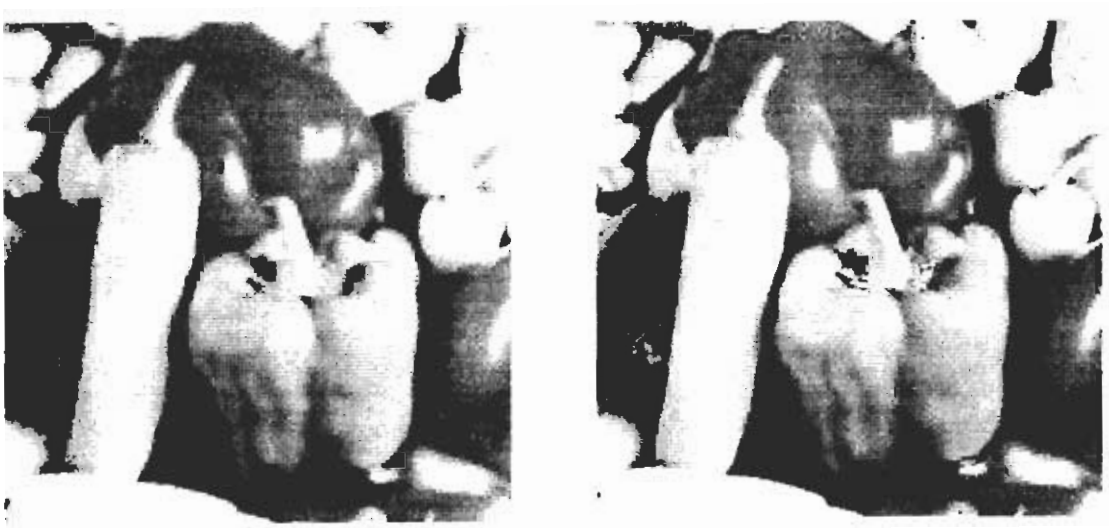

(a) (b)

Figure 6.8 Blind deconvolution of images degraded by a linear and space-variant process with AWGN using space-variant neural network approach. a) Degraded image of 'peppers' having SNR= 30db. b) Restored image of 'peppers'.

(a) (b)

Figure 6.9 Blind deconvolution of images degraded by a linear and space-variant process with quantization noise using space-variant neural network approach. a) Degraded image of 'Lena' having SNR= 20db. b) Restored image of 'Lena'

(a) (b)

Figure 6.10 Blind deconvolution of images degraded by a linear and space-variant process with AWGN using space-variant neural network approach. a) Degraded image of 'Lena' having SNR= 20db. b) Restored image of 'Lena'

Table 6.3 NMSE of estimated blur and ISNR of restored images of 'Lena', after blind deconvolution of images degraded by a linear and space-variant process, having 20 db and 30db SNR, using space-variant neural network approach.

Performance measure	Degraded images with quantization noise having		Degraded images with AWGN having	
	SNR of 30db	SNR of 20db	SNR of 30db	SNR of 20db
ISNR	4.09484	3.765	3.9163	3.492
NMSE	0.0872	0.0143	0.0871	0.0124

The restoration results using the proposed network are shown in Figures 6.6–6.10 along with the degraded images. It is clear that the algorithm is effective in restoring the image by providing the clarity in the fine textured regions while suppressing the noise and ringing effects in the smooth backgrounds. This is in accordance with the ISNR of the restored images and NMSE of the identified blurs shown in Table 6.3. The ISNR of restored images of 'Lena' after blind deconvolution of degraded images having 30db SNR with small quantization noise and AWGN, are 4.09484 and 3.9163, respectively. However, the ISNR of resorted images of 'Lena', after blind deconvolution of degraded images having 20db SNR with small quantization noise and AWGN, are 3.765 and 3.492, respectively. The small NMSE values shown in Table 6.3 represents the close resemblance of the identified blurs to the Gaussian blurs. These satisfactory results illustrate that the proposed technique is useful in blind deconvolution of images degraded under different circumstances, namely Gaussian blurring functions with various noise levels.

Chapter 7

Conclusion

7.1 Summary of Results

In the field of blind image deconvolution, the recent advances in the use of artificial neural networks have been exciting. The artificial neural network provides a level of flexibility and adaptability which has not been fully exploited, so far. For this reason, this dissertation shows that this approach can be extended to handle the case on blind image deconvolution of images suffering from linear or nonlinear and space-invariant or space-variant degradations. Another important factor is visual improvement in the quality of the image which requires that the concepts of human visual perception system should be incorporated in the identification and restoration process by modifying the cost function of the network. Therefore, a very important objective of this dissertation is to develop useable cost functions based on matching of the second order statistics of the images which can describe important human visual criteria.

In this dissertation, we have used the artificial neural network based on autoregressive moving average ARMA network with random Gaussian process in which the noisy and blurred images are modeled as continuous associative networks, where as auto-associative part determines the image model coefficients and the hetero-associative part determines the blur function of the system. We have used genetic algorithms to search for

global minimum of the error performance surface of a blind image restoration problem using artificial neural networks. The weights of the network were first of all initialized using genetic algorithm. Once global minima is near, iterative gradient based algorithm was used to minimize the error function. The self-organization like structure of the proposed neural network provides the potential solution of the blind image restoration problem. The beauty of the algorithm lies in the fact that estimation and restoration are achieved simultaneously.

The neural network has been extended by modifying the linear ARMA process to nonlinear ARMA process in order to handle nonlinear degradations. The artificial neural networks based on nonlinear ARMA models provides better capabilities of restoration of degraded images and identification of blur, in terms of ISNR and NMSE, than the networks based on linear ARMA models.

A new approach to adaptive blind image deconvolution, for space-variant degraded images, based on multilayer neural network has also been proposed. The first subnetwork was treated as space-variant autoassociative network which determine the image model coefficients. The second subnetwork was treated as space-variant heteroassociative network which determines the space-variant blur function. These subnets are space-variant because they convert images into smaller blocks, categorize them according to activity in the blocks and then process the image according to their activities. The highly textured blocks were treated as very high activity regions while slightly less highly textured block were treated as high activity blocks, even less activity block were treated as low activity regions, and smooth blocks were treated as very low activity regions. Therefore, the subnetworks perform their operations in such a way that the sharpness and contrast in very high and high activity regions should be increased as noise is not prominent in textured regions. However,

noise and ringing effects should be suppressed in low and very low activity regions. Therefore, such space-variant blind deconvolution method based on ARMA model was implemented using neural network methodology. The superior restoration results highlight the advantages of space-variant autoregressive and moving average process.

We have also proposed new terms in the cost function for this method which is based upon the human visual perception system. Human eye is not so sensitive to absolute pixel values as it is to edges and textures of images. These are related to local second order statistics i.e., local variances. This cost function contains two proposed terms which are error measures based on the local SOS of the images being compared.

An iterative steepest descent algorithm is implemented to minimize the square of the errors. Therefore, the proposed method provides the more reliable restoration as compared with the other methods in terms of ISNR of restored image and NMSE of identified blur. In addition it is shown that it provides more robustness towards additive noise.

7.2 Future Directions

- The performance of the developed algorithm needs to be further assessed using a range of both controlled and real-world still and moving noisy images representing various scenarios.
- Currently, the images are partitioned into blocks of equal size. In the future, the images could be partitioned into blocks of variable sizes and the size of each block could be set to be inversely proportional to the level of activity of the corresponding region.

- At present, simple thresholds have been used to categorize each block according to its level of activity. In the future, intelligent fuzzy logic based rules could be used to improve the categorization process.
- Currently, linear space-variant degradation processes have been modeled, and these can also be extended to 2^{nd} or 3^{rd} order nonlinear cases.
- In this thesis, the human visual perception based cost functions have been developed in this thesis to match second order statistics of the restored image. In future, the cost function could be extended to match the higher order statistics of the restored image.
- Compression issues have not been addressed in this thesis. These need to be investigated for both still and moving image scenarios.
- Also for the future work, the developed blind deconvolution algorithms could be implemented in hardware for real-time applications and their associated real-time relative computational complexity requirements investigated.
- Finally, the developed algorithms can also be extended to address the problem of multichannel blind image restoration using multiple degraded images of the same scene. The required multiple images of a single degraded image can also be obtained using the concept of directional filter banks.

References:

1 Andrews H. C. and B. R Hunt., Digital Image Restoration, Prentice-Hall, Inc., 1977.

2 Gonzalez, R. C. and R. E. Woods, Digital Image Processing, 2nd Ed., Pearson Edu. 2002.

3 Schulz, T., "Multiframe blind deconvolution of astronomical images", JOSA-A, vol. 10, no. 5, pp. 1064–1073, 1993.

4 Mutihac, R. and V. Hulle, "Bayesian restoration of medical X-ray digital images", Proceedings 2nd Int. Conf. on Electronics, Control and Signal Processing and E-Activities .World Scientific and Engineering Academy and Socicty (WSEA`S), Singapore, 7-12 December 2002, pp. 451-288, 2003.

5 Nguyen, N., P. Milanfar, and G. Golub, "Efficient generalized applications to parametric image restoration and resolution enhancement", IEEE Trans. on Image Processing, vol. 10, no. 9, pp. 1299-1308, 2001.

6 Gull, S. F. and G. J. Daniell, "Image reconstruction from incomplete and noisy data", Nature, vol. 272, pp. 686-690, 1978.

7 Angwin, D. L. and H. Kaufamn, Digital Image Restoration, Springer Verlage, New York, 1991.

8 Kunder D. and D. Hatzinakos, "Blind image deconvolution", IEEE Signal Processing Magazine, May 1996.

9 Tanaka, A., H. Imai and M. Miyakoshi, "On formulations and solutions in linear image restoration problems", IEICE Trans. on Fund. Electr. E87A, vol. 8, pp. 2144-2151, 2004.

10 Kokaram, A., "A statistical framework for picture reconstruction using 2D AR models", Image Vision Comput., vol. 22, no. 2, pp. 165-171, 2004.

11 Boncelet, C., "Image noise models", Handbook of Image and Video Processing, editor Al Bovik, Academic Press, 31 May, 2000.

12 Lagendijk, R. L. and J. Biemond, "Basic methods for image restoration and identification", Handbook of Image and Video Processing, editor Al Bovik, Academic Press, 31 May, 2000.

13 Likhterov, B. and N. S. Kopeika, "Motion-blurred image restoration using modified inverse all-pole filters", J. Electron. Imaging, vol. 13, no. 2, pp. 257-263, 2004.

14 Rajagopalan A. N., S. Chaudhuri and U. Mudenagudi, "Depth estimation and image restoration using defocused stereo pairs", IEEE Trans. on Pattern Anal., vol. 26, no. 11, pp. 1521-1525, 2004.

15 Stark, H., Image Recovery: Theory and Applications, Academic Press, London, 1987.

16 Zehngut, E., Iterative Image Restoration, Technion Press, Haifa, 1988.

17 Zhang D., and Z. Wang, "Impulse noise detection and removal using fuzzy techniques", IEE Elect. Lett., vol. 33, no. 5, pp. 378-379, 1997.

18 Feller, W., An Introduction to Probability Theory and Its Applications, John Wiley and Sons, New York, 1968.

19 Billingsley, P., Probability and Measure, John Wiley and Sons, New York. 1979.

20 Montgomery, D. C. and G. C. Runger, Applied Statistics and Probability for Engineers, John Wiley and Sons, 2nd ed., 1998.

21 Ho, C. W. and M. Nikolova, "Salt-and-pepper noise removal by median-type noise detectors and detail-preserving regularization", accepted for publication by IEEE Transactions on Image Processing.

22 Jain, A. K., "Advances in mathematical models for image processing", Proceeding of the IEEE, vol. 69, no. 5, pp. 502-528, May 1981.

23 Hunt, B. R., "The application of constrained least squares estimation to image restoration by digital computer", IEEE Trans. on Computers, vol. 2, pp. 805- 812, Sept. 1973.

24 Zhang, J., P. Fieguth, and D. Wang, "Random fields", Handbook of Image and Video Processing, editor Al Bovik, Academic Press, 31 May, 2000.

25 Jeng, F. and J. W. Woods, "Compound Gauss-Markov random fields for image estimation", IEEE Trans. on Signal Processing, vol. 39, pp. 683-697, 1991.

26 Tinku A. and A. K. Ray, Image Processing - Principles and Applications, John Wiley & Sons, 2005.

27 Biemond, J., R. L. Lagendijk and R. M. Mersereau, "Iterative methods for image deblurring", Proc. of the IEEE, vol. 78, no. 5, pp. 856-883, May 1990.

28 Sroubek, F. and J. Flussr, "Multichannel blind iterative image restoration", IEEE Trans. on Image Processing, vol. 12, no. 9, pp. 1094-1106, 2003.

29 Nagy, J. G., K. Palmer and L. Perrone, "Iterative methods for image deblurring: a matlab object-oriented approach", Numer. Algorithms, vol. 36, no. 1, pp. 73-93, 2004.

30 Figueiredo, M., and J. Leitão, "Unsupervised image restoration and edge location using compound Gauss-Markov random fields and the MDL principle", in IEEE Trans. on Image Processing, vol 6, n. 8, pp. 1089-1102, August 1997.

31 Shin, J., S. H. Hwang, S. W. Lee, J. Paik, B. Abidi and M. Abidi, "Real-time digital auto- focusing using *a priori* estimated set of PSFs", Opt. Eng. Lett., in preparation for submission, August 2004.

32 Zhou, Y. T., R. Chellappa, A. Vaid and B. K. Jenkins, "Image restoration using neural networks", IEEE Trans. On Acoustics, Speech and Signal Processing, vol. 36, no. 7, pp. 1141-1151, 1988.

33 Cho, C. M. and H. S. Don, "Blur identification and image restoration using a multilayer neural network", IEEE Int. Joint Conf. On Neural Networks, vol. 3, pp, 2558-2563, 1991.

34 Pail, J. K. and A. K. Katsaggelos, "Image restoration using a modified Hopfield network", IEEE Trans. on Image Processing, vol. 1, no. 1, pp. 49-63, 1992.

35 Sun, Y., J. G. Li, and S. Y. Yu, "Improvement on performance of modified Hopfield neural network for image restoration", IEEE Trans. on Image Processing, vol. 4, no. 5, pp. 688-692, 1995.

36 Muneyasu, M., K. Yamamoto and T. Hinamoto, "Image restoration using layered neural networks and Hopfield networks", Proc. of the 1995 Int. conf. on Image Processing (ICIP), pp. 33-36, 1995.

37 Wong, H. S., and L. Guan, "Adaptive regularization in image restoration using a model based neural network", Opt. Eng., vol. 36, no. 12, pp. 3297-3308, 1997.

38 Perry, S. W. and L. Guan, "Weight assignment for adaptive image restoration by neural networks", IEEE Trans. on Neural Networks, vol. 11, no. 1, pp. 156-170, 2000.

39 Wong, H. S. and L. Guan, "A neural learning approach for adaptive image restoration using fuzzy model based network architecture", IEEE Trans. on Neural Networks, vol. 12, no. 3, pp. 516-531, 2001.

40 Yap. K.H., L. Guan, and W. Liu, "A recursive soft decision approach to blind image deconvolution", IEEE Trans. on Signal Processing, vol. 51, no. 2, pp. 515-526, 2003.

41 Robini, M. C. and I. E. Magnin, "Stochastic nonlinear image restoration using the wavelet transform", IEEE Trans. on Image Processing, vol 12, no. 8, pp. 890-905, 2003.

42 Figueiredo, M. A. T., and R. D. Nowak, "An EM algorithm for wavelet based image restoration", IEEE Trans. on Image Processing, vol 12, no. 8, pp. 906-916, 2003.

43 Antoniadis, A. and J. Fan, "Regularized wavelet approximations", J. Amer. Statist. Assoc., vol. 96, pp. 939-967, 2001.

44 Banham, M. and A. Katsaggelos, "Spatially adaptive wavelet based multiscale image restoration", IEEE Trans. on Image Processing, vol. 5, pp. 619-634, 1996.

45 Belge, M., M. E. Kilmer and E. L. Miller, "Wavelet domain image restoration with adaptive edge preserving regularity", IEEE Trans. on Image Processing, vol. 9, pp. 597-608, 2000.

46 Qureshi, I. M., T. A. Cheema, A. Naveed and A. Jalil, "Genetic algorithms based artificial neural networks for blur identification and restoration of degraded images", Pakistan Journal of Information and Technology, vol. 2, no. 1, pp. 21-24, 2003.

47 McCallum, B. C., "Blind deconvolution by simulated annealing", Opt. Comm., vol. 75, no. 2, pp. 101-105, 1990.

48 Alder, D., "Genetic algorithms and simulated annealing: a marriage proposal", IEEE Int. Conf. on Neural Networks, pp. 1104-1109, 1993.

49 Robini, M. C., T. Rastello, and I. E. magnin, "Simulated annealing, acceleration techniques and image restoration", IEEE Tran. on Image Processing, vol. 8, no. 10, pp. 1374-1387, 1999.

50 May K., T. Stathaki and A. G. Constantinides, "A simulated annealing genetic algorithm for blind deconvolution of nonlinearly degraded images", IEEE Workshop on Nonlinear Signal and Image Processing, Mackinac Island, September 1997.

51 Giannakis, G. B., and R. W. Heathe, "Blind identification of multichannel FIR blurs and perfect image restoration", IEEE Trans. on Image Processing, vol. 9, no. 11, pp. 1877-1896, 2000.

52 Pai, H. T. P., and A. C. Bovik, "Exact multichannel blind image restoration", IEEE Signal processing Lett., vol. 4, no. 8, pp. 217-220, 1997.

53 Vrhel, M. J., and M. Unser, "Multichannel restoration with limited *A priori* information", IEEE Trans. on Image Processing, vol. 8, no. 4, pp. 527-536, 1999.

54 Molina, R., J. Mateos and A. K. Katsaggelos, "Bayesian Multichannel image restoration using compound Gauss-Markov random fields", IEEE Trans. on Image Processing, vol. 12, no. 12, pp. 1642-1654, 2003.

55 Galatsanos N. P., and R. T. Chin, "Digital restoration of multichannel images", IEEE Trans. on Acoustics, Speech, and Signal Processing, vol. 37, no. 3, pp. 415-421, 1989.

56 Hunt B. R., and O. Kubler, "Karhunen-Loeve multispectral image restoration. Part 1: Theory", IEEE Trans. on Acoustics, Speech, and Signal Processing, vol. ASSP-32, no. 3, pp. 592–600, 1984.

57 Galatsanos, N. P., A. K. Katsaggelos, R. T. Chin, and A. D. Hillery, "Least squares restoration of multichannel images", IEEE Trans. on Signal Processing, vol. 39, pp. 2222–2236, Oct. 1991.

58 Guo, Y. P., H. P. Lee, and C. L. Teo, "Multichannel image restoration using an iterative algorithm in space domain", Image Vis. Comput., vol. 14, no. 6, pp. 389–400, 1996.

59 Molina, R. and J. Mateos, "Multichannel image restoration in astronomy", Vistas Astron., vol. 41, no. 3, pp. 373–379, 1997.

60 Molina, R., A. K. Katsaggelos, J. Mateos, A. Hermoso, and C. A. Segall, "Restoration of severely blurred high range images using stochastic and deterministic relaxation algorithms in compound Gauss Markov random fields", Pattern Recognit., vol. 33, no. 3, pp. 557–571, 2000.

61 Molina, R., J. Mateos, and A. K. Katsaggelos, "Multichannel image restoration using compound Gauss-Markov random fields", in Proc. Int. Conf. on Acoustics, Speech, and Signal Processing, (ICASSP 2000), vol. 1, Vancouver, BC, Canada, pp. 141–144, 2000.

62 Vese, L. A. and S. J. Osher, "Image denoising and decomposition with total variation minimization and oscillatory functions", J. Math. Imaging Vis., vol. 20, no. 1-2, pp. 7-18, 2004.

63 Lagendijk R. L., J. Biemond and D. E. Boekee, "Identification and restoration of noisy blurred images using the expectation-maximization algorithm", IEEE Trans. on Acoustics, Speech, and Signal Processing, vol. 38, July 1990,

64 Cheema, T. A., I. M. Qureshi, A. Jalil, and A. Naveed, "Blurred image restoration of nonlinearly degraded images using ANN and nonlinear ARMA model", Journal of Intelligent Systems, vol. 11, no. 5, pp. 299–312, 2001

65 Reeves, S. J. and R. M. Mersereau, "Blur identification by the method of generalized cross-validation", IEEE Trans. on Image Processing, vol. 1, pp. 301-311, July 1997.

66 Acton, S. T., and A. C. Bovik, "Piecevise and local image models for regularized image restoration using cross-validation", IEEE Trans. on Image Processing, vol. 8, no. 5, pp. 652-665, 1999.

67 Golub, G. H., M. Heath and G. Wahba, "Generalized cross-validation as a method for choosing a good rigid parameter", Technometrics, vol. 21, no. 2, pp. 215-223, 1979.

68 Cheema, T. A., I. M. Qureshi, A. Jalil, and A. Naveed, "Artificial neural networks for blur identification and restoration of nonlinearly degraded images", International Journal of Neural Systems, vol. 11, no. 5, pp. 455–461, 2001.

69 McCulloch, W. S. and W. Pits, "A logical calculus of the ideas immanent in nervous activity", Bulletin of Mathematical Biophysics, vol. 5, pp. 115-133, 1943.

70 Minsky, M. and S. Papert, Perceptrons: An Introduction to Computation Geometry, The MIT press, 1969.

71 Carratio, S., Neural Networks: Advances and Applications, 2, ch. 9, North-Holland, pp. 177-198, 1992.

72 Coello, A and C. Carlos, "An updated survey of GA-based multiobjective optimization techniques", ACM Computing Surveys, vol.32, no.2, pp.109-143, June 2000.

73 Haupt, R. and S. E. Haupt, Practical Genetic Algorithms, John Wiley & Sons, 1998.

74 Chellappa, R. and A. Jain, Markov Random Fields - Theory and Applications, Academic Press, New York, 1993.

75 Rawlins G. J. E., Foundations of Genetic Algorithm, San Mateo, CA: Morgan Kaufmann, 1991.

76 Davis L. E., Handbook of Genetic Algorithms, New York: Van Nostrand Reinhold, 1991.

77 Yap, K. M., L. Guan, and W. Liu, "A recursive soft-decision approach to blind image deconvolution", IEEE Trans. on Signal Processing", vol. 51, no. 2, pp. 515-526, Feb. 2003.

78 Branin, F. H., "A widely convergent method for finding multiple solutions of simultaneous nonlinear equations", IBM Journal of Research and Development, vol. 16, pp. 504-522, 1972.

79 Nagy, J. G. and D. P. O'Leary, "Fast iterative image restoration with spatially-varying PSF", Advanced Signal Processing Algorithms, Architectures, and Implementations IV, Editor Franklin T. Luk, 3162, pp.388-399, 1997.

80 Nagy, J. G. and D. P. O'Leary, "Restoring images degraded by spatially-variant blur", SIAM J. Sci. Comput., vol. 19, pp. 1063- 1082, 1998.

81 McNown, S. R. and B. R. Hunt, "Approximate shift-invariance by warping shift-variant systems", in the Restoration of HST Images and Spectra II, R. J. Hanisch and R. L. White, eds., pp. 181-187, 1994.

82 Adorf, H. M., "Towards HST restoration with space-variant PSF, cosmic rays and other missing data", in the Restoration of HST Images and Spectra II, R. J. Hanisch and R. L. White, eds., pp. 72-78, 1994.

83 Fish, D. A., J. Grochmalicki, and E. R. Pike, "Scanning singular-value-decomposition method for restoration of images with space variant blur", J. Opt. Soc. Am. A., vol. 13, pp. 1-6, 1996.

84 Simon Haykin, Neural Networks, Prentice Hall Pub, 1997.

85 Yap, K. M., L. Guan, and W. Liu, "A recursive soft-decision approach to blind image deconvolution" IEEE Trans. on Signal Processing", vol. 51, no. 2, pp. 515-526, Feb. 2003.

86 Perry, S. W. and L. Guan, "Perception based adaptive image restoration", Proc. Of ICASSP'98, pp. 2893-2896, May 1998.